UNIVERSITY OF OKLAHOMA

GRADUATE COLLEGE

EFFECTS OF PH, INORGANIC ANIONS, AND SURFACTANTS ON THE PHOTOCATALYTIC DEGRADATION OF AQUEOUS AMMONIA IN GRAYWATER

A DISSERTATION

SUBMITTED TO THE GRADUATE FACULTY

in partial fulfillment of the requirements for the

degree of

Doctor of Philosophy

By

XINGDONG ZHU
Norman, Oklahoma
2007

Downloaded from SHAREOK. Persistent Handle URL: https://hdl.handle.net/11244/1320

UMI Number: 3307012



UMI Microform 3307012

Copyright 2008 by ProQuest Information and Learning Company.
All rights reserved. This microform edition is protected against unauthorized copying under Title 17, United States Code.

ProQuest Information and Learning Company
300 North Zeeb Road
P.O. Box 1346
Ann Arbor, MI 48106-1346

EFFECT OF PH, INORGANIC ANIONS, AND
SURFACTANTS ON THE PHOTOCATALYTIC
DEGRADATION OF AQUEOUS AMMONIA IN GRAYWATER

A DISSERTATION APPROVED FOR THE
SCHOOL OF CIVIL ENGINEERING AND ENVIRONMENTAL SCIENCE

BY

_____
Dr. Elizabeth C. Butler

_____
Dr. Lance L. Lobban

_____
Dr. Mark A. Nanny

_____
Dr. Daniel E. Resasco

_____
Dr. David A. Sabatini

© Copyright by XINGDONG ZHU 2007
All Rights Reserved.

ACKNOWLEDGEMENTS

I cordially thank my advisor Dr. Elizabeth Butler for everything she did for me through my study. I am grateful to her profound knowledge and a serious attitude on research. Her encouragement, understanding, and financial support are vital in the completion of this dissertation. Whenever I encountered problems with experiments, she was the person to help me solve problems. She encouraged me to not only grow as an experimentalist but also as an instructor and an independent thinker. Being English a second language, it is almost impossible to finish this dissertation without her patience and time in helping with writing.

I sincerely thank my committee members Drs. Lance L. Lobban, Mark A. Nanny, Daniel E. Resasco, and David A. Sabatini for their input. Their comments and suggestions are very insightful and invaluable on the completion of this dissertation. I also thank Dr. Tohren C. G. Kibbey for his nice help with the measurement of surfactants using UV-vis spectroscopy.

A special thank will be given to my Mother, Ms. Xuemei Qian. Without her faith in my going to the college, it is impossible for me to come to the USA to pursue my Ph. D. She gave me confidence and hope through my life and study. I also greatly thank my entire family back in China for their encouragement and support.

I would also thank my husband, Xuhui Zhou, and my daughter Lucy Zhou. My husband's unwavering love is my biggest support upon the completion of this dissertation. Lucy's coming to this world in 2005 was the greatest present during my Ph. D. study. She gives me fun and joys and fades my fret from school. They made me more comfortable in doing my research in the laboratory.

Funding for this research was provided by the National Aeronautics and Space Administration (NCC 5-586), the Oklahoma State Regents for Higher Education, and the University of Oklahoma College of Engineering. I thank Dr. Taha Elmorsi and the anonymous reviewers for helpful comments on part of this dissertation. I also thank the Degussa Corporation for the gift of the P25 TiO_2.

TABLE OF CONTENTS

Acknowledgements……...iv

List of Tables……..viii

List of Figures……ix

Abstract…….…...xii

Chapters

1. Introduction…….……...1
1.1. Motivation of this research……..1
1.2. Principle of TiO_2 photocatalysis.……..…...3
1.3. Objective of this research ……5

2. Effect of pH and catalyst concentration on photocatalytic oxidation of aqueous ammonia and nitrite in titanium dioxide suspensions
2.1. Introduction…….…9
2.2 Experimental section……..……12
2.2.1 Chemicals……...12
2.2.2. Experimental setup…….13
2.2.3. Analytical methods …….…….…….15
2.3. Results and discussion……...16
2.3.1. Influence of TiO_2 concentration on NH_4^+/NH_3 photocatalytic oxidation……....16
2.3.2. Influence of pH on NH_4^+/NH_3 photocatalytic oxidation…….…...22
2.3.3. Influence of pH on NO_2^- photocatalytic oxidation……27
2.4 Conclusions……....35

3. Effect of inorganic anions on the titanium dioxide-based photocatalytic oxidation of aqueous ammonia and nitrite ……...36
3.1. Introduction ……..…36
3.2. Materials and methods……...39
3.2.1. Chemicals ……..…...39
3.2.2. Photocatalytic oxidation experiments……39
3.2.3. Adsorption experiments……....40
3.2.4. Analytical methods……..……..41
3.3. Results and discussion ……..……42
3.3.1. NH_4^+/NH_3 photocatalytic oxidation……...42
3.3.1.1. Role of ·OH scavenging by anions and/or direct oxidation by anion radical……..44
3.3.1.2. Role of anion adsorption……...……47
3.3.2. NO_2^- photocatalytic oxidation…….……...48

3.3.2.1. Role of anion adsorption……51
3.4. Conclusions ……...……52

4. Effect of surfactants on the titanium dioxide-based photocatalytic oxidation of aqueous ammonia in graywater
4.1. Introduction……54
4.2. Experimental section …… 56
4.1.1 Chemicals ……..……..……..56
4.1.2 Photocatalytic oxidation experiments……..……59
4.1.3 Adsorption experiments……..……59
4.1.4 Analytical methods……..……60
4.2 Results and discussion……...61
4.2.1 Role of surfactant adsorption……..……64
4.3.2 Role of ·OH radical scavengers……..……68
4.3 Conclusions……78

5 Conclusions and recommendations
5.1 Conclusions……...80
5.2 Recommendations for graywater recycling……...…….…….81
5.3 Recommendations for future work……...82

References cited……84

Appendices

Appendix A Detailed experimental procedures ……...……...…100

Appendix B Calculation of illuminated water volume versus TiO_2 concentration …...107

Appendix C Sequential first order reaction rate law……..…111

Appendix D Measurement of the concentration of ·OH in UV/H_2O_2 system ……112

Appendix E Determination of critical micelle concentration (CMC) and surface coverage of surfactant on the TiO_2 surface……123

Appendix F Profiles of the photocatalytic degradation of ammonia in the presence of surfactants/monosaccharides……...132

LIST OF TABLES

Table 2.1. Initial rates, product yields, and rate constants of NH_4^+/NH_3 photocatalytic oxidation at different concentrations of TiO_2…….17

Table 2.2. Initial rate constants and photoadsorption equilibrium constants for the Langmuir–Hinshelwood model……...25

Table 4.1. Physical/chemical properties of surfactants and monosaccharides……..58

Table 4. 2. Second order rate constants of ·OH with organic/inorganic compounds…....74

APPENDICES

Table A1. Calibration standards for IC analysis …….103

Table A2. Calibration standards for GC/FID analysis ……104

Table D1. Pseudo first order rate constants of *n*-BuCl degradation and steady-state concentration of ·OH in the presence of surfactant/monosaccharide at pH ~ 10.1 ……121

Table F1. Concentration of NP10 and surface tension ……...136

Table F2. Surface area of head group of surfactants and their surface coverage……138

LIST OF FIGURES

Figure 1.1. Scheme of the TiO_2-photocatalytic process.……4

Figure 2.1. Experimental photocatalytic oxidation apparatus…….……..13

Figure 2.2. Initial rate of NH_4^+/NH_3 degradation versus TiO_2 concentration……....18

Figure 2.3. $[NH_3]_T$ and products versus time at different TiO_2 concentrations……....21

Figure 2.4. $[NH_3]_T$ disappearance and pH variation during NH_4^+/NH_3 photocatalytic oxidation versus initial pH……..…23

Figure 2.5. Initial rate of NH_4^+/NH_3 photocatalytic oxidation versus $[NH_3]_{T,0}$ at pH ~9 and pH ~10.2……....26

Figure 2.6. Initial rate of NO_2^- photocatalytic oxidation versus initial pH……..…..28

Figure 2.7. Initial rate of NO_2^- photocatalytic oxidation versus initial concentration at different initial pH values.…….……..32

Figure 3.1. Effect of inorganic anions on NH_4^+/NH_3 photocatalytic oxidation at pH ~9 and ~10……...……..44

Figure 3.2. Effect of inorganic anions on the homogeneous photochemical oxidation of NH_4^+/NH_3 by UV/H_2O_2 with a Vycor filter at pH ~10……....45

Figure 3.3. Adsorption of chloride (Cl^-), sulfate (SO_4^{2-}) and phosphate ($H_2PO_4^-/HPO_4^{2-}$)……...…….47

Figure 3.4. Effect of inorganic anions on NO_2^- photocatalytic oxidation between pH 4 and 11…….……..49

Figure 4.1. Photocatalytic degradation of NH_4^+/NH_3 and surfactant pH ~ 10.1 ……..….63

Figure 4.2. Initial rates of NH_4^+/NH_3 photocatalytic degradation in the presence of surfactants at pH ~ 10.1 ……..64

Figure 4.3. Mass concentration of surfactants and selected products during the photocatalytic degradation of NH_4^+/NH_3 and surfactants at pH ~ 10.1……...……67

Figure 4.4. Photodegradation of *n*-BuCl by UV/H_2O_2 at pH ~10.1 with initial addition of surfactants ……...69

Figure 4.5. Relative initial rate of NH_4^+/NH_3 degradation versus relative concentration of ·OH in the presence of surfactants/monosaccharides……..……...…..72

Figure 4.6. NH_4^+/NH_3 photocatalytic degradation and formate formation at pH ~ 10.1 …… ….75

Figure 4.7. Initial rate of NH_4^+/NH_3 degradation at pH 10.1 vs. the mass concentration of carbon……...78

Appendices

Figure B1. UV spectrum of 0.025 g/L TiO_2 suspension at pH 9.9……..107

Figure B2. Percentage of illuminated water volume versus TiO_2 concentration at the light intensity (I/I_0) of 0.01 at a wavelength of 388 nm…….……...…….110

Figure D1. Photodegradation of *n*-BuCl without surfactants (control) ……..…115

Figure D2. Photodegradation of *n*-BuCl with 2 $\times 10^{-5}$ M cetylpyridinium chloride ……..115

Figure D3. Photodegradation of *n*-BuCl with 2 $\times 10^{-5}$ M hexyl-β-D-glucoside …….116

Figure D4. Photodegradation of *n*-BuCl with 2 $\times 10^{-5}$ M 1-octanesulfonic acid sodium ……...116

Figure D5. Photodegradation of *n*-BuCl with 2 $\times 10^{-5}$ M dihexyl sulfosuccinate sodium ……...117

Figure D6. Photodegradation of *n*-BuCl with 2 $\times 10^{-5}$ M sodium dodecylsulfate……...117

Figure D7. Photodegradation of *n*-BuCl with 2 $\times 10^{-5}$ M cetyltrimethylammonium chloride ……118

Figure D8. Photodegradation of *n*-BuCl with 1.2 $\times 10^{-5}$ M Brij® 23 lauryl ether ……...118

Figure D9. Photodegradation of *n*-BuCl with 1.2 $\times 10^{-5}$ M Brij® 23 lauryl ether and 0.01 M H_2O_2 ……...119

Figure D10. Photodegradation of *n*-BuCl with 2 $\times 10^{-5}$ helicin……...……119

Figure D11. Photodegradation of *n*-BuCl with 2 $\times 10^{-5}$ ally-tetra-O-acetyl -β-D-glucopyranoside ……120

Figure E1. Homogeneous degradation of SDBS, CPC and NP10 at pH ~10.1……..…124

Figure E2. Photocatalytic degradation of NH_4^+/NH_3 without surfactants (control) ..….125

Figure E3. NH_4^+/NH_3 degradation with 2×10^{-5} M sodium dodecylbenzene sulfonate ……...125

Figure E4. NH_4^+/NH_3 degradation with 2×10^{-5} M 1-octanesulfonic acid sodium ……126

Figure E5. NH_4^+/NH_3 degradation with 2×10^{-5} M dihexyl sulfosuccinate sodium …..126

Figure E6. NH_4^+/NH_3 degradation with 2×10^{-5} M sodium dodecylsulfate ……..…127

Figure E7. NH_4^+/NH_3 degradation with 2×10^{-5} M cetylpyridinium chloride ……..127

Figure E8. NH_4^+/NH_3 degradation with 2×10^{-5} M cetyltrimethylammonium chloride……128

Figure E9. NH_4^+/NH_3 degradation with 2×10^{-5} M NP10 ……...……..128

Figure E10. NH_4^+/NH_3 degradation with 2×10^{-5} M hexyl-β-D-glucosid…….……..129

Figure E11. NH_4^+/NH_3 degradation with 1.2×10^{-5} M Brij®35 …….……129

Figure E12. NH_4^+/NH_3 degradation with 1.2×10^{-5} M Brij® 35 and 0.01 M H_2O_2……130

Figure E13. NH_4^+/NH_3 degradation with 2×10^{-5} M ally-tetra-O-acetyl- β-D-glucopyranoside ……..130

Figure E14. NH_4^+/NH_3 degradation with 2×10^{-5} M helicin …….….131

Figure F1. Surface tension vs. concentration of SDBS ……..……133

Figure F2. Surface tension vs. concentration of CPC ……...…..134

Figure F3. Critical micelle concentration of NP10 …….…... 135

Figure F4. Surface tension as function of natural logarithm of surfactant concentrations ……..…..137

ABSTRACT

Global water consumption has been increasing due to population growth. Accordingly, water recycling is a good strategy to compensate for the increased water demand. The overall objective of this study was to investigate the feasibility of using titanium dioxide (TiO_2)-photocatalysis to recycle graywater in a simplified model system. We evaluated effects of three major parameters, including pH, inorganic anions, and surfactants, on the photocatalytic degradation of aqueous ammonia (NH_4^+/NH_3) in graywater in a bench scale reactor. Our results show that higher initial rates of NH_4^+/NH_3 photocatalytic oxidation were obtained in higher pH solutions, and the initial rates were proportional to the initial concentrations of neutral NH_3, and not total NH_3 (i.e., $[NH_4^+] + [NH_3]$). We conducted experiments on the effects of four inorganic anions (Cl^-, SO_4^{2-}, $H_2PO_4^-/HPO_4^{2-}$, and HCO_3^-/CO_3^{2-}) on NH_4^+/NH_3 degradation at pH ~9 and ~10 and nitrite (NO_2^-) oxidation over the pH range of 4-11. Cl^-, SO_4^{2-}, and HCO_3^- had no effect on NH_4^+/NH_3 and NO_2^- photocatalytic oxidation at pH ~9 and ~10, whereas CO_3^{2-} slowed NH_4^+/NH_3 but not NO_2^- photocatalytic oxidation at pH ~11. While HPO_4^{2-} enhanced NH_4^+/NH_3 photocatalytic oxidation at pH ~9 and ~10, $H_2PO_4^-/HPO_4^{2-}$ inhibited NO_2^- oxidation at low to neutral pH values. Photocatalytic oxidation of NH_4^+/NH_3 to NO_2^- is the rate-limiting step in the complete oxidation of NH_4^+/NH_3 to NO_3^- in the presence of common wastewater anions at pH > 9. As for surfactants, their degradation rates were faster than that of NH_4^+/NH_3 at pH ~10.1. Surfactant significantly slowed the initial rates of NH_4^+/NH_3 degradation, with the detrimental effect increasing in the order sodium dodecylbenzene sulfonate (SDBS) < cetylpyridinium chloride (CPC) < nonylphenol

polyethoxylate (10) (NP10). Adsorption of surfactants could not explain the slower initial rates of NH_4^+/NH_3 photocatalytic degradation in the presence of 2×10^{-5} M surfactants. We concluded that formation of hydroxyl radical (·OH) scavengers, including formate and carbonate, from the photocatalytic degradation of surfactants was the main reason for decreasing initial rates of NH_4^+/NH_3 degradation. Our results show that TiO_2 photocatalysis can remove both carbonaceous and nitrogenous biological oxygen demand (CBOD and NBOD), which has implications in graywater recycling.

Key words: Aqueous ammonia, Titanium dioxide, pH, Inorganic anions, Surfactants, Hydroxyl radicals, Graywater.

CHAPTER 1

Introduction

1.1. Motivation of This Research

According to the United Nation population fund (UN FPA, 2001), global water consumption has increased six-fold over the past 70 years, due to population growth, industrial development, and increased use of irrigation. Accordingly, if we can properly treat wastewater, it could ultimately be used for agriculture purpose and groundwater recharge, or even for indirect sources of drinking water. This could alleviate the increasing water demand in the world. In addition to the increased water demand, there are many drought areas in the world, including Arizona in the southwest of the U.S.A., sub-Saharan Africa, and northern regions of China, where people lack of basic water supply. For example, the Yellow River in China ran dry from 600 kilometers upstream to the river's mouth every year in the 1990s. Particularly, in 1997, it ran dry a record of 226 days (UN FPA, 2001). This makes it difficult for local residents to obtain the minimum amount of water necessary for their lives, particularly during drought seasons. Therefore, it is vital to recycle wastewater to provide the solution to urgent needs of water supply. Furthermore, reuse of water can decrease the load of wastewater produced by crews on space shuttles and navy ships, which is crucial for their lives during Space (Lyndon, 1996; Yoon and Lueptow, 2005) and Navy missions (Lard et al., 1976; Benson et al., 1999).

Graywater, or wastewater generated in the households from showers, bathtubs, washing machines, and sinks, accounts for more than 50% of wastewater (Roesner et al., 2006). Thus, it makes a potential resource for water recycling. There are various

inorganic/organic pollutants in graywater including inorganic anions, nitrogen-containing species, and surfactants (Rose et al., 1991, Eriksson et al., 2002; Ramon et al., 2004). Among these, aqueous ammonia (NH_4^+/NH_3), one of the major nitrogen-containing pollutants in wastewater, is a potential source of oxygen depletion due to eutrophication (Delwiche, 1981; Lee et al., 2002). Also, an excess of NH_4^+/NH_3 is toxic to aquatic life including fish (Randall and Tsui, 2002; Tilak et al., 2002). For instance, it has been shown that NH_4^+/NH_3 is toxic to fish at a concentration of 1 mg/L (6×10^{-5} M) NH_3 in water (Hued et al., 2006). Indian carp are more sensitive to NH_3 — a concentration as low as 2.6×10^{-6} M NH_3 killed 50% of Indian carp studied (Tilak et al., 2002). The United States Environmental Protection Agency (US EPA) has not established a maximum contaminant level (MCL) for NH_4^+/NH_3 in drinking water, many European nations, however, have adopted a drinking water standard of 0.5 mg/l (3×10^{-5} M) NH_3 (EU drinking water standards, 1998).

While there are several methods for NH_4^+/NH_3 removal from water and wastewater, including biological nitrification, NH_4^+/NH_3 stripping, breakpoint chlorination, and ion exchange, each of these methods has disadvantages (Delwiche, 1981). For example, although biological nitrification is a widely used process to remove NH_4^+/NH_3, the efficiency of biological nitrification is highly dependent on temperature, dissolved oxygen, carbon source, pH, and the concentrations of toxic substances (Christensen et al, 1978, Fang et al., 1993; Hurse and Connor, 1999). Ammonia stripping can remove ammonia from wastewater, but it simply transfers the pollution from the water to the air without ultimately solving the problem (US EPA, 2000). As for the chlorination method, residual chlorine left in the discharge is toxic to

aquatic organisms, and chlorine could react with organic compounds producing a number of known and suspected carcinogens (Delwiche, 1981). As far as ion exchange is concerned, concentrated brine has to be treated (Jørgensen et al., 1976), and regeneration of ion exchange materials is needed.

Alternatively, the titanium dioxide (TiO_2)-based photocatalytic oxidation process has been considered as a promising technique to remove NH_4^+/NH_3 from water (Low et al., 1991; Wang, 1991; Pollema et al., 1992; Bravo, 1993; Wang et al., 1994; Takeda and Fujiwara, 1996; Bonsen et al., 1997) because TiO_2 is a cheap, stable, and non-toxic catalyst (Litter 1999). TiO_2 photocatalysis could be used as the polishing step after biological treatment, where lower concentrations of organic and inorganic contaminants are still present. Potential disadvantage of this technique is that nitrite (NO_2^-) and nitrate (NO_3^-), more toxic nitrogen species, are intermediates/products of NH_4^+/NH_3 oxidation (Wang et al., 1991; Pollema et al., 1992; Bravo et al., 1993; Bonsen et al., 1997). However, this can be overcome by combining ion-exchange process.

1.2. Principle of TiO_2 Photocatalysis

TiO_2 is an n-type semiconductor with a conduction band (cb) and a valence band (vb) and there is a band gap between those two bands, as shown in Figure 1.1. When the energy of the UV light is greater than the band gap (e.g., 3.2 eV for anatase form of TiO_2) (Bhatkhande et al., 2001), electrons can be ejected from the valence band to the conduction band; correspondingly photo-generated holes (h^+) are formed in the valence band.

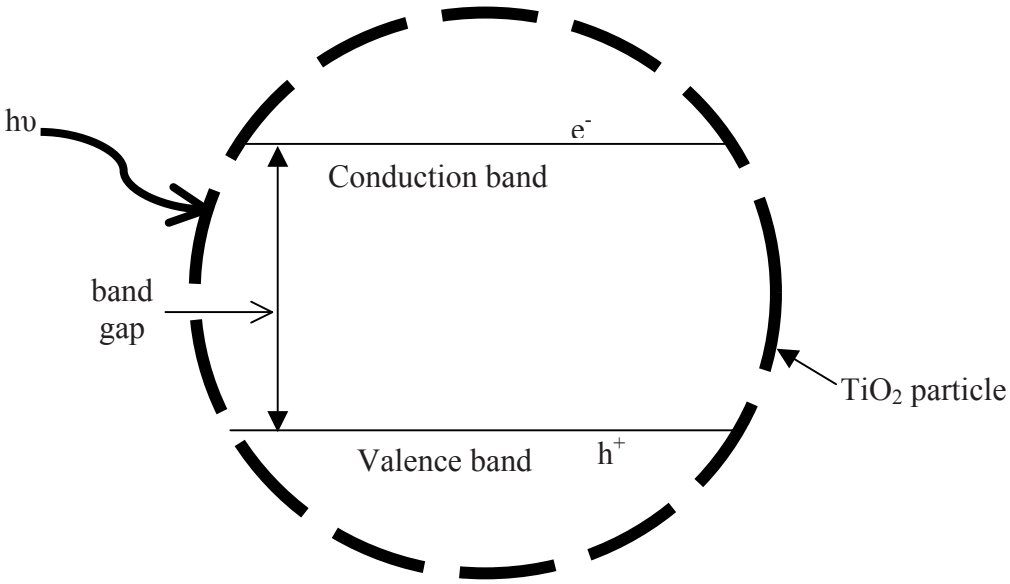


Figure 1.1. Scheme of the TiO_2- photocatalytic process

As shown in equations 1.1 and 1.2, photo-generated holes can react with OH^- and/or H_2O to form a non-selective oxidant, hydroxyl radical (·OH), which can oxidize organic and inorganic substrates near/on the surface (Fox and Dulay, 1993; Mills et al., 1993; Hoffmann et al., 1995; Herrmann, 1999; Pirkanniemi and Sillanpää, 2002; Bhatkhande et al., 2001).

$$H_2O/OH^- + h^+ \rightarrow \cdot OH \quad (1.1)$$

$$\cdot OH + \text{reactant} \rightarrow \text{products} \quad (1.2)$$

Photo-generated holes can also directly oxidize substrates on/near the TiO_2 surface (equation 1.3). Meanwhile, photo-generated electrons (e^-) can react with dissolved oxygen to form super oxide ($O_2^{\cdot -}$ and its conjugate acid HOO·, with a pK_a value of 11.6 (Staehelin and Hoigné, 1982)), which can reduce substrates (Kudo 1987, Li and Wasgestian 1998), as shown in equations 1.4 and 1.5.

$$h^+ + \text{reactant} \rightarrow \text{products} \quad (1.3)$$

$$O_2 + e^- \rightarrow O_2^{\cdot -} \quad (1.4)$$

$$HOO\cdot + \text{reactant} \rightarrow \text{products} \quad (1.5)$$

The holes and electrons can recombine on the surface or in the bulk of the particle to produce heat if there are no species that can scavenge the holes or electrons.

1.3. Objectives of This Research

While it has been shown that the mass loading of TiO_2 influences NH_4^+/NH_3 degradation rates (Wang et al., 1991; Pollema et al., 1992; Bonsen et al., 1997), no explanations were provided on why TiO_2 mass loading affected the degradation rates. In addition to the TiO_2 loading, pH is also important in photocatalysis. TiO_2 point of zero charge (pH_{pzc}) is ranged 6.2-7.5 for Degussa P25 (Hoffmann et al., 1995; Fernández-Nieves et al., 1998). At $pH < pH_{pzc}$, the TiO_2 surface is positively charged, which would favor adsorption of anion species, phosphate (PO_4^{2-}) and sodium dodecylbenzene sulfonate (SDBS), for example; at $pH > pH_{pzc}$, vice versa. Previous researchers have studied the effect of pH on the photocatalytic oxidation of NH_4^+/NH_3

and found higher reaction rates in alkaline solution versus neutral or acidic solution (Low et al., 1991; Wang, 1991; Pollema et al., 1992; Bravo, 1993; Wang et al., 1994; Takeda and Fujiwara, 1996; Bonsen et al., 1997), which is possibly due to the pH dependency of the TiO_2 surface charge (Bravo et al., 1993), or due to the rate-limiting step of NH_3 adsorption to the TiO_2 surface. However, there was no direct evidence to explain this trend. In addition, NO_2^- and NO_3^- are the intermediates or products of NH_4^+/NH_3 oxidation, understanding whether NO_2^- oxidation to NO_3^- is a rate-limiting step in the oxidation of NH_4^+/NH_3 to NO_3^-, and also how pH affects the oxidation rate of NO_2^- to NO_3^-, are important for an effective graywater treatment system design. Therefore, the first objective of this research was to investigate how the suspension pH and mass concentration of TiO_2 influence the photocatalytic degradation of NH_4^+/NH_3 and NO_2^-. To achieve this objective, several initial pH values and mass concentrations of TiO_2 were chosen to investigate their effects on the initial rates of NH_4^+/NH_3 and NO_2^- photocatalytic oxidation. Chapter 2 will discuss this in great detail.

Inorganic anions are commonly present in graywater (Rose et al., 1999, Eriksson et al., 2002; Ramon et al., 2004), and inorganic anions also influence the photocatalytic degradation rates of substrates (Abdullah et al., 1990; Chen et al., 1997; Wang et al., 1999; Xia et al., 2002, Hu et al., 2003, 2004; Zhang et al., 2005), due to their adsorption and/or competitive reactions with substrates for ·OH, as shown in equation 2. To the best of our knowledge, only Chen and Cao (2002) have studied the effect of inorganic anions, including Cl^-, SO_4^{2-} and NO_3^-, on NO_2^- photocatalytic oxidation using TiO_2 supported on hollow glass microbeads at pH 5. However, no systematic study has been done on the effect of inorganic anions on the TiO_2–based photocatalytic oxidation of

both NH_4^+/NH_3 and NO_2^- as a function of pH. Hence, this formed the focus of the second objective, i.e., to study whether inorganic anions would decrease the photocatalytic degradation rates of NH_4^+/NH_3 and NO_2^-. In this study, we examined the effects of four inorganic anions (Cl^-, SO_4^{2-}, $H_2PO_4^-/HPO_4^{2-}$, and HCO_3^-/CO_3^{2-}) on the photocatalytic oxidation of NH_4^+/NH_3 at pH ~9 and ~10 and NO_2^- over the pH range of 4-11. More details are presented in Chapter 3.

Surfactants are also commonly present in graywater due to the use of personal care products (Karsa, 1999; Eriksson et al., 2002). Biodegradation of surfactants would decrease the dissolved O_2 in water due to biochemical oxygen demand. Competitive adsorption of surfactants with NH_4^+/NH_3 for active sites on the TiO_2 surface and the competing reaction of surfactants with NH_4^+/NH_3 for ·OH would decrease initial rates of NH_4^+/NH_3 degradation. Therefore, it would be interesting to know whether surfactants could be removed by photocatalysis and how they influence NH_4^+/NH_3 photocatalytic degradation in graywater recycling. Hence, the third objective was to investigate whether surfactants would decrease initial rates of NH_4^+/NH_3 degradation at pH ~10.1. Nine surfactants and two monosaccharides were chosen as model compounds. We investigated whether competitive adsorption of the model compounds or the formation of ·OH scavengers from the photocatalytic degradation of the model compounds is responsible for the slower initial rates of NH_4^+/NH_3 photocatalytic degradation. Chapter 4 provides details of this study.

Chapter 5 provides a summary and recommendations for graywater recycling and future work on this research. Generally, the results from this research will help water and wastewater professionals to understand the effects of several main parameters

in graywater on the removal efficiency of biological oxygen demand (BOD) (e. g., surfactants) and inorganic contaminants (NH_4^+/NH_3), and provide theoretical results that can serve as a guide for graywater recycling. This work can be applicable for graywater reuse in space shuttles and emerging regions where potable or non-potable water is limited. This work can also be applied for temporary wastewater treatment system used in disaster relief and refugee camp.

CHAPTER 2*

Effect of pH and Catalyst Concentration on Photocatalytic Oxidation of Aqueous Ammonia and Nitrite in Titanium Dioxide Suspensions

2.1. Introduction

Aqueous ammonia, one of the major nitrogen-containing pollutants in wastewater, is a potential source of oxygen depletion due to eutrophication (Delwiche, 1981; Lee et al., 2002). Both ammonium, NH_4^+, (pK_a = 9.3 at 25 ºC (Stumm and Morgan, 1996)), and its conjugate base, NH_3, can be present in water and wastewater. While there are several methods for NH_4^+/NH_3 removal from water and wastewater, including biological nitrification, ammonia stripping, breakpoint chlorination, and ion exchange, each of these methods has disadvantages (Delwiche, 1981). For example, the efficiency of biological nitrification is highly dependent on temperature, dissolved oxygen, the carbon source, pH, and the concentrations of toxic substances (Christensen and Harremoes, 1978; Focht and Chang, 1975). Titanium dioxide (TiO_2)-based photocatalytic oxidation is a promising technology in water and wastewater treatment because TiO_2 is a cheap, stable, and non-toxic catalyst (Litter, 1999). It has been shown that solar radiation can be used in photocatalysis, which would make it economically competitive for water and wastewater treatment (Nagaveni et al.; 2004). Photocatalytic oxidation of NH_4^+/NH_3 using TiO_2 has been shown in several studies (Gopalarao et al.,

* Reproduced with permission from "Environmental Science & Technology 39, Zhu, X. D.; Castleberry, R. S.; Nanny, M. A.; Butler, E. C. Effect of pH and catalyst concentration on photocatalytic oxidation of aqueous ammonia and nitrite in titanium dioxide suspensions, 3784-3791, Copyright (2007) American Chemical Society".

1941; Bravo et al., 1993; Low et al. 1991; Pollema et al.; 1992; Wang, 1991; Wang et al., 1994; Takeda and Fujiwara, 1996; Bonsen et al., 1997). While previous investigators studied the effect of pH on photocatalytic oxidation of NH_4^+/NH_3 and found higher reaction rates in alkaline solution versus neutral or acidic solution (Bravo et al., 1993; Low et al. 1991; Pollema et al.; 1992; Wang, 1991; Wang et al., 1994; Takeda and Fujiwara, 1996; Bonsen et al., 1997), no direct evidence to explain this trend has been reported. Bravo et al. (1993) speculated that the higher NH_4^+/NH_3 photocatalytic oxidation rate at alkaline pH was due to the pH dependence of the TiO_2 surface charge. Specifically, when the pH is lower than the TiO_2 point of zero charge (pH_{pzc}) (6.2-7.5 for Degussa P25 (Hoffmann et al., 1995; Fernández-Nieves et al., 1998)), the net surface charge is positive, which would hinder adsorption of NH_4^+ due to electrostatic repulsion (Bravo et al., 1993). On the other hand, when the pH is higher than the pH_{pzc} but lower than the pK_a of NH_4^+ (9.3), the negatively charged TiO_2 surface would favor adsorption of NH_4^+ and the highest reaction rates would be expected in this pH region if electrostatics determined reaction rates. Bonsen et al. (1997), however, proposed that adsorption of neutral NH_3, not NH_4^+, at the TiO_2 surface was the rate-limiting step during NH_4^+/NH_3 photocatalytic oxidation over the pH range 2.5-11.

Researchers have also studied the pH dependence of the products of NH_4^+/NH_3 photocatalytic oxidation (Pollema et al., 1992; Wang et al., 1994; Bonsen et al., 1997). For example, nitrate (NO_3^-) was the primary product of NH_4^+/NH_3 photocatalytic oxidation in acidic solution (pH 1.0), while nitrite (NO_2^-) was the main product in alkaline solution (pH 11.5) (Wang et al., 1994). In addition, Bonsen et al. (1997) found

that the product distribution in NH_4^+/NH_3 photocatalytic oxidation varied with TiO_2 concentration, but did not discuss the reasons for this phenomenon.

For NO_2^- photocatalytic oxidation, NO_3^- was found to be the major product, and the yield of NO_3^- increased dramatically with decreasing pH (Zafra et al., 1991; Milis and Domènech, 1993; Milis et al., 1994; Sun and Chou, 1999). Milis and Domènech (1993) have proposed that, as for NH_4^+, electrostatic interaction between NO_2^- and the TiO_2 surface affects the reaction rate of NO_2^- photocatalytic oxidation at different pH values. Since NO_2^- and NO_3^- are the intermediates or products of NH_4^+/NH_3 oxidation, understanding whether NO_2^- oxidation to NO_3^- is a rate-limiting step in the oxidation of NH_4^+/NH_3 to NO_3^-, and also how pH affects the oxidation rate of NO_2^- to NO_3^-, are important for an effective treatment system design.

The objectives of this research were: (i) to investigate the reasons why TiO_2 concentration affects the product distribution in NH_4^+/NH_3 photocatalytic oxidation and (ii) to determine why the NH_4^+/NH_3 and NO_2^- photocatalytic oxidation rates are pH dependent. Our hypothesis was that the pH dependence of the rates of photocatalytic oxidation of NH_4^+/NH_3 and NO_2^- could be explained by the pH-dependent extent of adsorption of these species to the TiO_2 surface. Accordingly, a series of experiments were conducted in which we measured initial photocatalytic oxidation rates for both NH_4^+/NH_3 and NO_2^- over a range of pH values. Since the mechanisms and extent of solute adsorption to the TiO_2 surface in the presence of UV light (photoadsorption) can differ from those for dark adsorption (Pelizzetti and Serpone, 1989), the Langmuir-Hinshelwood model was used to quantify the extent of photoadsorption in UV-illuminated TiO_2 systems and to relate it to initial reaction rates. The Langmuir-

Hinshelwood model can be expressed as:

$$r = \frac{kKC}{1 + KC} \qquad (2.1)$$

where r and k are the initial rate and rate constant, respectively, with units of M/min, C is the reactant initial concentration (M), and K is the photoadsorption equilibrium constant (M^{-1}).

2.2. Experimental Section

2.2.1. Chemicals

Degussa P25 TiO_2 (Akron, OH) was used without modification. This catalyst had a BET surface area of 50 ± 15 m^2/g and an average primary particle size of 21 nm (Degussa Corporation). According to personal communication with the Degussa Corporation, the estimated BET surface area for a specific batch of TiO_2 should be much narrower than this reported range. All solutions were prepared using nanopure water (18.1 MΩ cm) from an Infinity™ ultrapure water system (model D8961, Barnstead; Dubuque, IA). All chemicals were used as received. $(NH_4)_2SO_4$ (Alfa Aesar; Ward Hill, MA), $NaNO_2$ (Sigma-Aldrich; Milwaukee, WI), and $NaNO_3$ (Sigma-Aldrich), were used to make stock and standard solutions of NH_3, NO_2^-, and NO_3^-, respectively. Na_2SO_4 (Alfa Aesar) was used for ionic strength adjustment.

2.2.2. Experimental Setup

The experimental apparatus consisted of a cylindrical Pyrex glass reactor (7841-06, Ace Glass; Vineland, NJ), a double-walled quartz-cooling water jacket, and a 450 W medium pressure Hg lamp (7825-34, Ace Glass) (Figure 2.1).

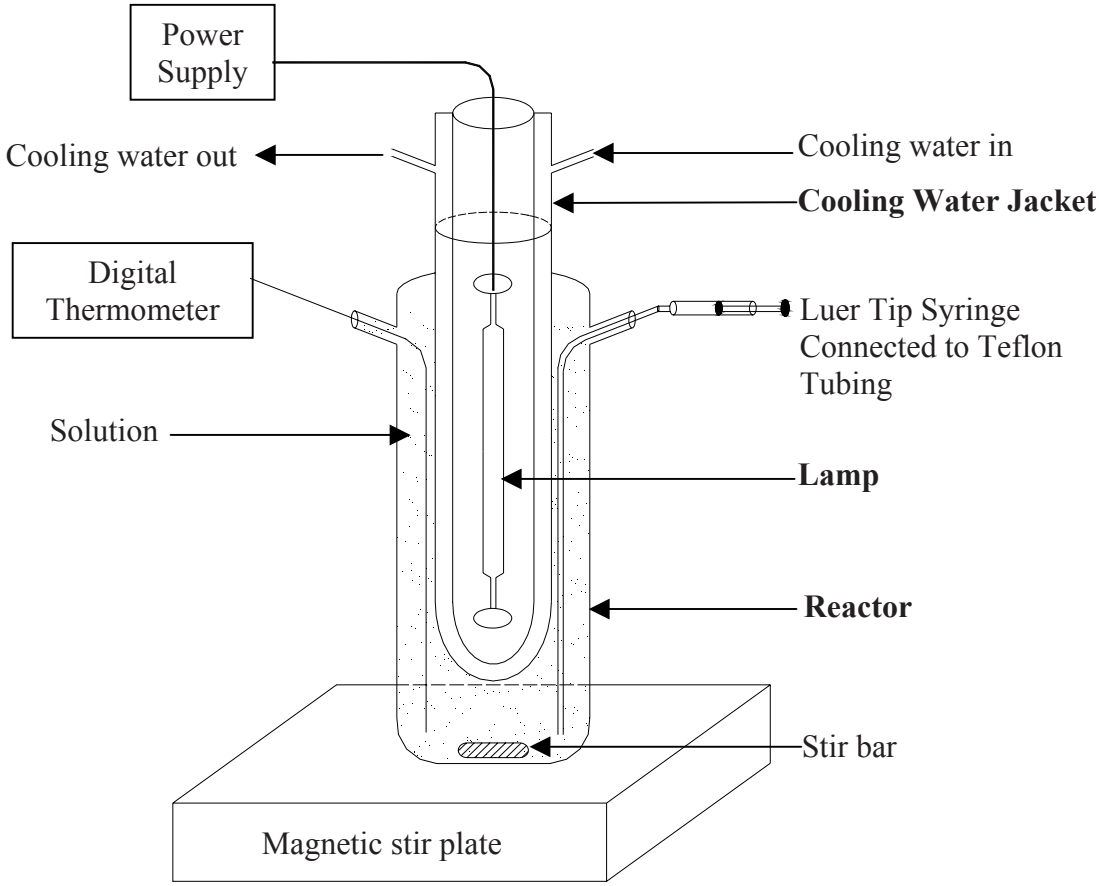


Figure 2.1. Experimental photocatalytic oxidation apparatus.

The total radiation output of the lamp was 175.8 W with the following specific radiation distribution: 220-280 nm: 27.0 W; 280-320 nm: 28.7W; 320-400 nm: 28.0 W;

400-600 nm: 75.7 W; and 1000-1400 nm: 16.4 W. Appendix A provides a step-by-step procedure for conducting kinetic experiments. Basically, the cooling water jacket was set up inside the reactor to maintain the temperature between 25 and 31 ºC, preventing excessive heating of the TiO_2 slurry. The lamp was placed inside the cooling water jacket. The volume of aqueous slurry in all experiments was 1300 mL, and TiO_2 concentrations ranged from 0.1 to 3 g/L. All experiments contained an excess of electrolyte, 1×10^{-3} M Na_2SO_4, in order to maintain a relatively constant ionic strength even when reactant concentrations were varied. The reaction slurry was stirred with a magnetic stirrer at a constant speed to maintain a well-mixed TiO_2 suspension during the experiments. Experiments with neither UV light nor TiO_2 showed that loss of NH_4^+/NH_3 due to volatilization was negligible during the time period of our experiments. Experiments with TiO_2, but no UV light, also showed that dark adsorption was negligible.

Before turning on the UV lamp, the pH of the suspension was adjusted to the desired value by dropwise addition of 1 M NaOH or 0.05 M H_2SO_4 (Fisher Scientific, Fairlawn, NJ). The suspension was placed in the dark, shielded with aluminum foil, and stirred until the pH was stable, indicating adsorption equilibrium. This occurred quickly (15 – 30 minutes) at pH values higher than 10 due to the high buffer capacity of water in this pH region. For lower pH values, it took 2-4 hours for pH equilibrium to be reached for NO_2^- solutions, while up to 24 hours were needed for NH_4^+/NH_3 solutions. At regular time intervals, samples were taken from the reactor using a 30 mL plastic sterile syringe with a leur slip tip, which was attached to an eighteen-inch piece of Teflon tubing (i.d. 3 mm). The sample was filtered into a 50 mL polypropylene tube

using a 47 mm filter holder (Millipore, Fisher Scientific) through a 0.1μm super®-100 filter membrane (Pall Life Sciences; Ann Arbor, MI). The filtrate was used for the measurement of pH, NH_4^+/NH_3, NO_2^-, and NO_3^-.

2.2.3. Analytical Methods

An ammonia gas-sensing electrode (model 95-12, Thermo Orion; Beverly, MA) and a pH electrode (model 9165BN, Thermo Orion), both connected to a model 420A+ Thermo Orion pH meter (Fisher Scientific), were used for NH_4^+/NH_3 and pH measurement, respectively. 200 μL of ionic strength adjustor (ISA, Thermo Orion), which contains deionized water, NaOH, disodium EDTA, and thymolphthalein (a pH indicator with a titration end point of 9.3-10.5 and a blue color above this pH range (Jenkins, 1980)), were added to the 10 mL standards and filtered samples immediately before NH_4^+/NH_3 measurement. The purpose of the ISA was to keep the samples and standards at a constant ionic strength and constant high pH value, so that essentially all NH_4^+/NH_3 would be in the neutral form, which is what the electrode measured ($[NH_3]_T = [NH_3]+[NH_4^+]$). The detection limit of the ammonia gas-sensing electrode was 5×10^{-6} M. Appendix A provides a detailed procedure for the measurement of NH_4^+/NH_3.

The concentrations of NO_2^- and NO_3^- were determined using a Dionex ion chromatograph (IC) with an Ion Pac® AG 11 guard column (4 × 50 mm), and an Ion Pac® AS 11 anion analytical column (4 × 250 mm), coupled with an ED 50 conductivity detector. A GP 50 gradient pump and an AS 40 automated sampler were employed. 5 mM and 100 mM NaOH solutions, prepared from 50% w/w NaOH, were used for the gradient eluents. The following gradient program was used to control the flow rates of

each individual solution. For the first 2.5 minutes, 90% nanopure water and 10% 5 mM NaOH were used. The flow was then changed to 100% 5 mM NaOH over 3.5 minutes. Finally, the flow was changed to 65% 5 mM and 35% 100 mM NaOH over 2.8 minutes. The sample loop volume was 25 μL. A Dionex Peaknet 6.3 chromatography workstation was used for peak integration.

The concentrations of NH_4^+/NH_3, NO_2^- and NO_3^- were calculated by five point external standard calibration curves. The standard solutions were prepared daily, and analysis of standards was repeated every twenty samples. For IC analysis, a blank sample was analyzed every 30 samples. The procedures of preparation of IC standard solutions are described in Appendix A. For NH_4^+/NH_3 analysis, a blank sample was measured once daily. Every fourth sample was run in duplicate, and duplicate analyses differed by less than 5%. Kinetic experiments were repeated periodically, and they were reproducible within 95% confidence intervals.

2.3. Results and Discussion

2.3.1. Influence of TiO_2 concentration on NH_4^+/NH_3 photocatalytic oxidation

First, we measured the initial rate of NH_4^+/NH_3 oxidation at pH 10.2 for TiO_2 concentrations ranging from 0 to 3 g/L. The purpose of these experiments was to determine the optimum TiO_2 concentrations for subsequent experiments and to investigate how the TiO_2 concentration affected the product distribution. Since the kinetics of NH_4^+/NH_3 oxidation for this range of TiO_2 concentrations did not always conform to a simple zero or first order rate law over several half lives, we quantified NH_4^+/NH_3 reactivity by comparing initial reaction rates for the first half life. Initial

rates, product yields, and mass recoveries for the different TiO_2 concentrations are shown in Table 2.1, and initial rates of NH_4^+/NH_3 photocatalytic oxidation as a function of TiO_2 concentration are also shown in Figure 2.2.

Table 2.1. Initial rates, product yields, and rate constants of NH_4^+/NH_3 photocatalytic oxidation at different concentrations of TiO_2[a]

TiO_2 Concentration (g/L)	Initial rate $\times 10^7$ ($M \cdot min^{-1}$)	% NH_3 remaining in 6 hrs	% NO_2^- yield in 6 hrs[b]	% NO_3^- yield in 6 hrs[c]	% Mass recovery in 6 hrs[d]	$k_1 \times 10^3$ (min^{-1})	$k_2 \times 10^3$ (min^{-1})
0	5.4 ± 1.4	45	28	BDL[e]	73	-[f]	-[f]
0.1	3.8 ± 1.1	19	45	21	86	-[f]	-[f]
0.2	2.42 ± 0.97	30	37	19	86	-[f]	-[f]
0.5	2.65 ± 0.82	26	16	43	85	-[f]	-[f]
1	2.74 ± 0.54	12	4	90	106	4.725 ± 0.083	39.4 ±3.5
2	3.83 ± 0.53	4	BDL[e]	97	101	6.34 ± 0.14	70 ± 19
3	4.12 ± 0.46	7	BDL[e]	93	100	6.356 ± 0.042	136 ± 28

[a]Initial concentration of total NH_3 ($[NH_4^+] + [NH_3]$): (9.45 to 9.98) $\times 10^{-5}$ M; initial pH:10.2; reaction time: t = 6h; uncertainties are 95% confidence intervals. [b]$100 \times [NO_2^-]_t / [NH_3]_{T,0}$. [c]$100 \times [NO_3^-]_t / [NH_3]_{T,0}$. [d]$100 \times ([NO_2^-]_t + [NO_3^-]_t + [NH_3]_{T,t})/[NH_3]_{T,0}$. [e]Below detection limits. [f]Not determined because the data for TiO_2 concentrations < 1 g/L did not fit the consecutive first-order model.

As shown in Table 2.1 and Figure 2.2, the initial rate of NH_4^+/NH_3 photocatalytic oxidation decreased when the TiO_2 concentration was increased from 0 to 0.2 g/L, then increased as the TiO_2 concentration was increased to 3 g/L, where it seemed to level off. These trends may be due to different contributions of distinct

homogeneous and heterogeneous photochemical reactions at different TiO_2 concentrations. Specifically, when no TiO_2 was present, only the homogeneous photochemical reaction was possible. When only a small amount of TiO_2 (< 0.2 g/L) was present, it may have acted mainly to absorb and/or scatter UV light, inhibiting the homogeneous reaction (evidence of this is shown in Appendix B), but not yet causing a significant heterogeneous reaction. This could explain the downward trend in initial rates of NH_4^+/NH_3 photocatalytic oxidation shown in Figure 2.2.

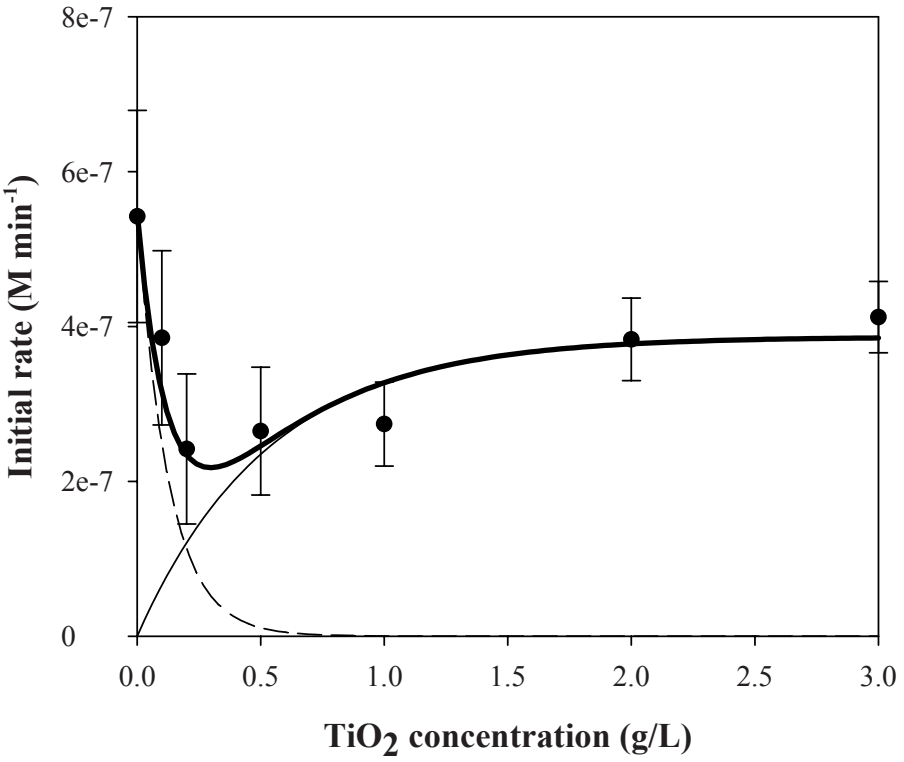


Figure 2.2. Initial rate of NH_4^+/NH_3 degradation versus TiO_2 concentration, initial pH: 10.2; $[NH_3]_{T,0}$ ranged from 9.38×10^{-5} to 9.76×10^{-5} M; error bars are 95% confidence intervals. Dashed and solid lines are schematic lines of homogeneous and heterogeneous degradation of NH_4^+/NH_3 that may occur in parallel, and the thicker line is the sum of these two processes.

At higher TiO_2 concentrations (> 0.2 g/L), however, the heterogeneous reaction likely increased in importance, which could explain the increase in rate constants in this TiO_2 concentration range. The eventual leveling-off of the initial rates of NH_4^+/NH_3 photocatalytic oxidation around 3 g/L (Figure 2.2) could be explained by the fact that TiO_2 was present at a high enough concentration to block UV transmittance to the interior portions of the reactor (Wang et al., 1994, Mills et al., 1993), making the homogeneous reaction insignificant (Appendix B).

The different mass recoveries measured at different TiO_2 concentrations (Table 2.1) support the idea that the relative contributions of homogeneous and heterogeneous reactions depend on TiO_2 concentration. Table 2.1 shows that the homogeneous reaction (i.e., 0 g/L TiO_2) yielded a 73% mass recovery in 6-hour of UV illumination (calculated as the sum of total NH_3 (i.e., $[NH_4^+] + [NH_3]$, $[NO_2^-]$ and $[NO_3^-]$), indicating formation of products other than NO_2^- and NO_3^-. These products could include N_2 and NH_2OH, which were detected by Ogata et al. (1981) in the photooxidation of NH_4^+/NH_3 with hydrogen peroxide. Unlike the homogeneous reaction, experiments with TiO_2 concentrations $\geq$ 1 g/L yielded approximately 100% mass recoveries during the same time period, indicating a different reaction mechanism under these conditions. Since TiO_2 concentration was the only variable that was changed between 0 and 3 g/L TiO_2, we conclude that the heterogeneous, TiO_2 mediated pathway, which produced a different distribution of reaction products than the homogeneous pathway, predominated at higher TiO_2 concentrations.

Unlike the heterogeneous photochemical reaction, the homogeneous photochemical oxidation of NH_4^+/NH_3 at pH 10.2 produced NO_2^-, but not NO_3^- after 6

hours of UV-illumination. This indicates that TiO_2 is required for the photochemical oxidation of NO_2^- at pH 10.2. (Homogeneous oxidation of NO_2^- by O_2 has been shown to be most important at low pH (Braida and Ong, 2000).) The higher NO_3^- yields for TiO_2 concentrations ≥ 1 g/L (Table 2.1) are additional evidence that the heterogeneous reaction predominates at these TiO_2 concentrations.

Figure 2.3 shows plots of $[NH_3]_T$ (i.e., $[NH_4^+] + [NH_3]$), $[NO_2^-]$, and $[NO_3^-]$ versus time for selected TiO_2 concentrations from Figure 2.2. We attempted to quantify in more detail the reaction kinetics for these experiments in order to predict which reaction products would predominate in treatment systems under different conditions.

For TiO_2 concentrations where both the homogeneous and heterogeneous photochemical reactions were significant (<1 g/L), no simple rate law accurately described the distribution of reactants and products over time. For TiO_2 concentrations ≥ 1 g/L, where the heterogeneous reaction predominated, however, the data conformed to a consecutive first order model, as shown in reaction 2.2

$$NH_4^+/NH_3 \xrightarrow{k_1} NO_2^- \xrightarrow{k_2} NO_3^- \qquad (2.2)$$

where k_1 and k_2 are pseudo-first-order rate constants with units of min^{-1}. (These rate constants are distinct from the Langmuir-Hinshelwood rate constant k in equation 2.1.)

Since near 100% nitrogen mass recovery was observed at TiO_2 concentrations ≥ 1 g/L, we concluded that NO_2^- and NO_3^- were the most stable intermediates/products under these conditions, justifying application of a consecutive first-order reaction model considering only the reactions shown in reaction 2.2. The integrated rate laws

corresponding to reaction 2.2 (Steinfeld et al., 1999) are shown in Appendix C. Sigma Plot (version 2001) was used to calculate k_1 and k_2 by nonlinear regression of the experimental concentrations of total NH_3, NO_2^-, and NO_3^- versus time using these integrated rate laws. The resulting k_1 and k_2 values were substituted into the rate laws (Appendix C) and the concentrations of each species in reaction 2.2 were calculated as functions of time, then plotted as the solid lines in Figure 2.3. The calculated values of k_1 and k_2 are summarized in Table 2.1.

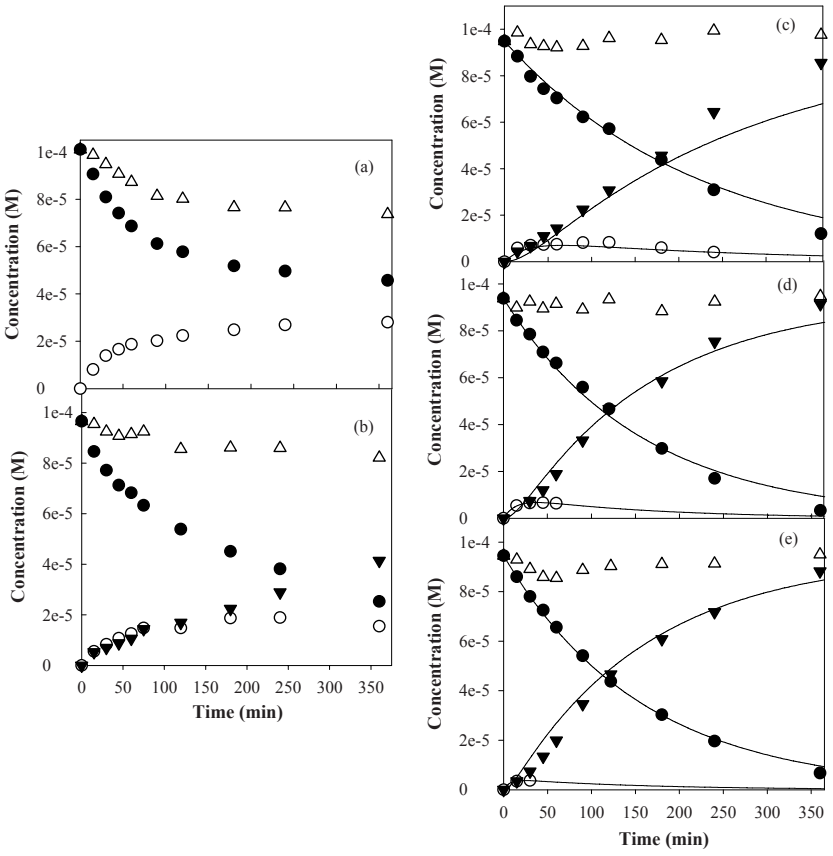


Figure 2.3. $[NH_3]_T$ and products versus time at different TiO_2 concentrations. (a) 0 g/L, (b) 0.5 g/L, (c) 1 g/L, (d) 2 g/L, (e) 3 g/L; data points represent experimentally measured concentrations, $[NH_3]_{T,t}$ ($[NH_3]+[NH_4^+]$ at time t) (●), $[NO_2^-]_t$ (○), $[NO_3^-]_t$ (▼), total nitrogen (Δ, sum of $[NH_3]_{T,t}$, $[NO_2^-]_t$, and $[NO_3^-]_t$); initial pH: 10.2; lines represent the consecutive first-order model fit for the concentrations of $[NH_3]_{T,t}$, $[NO_2^-]_t$, and $[NO_3^-]_t$ calculated from the rate constants k_1 and k_2 that were determined from the experimental data.

Table 2.1 shows that for all TiO_2 concentrations ≥ 1 g/L, the rate constant for NO_2^- oxidation, k_2, is significantly higher than the rate constant for NH_4^+/NH_3 oxidation, k_1, which means that the overall rate of NO_3^- formation is limited by the rate of NH_4^+/NH_3 oxidation to NO_2^- under these conditions. Table 2.1 also shows that as the TiO_2 concentration increased from 1 to 3 g/L, k_2 increased by more than three fold, while k_1 only increased by one third. This indicates that the rate of NO_2^- oxidation is more surface area dependent than the rate of NH_4^+/NH_3 oxidation.

2.3.2. Influence of pH on NH_4^+/NH_3 photocatalytic oxidation

In order to avoid the confounding effects of homogeneous photochemical processes on reaction kinetics, 3 g/L TiO_2 was chosen for all subsequent experiments. Since Bonsen et al. (1997) observed no significant difference in the initial rate of NH_4^+/NH_3 photocatalytic oxidation in the presence of O_2 versus N_2, we did not monitor the dissolved oxygen in our experiments. Experiments to study the influence of pH on the initial rate of NH_4^+/NH_3 photocatalytic oxidation were conducted at four initial pH values. The results are shown in Figures 2.4a-b. Figure 2.4a shows that there was no significant photocatalytic oxidation of NH_4^+/NH_3 at pH 6.3. For initial pH values of 7.7 and 9.0, photocatalytic oxidation of NH_4^+/NH_3 took place for a short period until the pH dropped to approximately 7.0, after which the reaction rate was negligible. At an initial pH of 10.2, however, the pH did not drop below 9.9 after four hours of UV illumination, and continuous photocatalytic oxidation of NH_4^+/NH_3 was observed during this period. These results indicate that there was no significant degradation of NH_4^+/NH_3 at pH values lower than approximately 7, which is consistent with previous

findings (Wang, 1991; Wang et al., 1994; Bonsen et al., 1997). The pH drop that occurred for initial pH values of 7.7 and 9.0 may be due to proton formation from NH_4^+/NH_3 oxidation (Pollema et al., 1992).

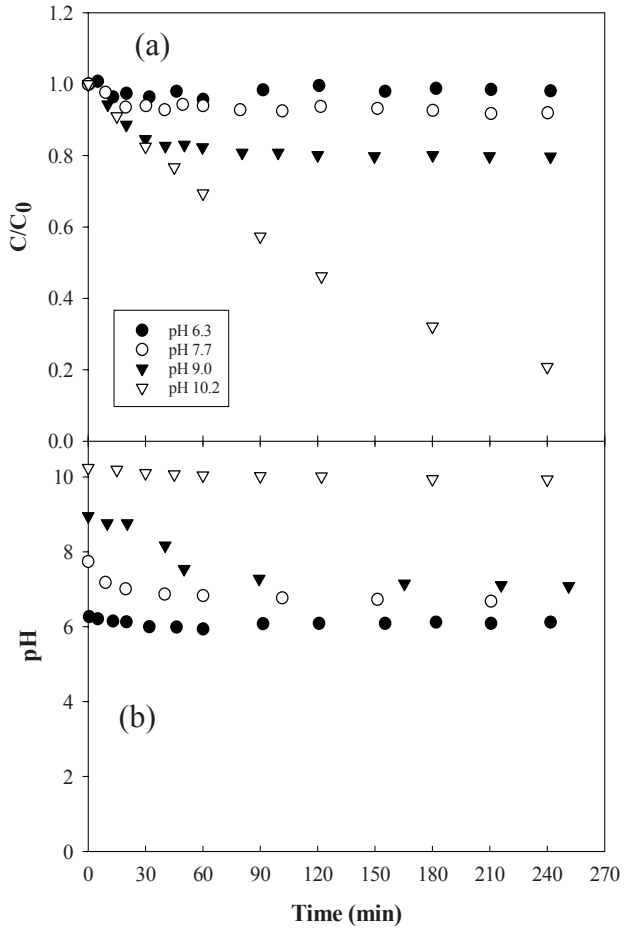


Figure 2.4. (a) $[NH_3]_T$ disappearance and (b) pH variation during NH_4^+/NH_3 photocatalytic oxidation versus initial pH. $[NH_3]_{T,0}$: 9.45×10^{-5} to 9.98×10^{-5} M, TiO_2 concentration: 3 g/L.

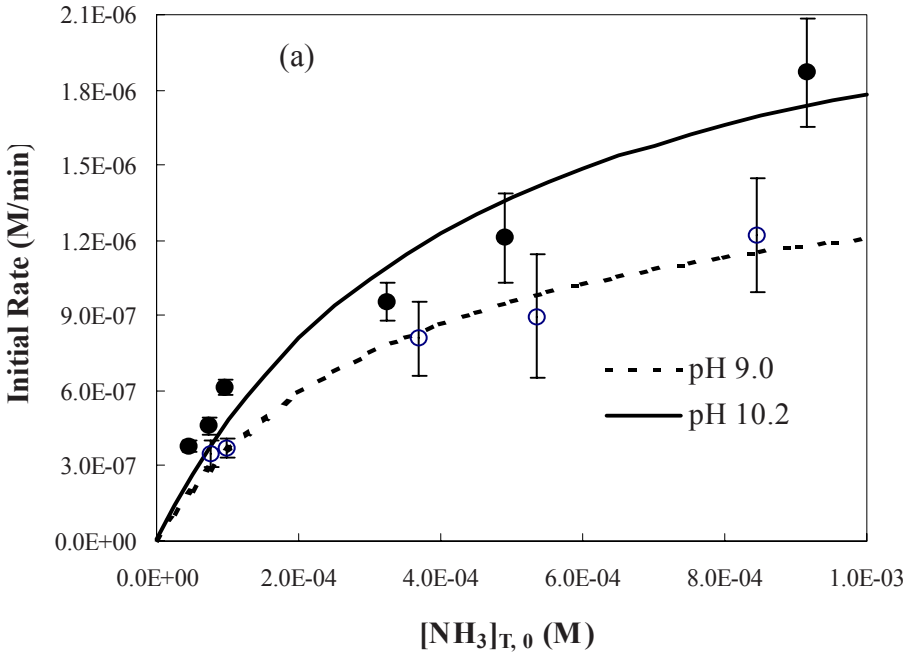
In order to test our hypothesis that the initial rates of NH_4^+/NH_3 oxidation were proportional to the extent of adsorption to the TiO_2 surface, we measured the initial rates of photocatalytic oxidation for a range of initial concentrations (4.4×10^{-5} - $9.2 \times$

10^{-4} M) and fit the data to the Langmuir-Hinshelwood model. The potentially confounding effect of variable pH over the course of the experiments was minimized by measuring initial rates, which were calculated from the best linear fit of NH_4^+/NH_3 concentration versus time for the initial time period where the slope (and pH) was approximately constant. The results in Figure 2.4 indicate that the reaction was too slow to measure for initial pH values lower than 9, so we performed these experiments at initial pH values of ~9.0 and ~10.2. (The initial pH values varied slightly around 9.0 and 10.2, as shown in Table 2.2.) The experimental data for pH 9.0 and 10.2, along with the Langmuir-Hinshelwood model fits, are shown in Figure 2.5a. The kinetic parameters *k* and *K*, shown in Table 2.2, were calculated by equation 2.1 using non-linear least-squares regression. Table 2.2 shows that neither *k* nor *K* differed significantly, considering 95% confidence intervals, for pH 9.0 versus 10.2. Despite the lack of a statistically significant difference in values of *k* and *K*, however, Figure 2.5a shows higher initial rates of NH_4^+/NH_3 photocatalytic oxidation at pH 10.2 versus 9.0 for every initial concentration of NH_4^+/NH_3, indicating a difference in reactivity at the two initial pH values. The greater initial rates at pH 10.2 versus 9.0 indicate that adsorption due to electrostatic attraction between NH_4^+ and the negatively charged TiO_2 surface is not sufficient to explain the pH dependence of NH_4^+/NH_3 photocatalytic oxidation rates, since the fraction of total NH_3 in the cation form is higher at pH 9.0 (67%) than at 10.2 (11%), and the TiO_2 surface is predominantly negative at both pH values.

Table 2.2. Initial rate constants (k) and photoadsorption equilibrium constants (K) for the Langmuir–Hinshelwood model[a]

Compound	Initial pH	k (M /min)	K (M^{-1})
[b]$[NH_3]_{T,0}$	~9.0 (8.9-9.3)[d]	$(1.64 \pm 0.70) \times 10^{-6}$	$(2.8 \pm 2.8) \times 10^{3}$
	~10.2 (9.9-10.3)	$(2.6 \pm 1.5) \times 10^{-6}$	$(2.3 \pm 2.8) \times 10^{3}$
[c]$[NH_3]_0$	(8.9-10.3)	$(2.34 \pm 0.79) \times 10^{-6}$	$(3.2 \pm 2.3) \times 10^{3}$
$[NO_2^-]_0$	~5.8 (5.7-5.9)	$(4.81 \pm 0.42) \times 10^{-6}$	$(6.8 \pm 4.0) \times 10^{4}$
	~8.6 (8.5-8.7)	$(4.52 \pm 0.48) \times 10^{-6}$	$(4.3 \pm 2.6) \times 10^{4}$
	~10.0 (9.9-10.1)	$(1.76 \pm 0.14) \times 10^{-6}$	$(3.0 \pm 1.3) \times 10^{4}$
	~11.0 (10.9-11.1)	$(1.67 \pm 0.21) \times 10^{-6}$	$(3.2 \pm 2.2) \times 10^{4}$

[a]Uncertainties are 95% confidence intervals. [b]$[NH_3]_{T,0} = [NH_4^+]_0 + [NH_3]_0$.
[c] $[NH_3]_0$ was calculated from $[NH_3]_{T,0}$ and pH was used to calculate the rate constant and the photoadsorption equilibrium constant. [d]Reported pH values in the second column are the median pH values; the values in the parenthesis represent the ranges of the initial pH values.



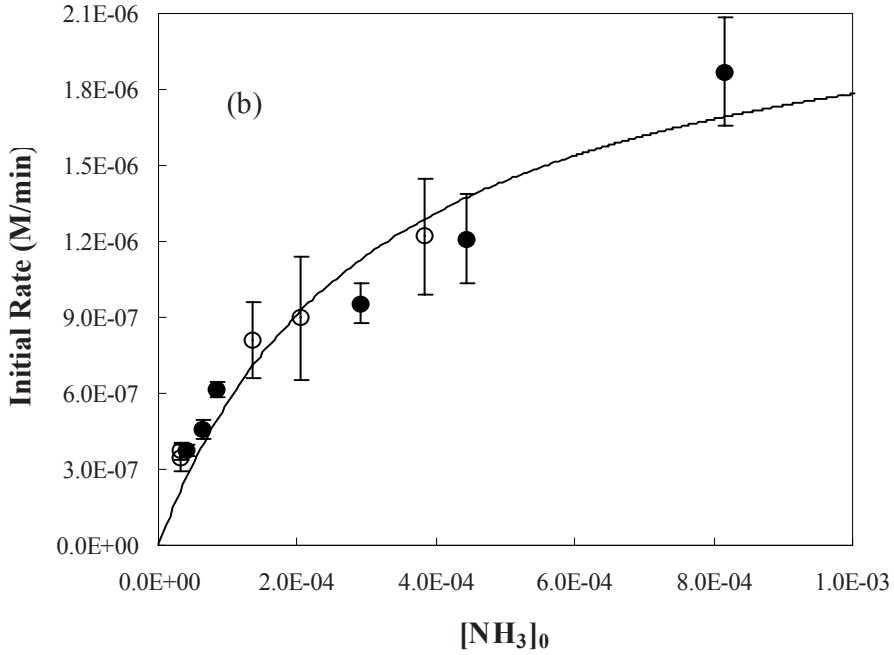


Figure 2.5[*]. Initial rate of NH_4^+/NH_3 photocatalytic oxidation versus (a) $[NH_3]_{T,0}$ at pH ~9 (○), and pH ~10.2 (●), and (b) $[NH_3]_0$. $[NH_3]_0 = K_a \times [NH_3]_{T,0} / ([H^+] + K_a)$. $[NH_3]_{T,0}$ was measured by the ammonia gas-sensing electrode, $pK_a = 9.3$ (Stumm and Morgan 1996); TiO_2: 3 g/L; $[NH_3]_{T,0}$: 4.4×10^{-5} to 9.2×10^{-4} M; error bars are 95% confidence intervals; lines are the Langmuir-Hinshelwood model fits.

[*] Sunny R. Castleberry measured initial rates of NH_4^+/NH_3 degradation at pH 9.0 and 10.2.

Previous researchers (Pagsberg, 1972; Neta et al., 1978) have studied the reaction between neutral NH_3 and ·OH and found a rate constant of 1×10^8 M^{-1} s^{-1}, while the reaction between NH_4^+ and ·OH was too slow to measure. Hence, the greater reactivity of electrophilic ·OH with neutral NH_3 versus NH_4^+ (Ogata et al., 1981; Kuo et al., 1997) may explain the higher initial rates at pH 10.2 versus 9.0.

To get further insight into the pH dependence of the reaction rate, all data shown in Figure 2.5a were reanalyzed and initial rates of photocatalytic oxidation versus initial concentrations of neutral NH_3, i.e., $[NH_3]_0$, not $[NH_3]_{T,0}$, were plotted (Figure 2.5b). Values of $[NH_3]_0$ were calculated as described in the caption to Figure 2.5. When treated this way, the pH 9.0 and 10.2 data converged and could be fit to the Langmuir-Hinshelwood model as a single data series (the calculated *k* and *K* values are reported in Table 2), which is evidence that the initial rates of NH_4^+/NH_3 TiO_2 photocatalytic oxidation are proportional to $[NH_3]_0$, and not $[NH_3]_{T,0}$. This shows again that the extent of adsorption of cationic NH_4^+ to the negatively charged TiO_2 surface does not appear to influence rates of NH_4^+/NH_3 photocatalytic oxidation.

2.3.3. Influence of pH on NO_2^- photocatalytic oxidation

Next, we studied how pH affects the second step in reaction 2.2, i.e., the photocatalytic oxidation of NO_2^-, though this is not the rate-limiting step in NH_4^+/NH_3 photocatalytic oxidation to NO_3^-. We measured the initial rate of photocatalytic oxidation of 1.8 (± 0.2) $\times$ 10^{-4} M NO_2^- over a range of pH values. Figure 2.6 shows that the pH values where the lowest initial rates of NO_2^- photocatalytic oxidation were observed (i.e., pH 10.1-11.0) corresponded to the pH values with the highest initial rates

of NH_4^+/NH_3 photocatalytic oxidation (Figure 2.5a). This is consistent with the fact discussed earlier that the pseudo first order rate constant for NO_2^- photocatalytic oxidation, k_2, was significantly greater than that for NH_4^+/NH_3 photocatalytic oxidation, k_1. Even at higher pH values, the initial rate of NO_2^- photocatalytic oxidation was still an order of magnitude higher than that of NH_4^+/NH_3. Thus we identified no conditions, in the presence of excess TiO_2, where photocatalytic oxidation of NO_2^- to NO_3^- would limit the overall rate of NH_4^+/NH_3 oxidation to NO_3^-.

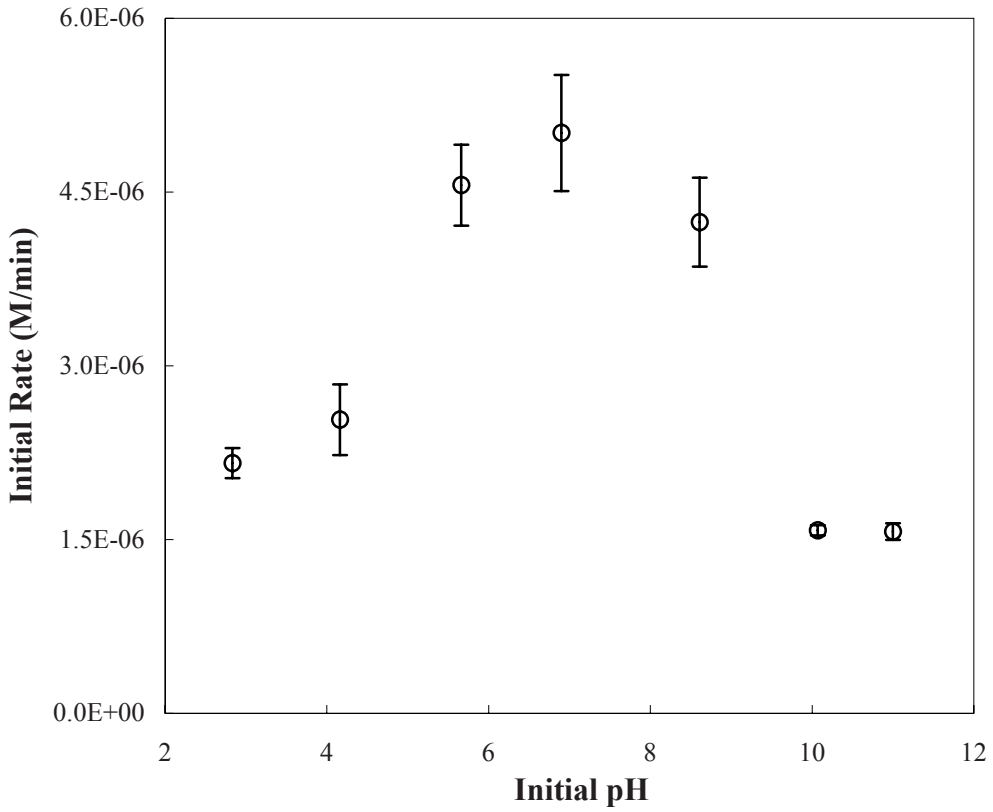


Figure 2.6. (a) Initial rate of NO_2^- photocatalytic oxidation versus initial pH; $[NO_2^-]_0$: $(1.8 \pm 0.2) \times 10^{-4}$ M; TiO_2: 3 g/L; uncertainties are 95% confidence intervals. pH values (from left to right) are 2.8, 4.2, 5.7, 6.9, 8.6, 10.1, and 11.0.

To assess the possible contribution of homogeneous photochemical oxidation of NO_2^- to the initial rates illustrated in Figure 2.6, two experiments were carried out with no TiO_2, but with UV light, at pH 5.8 and 9.9 and an initial NO_2^- concentration of 2.0×10^{-4} M. While no significant homogeneous photochemical oxidation of NO_2^- was observed at pH 9.9, there was considerable homogeneous photochemical oxidation at pH 5.8, with an initial rate of $(1.37 \pm 0.14) \times 10^{-6}$ M/min. As discussed earlier (discussion of Figure 2.2 and Table 2.1), however, we concluded that homogeneous photochemical oxidation of NH_4^+/NH_3 was not significant at TiO_2 concentrations ≥ 1 g/L due to absorbance and scattering of UV light by the TiO_2 particles. By the same reasoning, it is unlikely that homogeneous photochemical oxidation of NO_2^- significantly contributed to the initial rates of NO_2^- oxidation illustrated in Figure 2.6, since all experiments in this Figure were done with 3 g/L TiO_2. We also considered the possibility that non-photochemical oxidation of NO_2^- to NO_3^- by dissolved O_2 was partly responsible for the initial rates illustrated in Figure 2.6, since NO_2^- is susceptible to oxidation by O_2 in acidic solution (Staehelin and Hoigné, 1982; Braida and Ong, 2000). However, only a very slow dark NO_2^- oxidation rate of approximately 1.6×10^{-8} M/min at pH 2.8 was observed in our experiments, indicating that the rate of dark oxidation of NO_2^- by O_2 is not significant compared to the rate of oxidation by TiO_2 photocatalysis.

Figure 2.6 shows first an increase, then a decrease in initial rates over the pH range 2.8 – 11.0. Several processes likely contribute to this trend. We first considered that coagulation and flocculation of the TiO_2 particles as a function of pH could explain the variation in initial rates with pH. This explanation was not consistent with our data,

however. At pH values near the pH_{pzc} where the net TiO_2 surface charge is neutral, the extent of coagulation would be the largest, which would result in decreased surface area due to flocculation and would slow the surface reaction rate (Letterman, 1999). O'Shea et al. (1999) observed the greatest flocculation rate at pH values near the TiO_2 pH_{pzc} in the presence of sodium sulfate (the same electrolyte used in our experiments). However, as shown in Figure 2.6, we measured the highest initial rates of NO_2^- photocatalytic oxidation near the TiO_2 pH_{pzc} (6.2 – 7.5 (Hoffmann et al., 1995; Fernandez-Nieves et al., 1998)), indicating that the effect of coagulation/flocculation on reaction rates was not significant compared to the effect of other parameters such as pH.

We considered several explanations for the increase in rates of NO_2^- phtotcatalytic oxidation between pH 2.8 and 5.7, and especially between pH 4.2 and 5.7. First, adsorption of negatively charged NO_2^- to the TiO_2 surface (which would be positively charged below the TiO_2 pH_{pzc}) would increase at pH values above the HNO_2 pK_a. HNO_2 has a pK_a of 3.23 (calculated from the standard Gibbs energy change for the acid dissociation reaction at 25 ^oC using data from reference (Stumm and Morgan, 1996)), so if the extent of NO_2^- adsorption were solely responsible for the pH dependence of the initial rate, then a significant increase in initial rate would be expected above pH 3.23, which we did not observe (Figure 2.6). This indicates that the extent of adsorption is not the sole factor influencing initial rates of NO_2^- oxidation in this pH region.

It is possible that the equilibrium distribution between another acid/conjugate base pair, for example $HO_2\cdot$ and $O_2^{-}\cdot$, could be responsible for the increase in initial rates between 4.2 and 5.7. At pH values higher than the $HO_2\cdot$ pK_a of 4.8 (Bielski et al., 1985),

$O_2^{-}\cdot$ could serve as an additional source of ·OH (Litter, 1999; Pirkanniemi and Sillanpää, 2002).

The decline in initial rates shown in Figure 2.6 as the initial pH was increased from pH 6.9 to 10.1 could be at least partly due to the decreasing extent of adsorption of NO_2^- to the TiO_2 surface due to the increasingly negative surface charge. Consistent with this hypothesis, previous studies (Fernandez-Nieves et al., 1998; Bourikas et al., 2003) showed that the TiO_2 surface charge or zeta potential became more negative when the pH increased from 8 to 10. Bravo et al. (1993) proposed that at strongly basic pH values, competition for surface sites by OH^- inhibits adsorption of other species such as NO_2^-, which might explain the essentially constant initial rate between pH 10.1 and 11.0.

To test whether the decline in initial rates of NO_2^- photocatalytic oxidation above pH 6.9 was due solely to decreasing NO_2^- adsorption to the TiO_2 surface, initial rates were measured for a range of initial NO_2^- concentrations at four different initial pH values ranging from ~5.8 to ~11.0, and the data were fit to the Langmuir-Hinshelwood model. The results are shown in Figure 2.7, and the values of *k* and *K* were calculated from equation 1 and are summarized in Table 2.2.

Table 2.2 shows that the photoadsorption equilibrium constant *K* declined as the pH increased from 5.8 to 10.0, then remained approximately constant between pH 10.0 and 11.0, which is consistent with the idea that the extent of NO_2^- adsorption decreased with increasing pH above the TiO_2 pH_{pzc}. In addition, the values of *K* for photocatalytic oxidation of NO_2^- were all at least one order of magnitude higher than those for NH_4^+/NH_3, indicating that NO_2^- has a higher photoadsorption affinity to the TiO_2 surface than does NH_4^+/NH_3. This supports the finding discussed earlier that, at least in

alkaline solution, NO_2^- photocatalytic oxidation is more surface area dependent than is NH_4^+/NH_3.

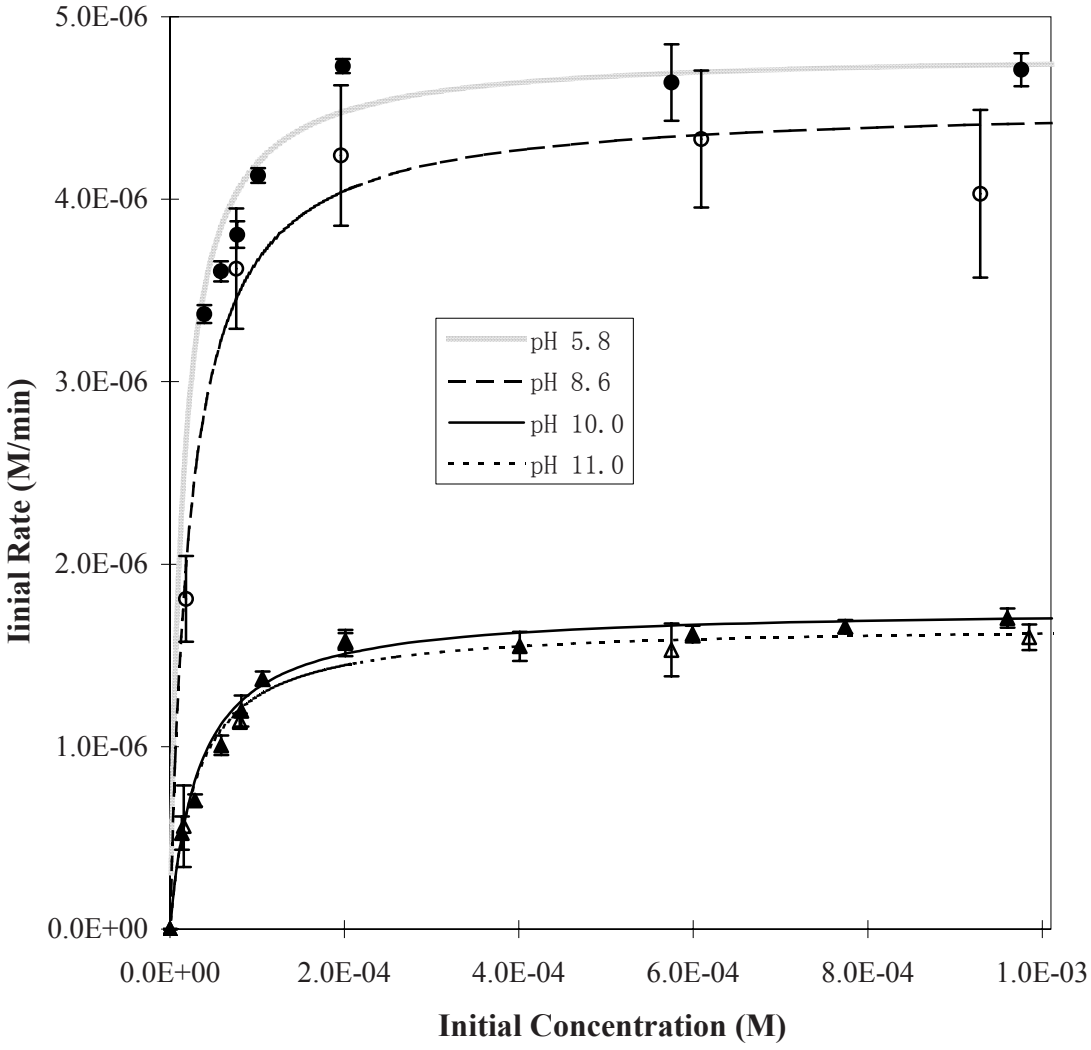


Figure 2.7. Initial rate of NO_2^- photocatalytic oxidation versus initial concentration at different initial pH values, the symbols represent the initial rates at different pH, pH ~5.8 (●), pH ~8.6 (○), pH ~10.0 (▲), pH ~11.0 (Δ); $[NO_2^-]_0$: $1.37 \times 10^{-5} – 9.85 \times 10^{-4}$ M; error bars are 95% confidence intervals; lines are the Langmuir-Hinshelwood model fits.

The Langmuir-Hinshelwood rate constant *k*, also decreased significantly between pH 5.8 and 11.0, especially between pH 8.6 and 10.0, indicating that decreasing adsorption alone cannot entirely explain the decline in NO_2^- photocatalytic oxidation rates between pH 5.8 and 11.0, and that one or more kinetic factors are also involved. O'Shea and Cardona (O'Shea and Cardona, 1995) also observed that the Langmuir-Hinshelwood parameters were dependent on the solution pH during phenol photocatlaytic oxidation. They explained the results by the involvement of unprotonated ·OH, $\cdot O^-$, at pH values greater than 12, which was outside the pH range that we studied.

For our experimental system, we considered several possibilities to explain the decrease in *k* values between pH 5.8 and 11. These explanations assume that the rate constant *k* is the sum of two or more rate constants for independent processes involved in NO_2^- photocatalytic oxidation, where at least one of the processes is pH-dependent. We first speculated that ·OH formation from H_2O_2 might be an important source of ·OH below the H_2O_2 pK_a, but not above the pK_a, where H_2O_2 would undergo acid dissociation:

$$H_2O_2 \leftrightarrow HO_2^- + H^+ \qquad (2.3)$$

The pK_a of H_2O_2, however, is 11.6 (Staehelin and Hoigné, 1982), so its concentration would not decline significantly due to acid dissociation below pH 10.0, and this equilibrium cannot explain our pH trend in *k* values. Second, we considered that an increase in the concentration of carbonate, CO_3^{2-}, a known ·OH scavenger (Larson and

Zepp, 1988), at pH values near the HCO_3^- pK_a (10.3, (Stumm and Morgan, 1996)), could decrease the concentration of reactive ·OH and thereby decrease the apparent rate constant, *k*. However, we measured a negligible concentration of CO_3^{2-} in our system by alkalinity titration at pH 10.4, so ·OH scavenging by CO_3^{2-} cannot explain the decrease in the *k* values with increasing pH.

Our best explanation for the decrease in *k* values above pH 6.9 is the formation of one or more acid/conjugate base pairs during NO_2^- photocatalytic oxidation, where the conjugate base acts as an ·OH scavenger, or otherwise slows the forward reaction of NO_2^- to NO_3^- since photoreduction of NO_3^- to NO_2^- occurs even in the absence of TiO_2 (Daniels et al., 1968; Alif and Boule, 1991; Mack and Bolton, 1999). Changing the pH around this pK_a could in this way affect the rate constant *k* for NO_2^- photocatalytic oxidation. Peroxynitrate ($^-OONO_2$), the conjugate base of peroxynitric acid ($HOONO_2$, pK_a 6.0 (Goldstein et al., 1998)) and peroxynitrite (^-OONO), the conjugate base of peroxynitrous acid (HOONO, pK_a 6.5 (Løgager and Sehested, 1993)), are formed in the photoreduction of NO_3^- (Daniels et al., 1968; Alif and Boule, 1991; Mark et al., 1996; Sharpless and Linden, 2001) and are possible intermediates in our system. Peroxynitrite, ^-OONO, can scavenge ·OH and also lead to formation of NO_2^- (Sharpless and Linden, 2001) both of which would decrease the apparent rate constant *k* for the forward reaction of NO_2^- to NO_3^-. Similarly, peroxynitrate, $^-OONO_2$, could have the same effect of decreasing the apparent rate constant *k* for the forward reaction of NO_2^- to NO_3^-. Further evidence is required to support or refute the involvement of any intermediates discussed in this paragraph.

2.4. Conclusions

This research provides theoretical results that could serve as a guide for an effective design of NH_4^+/NH_3 removal in water and wastewater treatment systems. Efforts to optimize rates of NH_4^+/NH_3 photocatalytic oxidation should focus on pH control to increase the fraction of total NH_4^+/NH_3 in the form of NH_3 and should provide sufficient TiO_2 for complete oxidation of NO_2^- and NO_3^-. If followed by a treatment process such as ion exchange for NO_3^- removal, TiO_2 photocatalytic oxidation of NH_4^+/NH_3 could be an alternative to biological nitrification for specialized applications such as water recycling on long-term space missions, small-scale water treatment systems, and temporary wastewater treatment systems used in disaster relief.

CHAPTER 3*

Effect of Inorganic Anions on the Titanium Dioxide-Based Photocatalytic Oxidation of Aqueous Ammonia and Nitrite

3.1. Introduction

Inorganic anions, such as chloride (Cl^-), sulfate (SO_4^{2-}), phosphate ($H_2PO_4^-$/HPO_4^{2-}), and bicarbonate/carbonate (HCO_3^-/CO_3^{2-}), are commonly present in wastewater with concentrations up to 1.5×10^{-3} M (Tchobanoglous et al., 2003). Many researchers have investigated the effects of inorganic anions on titanium dioxide (TiO_2)-based photocatalytic degradation of organic compounds (Abdullah et al., 1990; Chen et al., 1997; Wang et al., 1999; Calza and Pelizzetti, 2001; Xia et al., 2002; Sökmen and Özkan, 2002; Hu et al., 2003, 2004; Özkan et al., 2004; Zhang et al., 2005). To the best of our knowledge, only Chen and Cao (2002) have studied the effect of Cl^-, SO_4^{2-} and NO_3^- on NO_2^- photocatalytic oxidation using TiO_2 supported on hollow glass microbeads at pH 5. However, no systematic study has been done on the effect of inorganic anions on the TiO_2–based photocatalytic oxidation of both NH_4^+/NH_3 and NO_2^- as a function of pH. Accordingly, to effectively remove NH_4^+/NH_3 and NO_2^- from water and wastewater, it is critical to study whether inorganic anions could influence their photocatalytic oxidation. In this research, we investigated the effects of Cl^-, SO_4^{2-},

* This chapter reprinted from "Journal of Photochemistry and Photobiology A: Chemistry 185, Zhu, X. D.; Nanny, M. A.; Butler, E. C. Effect of inorganic anions on the titanium dioxide-based photocatalytic oxidation of aqueous ammonia and nitrite, 289-294, 2007, Copyright (2007), with permission from Elsevier".

$H_2PO_4^-/HPO_4^{2-}$, and HCO_3^-/CO_3^{2-} on NH_4^+/NH_3 and NO_2^- photocatalytic oxidation in TiO_2 suspensions for the pH range of 4-11.

Previous studies have shown that inorganic anions can scavenge ·OH to form the corresponding anion radicals (Jayson et al., 1973; Neta et al., 1988; Kochany and Lipczynska-Kochany, 1992; Wu et al., 2002; Brusa and Grela, 2003). An example of ·OH scavenging by CO_3^{2-} to form the carbonate radical ($CO_3\cdot^-$) (Neta et al., 1988) is shown below:

$$CO_3^{2-} + \cdot OH \rightarrow OH^- + CO_3\cdot^- \qquad (3.1)$$

Hydroxyl radical scavenging by the anions Cl^-, SO_4^{2-}, and $H_2PO_4^-/HPO_4^{2-}$ as well as formation of the corresponding anion radicals ($HOCl\cdot^-$, $SO_4\cdot^-$, $H_2PO_4\cdot/HPO_4\cdot^-$) have also been shown in aqueous solutions (Neta et al., 1988). Hydroxyl radical scavenging of the anions Cl^-, HCO_3^-/CO_3^{2-}, SO_4^{2-}, and $H_2PO_4^-/HPO_4^{2-}$ may influence the photocatalytic oxidation of organic compounds (Wang et al., 1999; Hu et al., 2003, 2004; Zhang et al., 2005; Liao et al., 2001) by destroying the reactive species ·OH. The corresponding anion radicals can themselves oxidize organic and inorganic compounds at different rates (Neta et al., 1988; Paruthamuthu and Neta, 1978; Neta et al., 1978), which can also influence overall rates of photocatalytic oxidation.

Previous researchers (Abdullah et al., 1990; Chen et al., 1997; Wang et al., 1999; Calza and Pelizzetti, 2001; Xia et al., 2002; Zhang et al., 2005) have proposed that competitive adsorption of the inorganic anions for active sites on the TiO_2 surface may also influence the photocatalytic degradation of organic compounds. For example, 0.01 M Cl^- was found to decrease the degradation rate of 2-chlorophenol and 2-nitrophenol at pH values lower than the TiO_2 point of zero charge (pH_{pzc}) (6.2-7.5 for

Degussa TiO_2 P 25 (Fernández-Nieves et al., 1998; Kosmulski, 2004)), while Cl^- had no inhibitory effect at pH values greater than the pH_{pzc} due to negligible adsorption to the negatively charged TiO_2 surface (Wang et al., 1999). Similarly, SO_4^{2-} and $H_2PO_4^-$ decreased the rate of photocatalytic degradation of ethanol, salicylic acid, and aniline at pH 4.1, which was attributed to electrostatic adsorption of these anions to the TiO_2 surface (Abdullah et al., 1990). Decreased photocatalytic oxidation rates of an azo dye at neutral pH in the presence of $H_2PO_4^-/HPO_4^{2-}$ were also observed (Hu et al., 2004). This was possibly because of specific (i.e., non-electrostatic) adsorption of $H_2PO_4^-/HPO_4^{2-}$ to the TiO_2 surface (Connor and McQuillan, 1999, Chen et al., 2003).

In this research, we hypothesized that inorganic anions would influence rates of NH_4^+/NH_3 and NO_2^- photocatalytic oxidation in one of the following ways: (i) ·OH scavenging by inorganic anions, (ii) direct oxidation of NH_4^+/NH_3 and NO_2^- by anion radicals, or (iii) adsorption of inorganic anions to the TiO_2 surface. We studied the photocatalytic oxidation of NH_4^+/NH_3 and NO_2^- as a function of pH with the four inorganic anions (Cl^-, SO_4^{2-}, $HPO_4^{2-}/H_2PO_4^-$, and HCO_3^-/CO_3^{2-}) that are commonly present in water and wastewater. Since ·OH can be generated by UV illumination of H_2O_2 (Chu, 2001), we used UV-illuminated H_2O_2 to study ·OH scavenging by inorganic anions and direct oxidation of NH_4^+/NH_3 and NO_2^- by anion radicals. Adsorption experiments were also conducted to measure the extent of adsorption of the different anions to the TiO_2 surface.

3.2. Materials and Methods

3.2.1. Chemicals

Degussa TiO_2 P 25 (Akron, OH) was used without purification unless specifically mentioned. This catalyst had a BET surface area of 50 ± 15 m^2/g and an average primary particle size of 21 nm (Degussa Corporation). Nanopure water (18.1 $M\Omega \cdot cm$) from an Infinity^{TM} ultrapure water system (model D8961, Barnstead; Dubuque, IA) was used to prepare solutions in this study. The chemicals $NaNO_2$, $NaNO_3$ (Sigma-Aldrich; Milwaukee, WI), NH_4Cl, $(NH_4)_2SO_4$ (Alfa Aesar, Ward Hill, MA), $(NH_4)_2CO_3$, and $(NH_4)_2HPO_4$ (Fisher Scientific, Fairlawn, NJ) were used as NO_2^-, NO_3^-, and NH_4^+/NH_3 sources. Sodium salts [Na_2SO_4, NaCl (Alfa Aesar), Na_2HPO_4/NaH_2PO_4 (Aldrich), and $NaHCO_3/Na_2CO_3$ (Fisher Scientific)] were used as inorganic anion sources. Thirty percent H_2O_2 (Fisher Scientific) was used for the homogeneous photochemical oxidation of NH_4^+/NH_3 and NO_2^-.

3.2.2. Photocatalytic Oxidation Experiments

The photochemical reactor (model 7840-185, Ace Glass, Vineland, NJ) consisted of three major components: a cylindrical Pyrex glass reactor, a double-walled quartz cooling water jacket, and a 450 W medium pressure Hg lamp. The cooling water jacket was inserted into the reactor, and the UV lamp was then placed inside the quartz cooling jacket. More details about the experimental apparatus have been reported in chapter 2. Our previous study showed that when 3 g/L TiO_2 was used there was no significant homogeneous photochemical reaction of NH_4^+/NH_3, because the high concentration of TiO_2 blocked UV transmittance to the interior portions of the reactor

(chapter 2). Therefore, to accurately evaluate photocatalytic oxidation of NH_4^+/NH_3 and NO_2^- in the presence of inorganic anions, 3 g/L TiO_2 was used in this study, except for homogeneous photochemical reactions where H_2O_2 and not TiO_2 was used as the ·OH source. The reaction solution was stirred with a magnetic stirrer to maintain a homogeneous TiO_2 suspension. Samples were taken during kinetic studies and filtered through 0.1 μm filter membranes, and the filtrates were used for measurement of pH, NH_4^+/NH_3, NO_2^-, and NO_3^-.

3.2.3. Adsorption Experiments

Since the commercial Degussa TiO_2 P 25 contains ≤ 0.3% Cl^- by weight (Degussa Website) and we measured 0.95 mg dissolved Cl^-/g TiO_2 as an impurity, the TiO_2 was washed with nanopure water until the aqueous concentration of Cl^- was lower than the detection limit of the ion chromatograph (1×10^{-6} M). No significant difference in the initial rate of NO_2^- photocatalytic oxidation at pH ~10 in the presence of 1×10^{-3} M Na_2SO_4 between the washed and unwashed TiO_2 was observed. In addition, the extent of adsorption to the washed and unwashed TiO_2 was the same when $H_2PO_4^-/HPO_4^{2-}$ and SO_4^{2-} were used as the adsorbates. These experiments show that neither the Cl^- impurity nor the washing treatment affected the TiO_2 reactivity or adsorption behavior.

Sodium perchlorate ($NaClO_4$, 0.01 M) was used as an inert electrolyte for adsorption experiments to maintain a constant ionic strength. To obtain a range of anion adsorption densities on the TiO_2 (3 g/L) surface over the pH range of 3-11, 2×10^{-4} M was chosen as the initial concentration of Na_2SO_4, NaH_2PO_4, or NaCl.

Adsorption of HCO_3^-/CO_3^{2-} to the TiO_2 surface in acidic solutions was not measured because HCO_3^- would be protonated to form dissolved CO_2 and carbonic acid under these conditions. Adsorption of HCO_3^-/CO_3^{2-} to the TiO_2 surface also was not measured in alkaline solutions due to interference by desorption of CO_2 from the Degussa TiO_2 P 25, as determined by a Shimadzu Total Organic Carbon Analyzer (TOC 5050A/ASI 5000A). At neutral pH, however, no significant adsorption of HCO_3^- was observed by measuring the inorganic carbon in the equilibrated aqueous solution using the TOC 5050A/ASI 5000A, and adsorption would likely be even lower in alkaline solutions, due to the increased negative charge of the TiO_2 surface at higher pH values.

The suspensions were adjusted to the target pH values using 1 M $HClO_4$ or NaOH and shaken for 24 hours in a constant temperature chamber (Sheldon Manufacturing, Model 2020, Cornelius, OR) at 25 ºC. The equilibrated suspensions were then filtered through the 0.1 μm membranes, and the filtrates were used for measurement of Cl^-, SO_4^{2-}, $H_2PO_4^-/HPO_4^{2-}$, and HCO_3^-. The percent adsorbed for each anion was calculated by dividing the adsorbed concentration of the anion by its total concentration.

3.2.4. Analytical Methods

The concentrations of NO_2^-, NO_3^-, Cl^-, SO_4^{2-}, and $H_2PO_4^-/HPO_4^{2-}$ were determined using a Dionex ion chromatograph with an Ion Pac® AG 11 guard column (4 × 50 mm), an Ion Pac® AS 11 anion analytical column (4 × 250 mm), and an ED 50 conductivity detector, as described in chapter 2. An ammonia gas-sensing electrode (model 95-12, Thermo Orion; Beverly, MA) was used to determine the concentration of

NH_4^+/NH_3, and the measurement procedure is also reported in chapter 2. A pH electrode (91-56, Thermo Orion) was used for pH measurement.

Five-point external standard calibration curves were used to calculate the concentrations of NH_4^+/NH_3, NO_2^-, NO_3^-, Cl^-, HCO_3^-, SO_4^{2-}, and $H_2PO_4^-/HPO_4^{2-}$. The standard solutions were prepared daily, and analysis of the standards was repeated every 20 samples. To minimize the potentially confounding effect of variable pH during the reaction, the initial rate was calculated from the best linear fit of NH_4^+/NH_3 or NO_2^- concentration versus time for the time period where both the pH and slope were nearly constant, and the error bars in Figures 3.1 and 3.4 are 95% confidence intervals of the initial rates.

3.3. Results and Discussion

3.3.1. NH_4^+/NH_3 Photocatalytic Oxidation

To examine the effects of inorganic anions on NH_4^+/NH_3 photocatalytic oxidation, we chose pH values of ~9 (8.7-9.1) and ~10 (10.1-10.3), because the photocatalytic oxidation of NH_4^+/NH_3 is very slow or negligible at pH values lower than 9 (Pollema et al., 1999; Wang et al., 1994; Bonsen et al., 1997; chapter 2). In addition, pH ~11 (11.0-11.1) was chosen to separate the effects of HCO_3^- and CO_3^{2-} on NH_4^+/NH_3 photocatalytic oxidation, because the speciation of HCO_3^-/CO_3^{2-} is pH dependent with a pK_a value of 10.3 for HCO_3^- (Stumm and Morgan, 1996). The pH change we used was higher than the pH_{pzc} of the Degussa TiO_2 (6.2-7.5 (Hoffmann et al., 1995; Fernandez-Nieves et al., 1998)). For comparison, three control experiments (where no anions were added) were also conducted at pH ~9, ~10, and ~11. Figure 3.1

illustrates the initial rates of NH_4^+/NH_3 photocatalytic oxidation in the presence of inorganic anions, as well as the control experiments, at these pH values.

When no anions were added, the initial rate of NH_4^+/NH_3 photocatalytic oxidation was approximately 50% higher at pH ~10 compared to pH ~9, and the same trend was observed in the presence of Cl^- and SO_4^{2-} (Figure 3.1). This increase in rates with pH is consistent with the fact that at pH ~10 versus ~9 a greater fraction of NH_4^+/NH_3 is in the form of neutral NH_3, which is more reactive with electrophilic ·OH than is NH_4^+ (Ogata et al., 1981). Compared to the control experiments, SO_4^{2-}, Cl^-, and HCO_3^- yielded similar rates of NH_4^+/NH_3 photocatalytic oxidation at a given pH, while HPO_4^{2-} yielded a higher rate, and CO_3^{2-} yielded a lower rate (Figure 3.1). We first postulated that these differences were due to either (i) different rates of ·OH scavenging by Cl^-, SO_4^{2-}, HPO_4^{2-}, HCO_3^-/CO_3^{2-} (Buxton et al., 1988) and/or (ii) different rates of direct oxidation of NH_4^+/NH_3 by anion radicals.

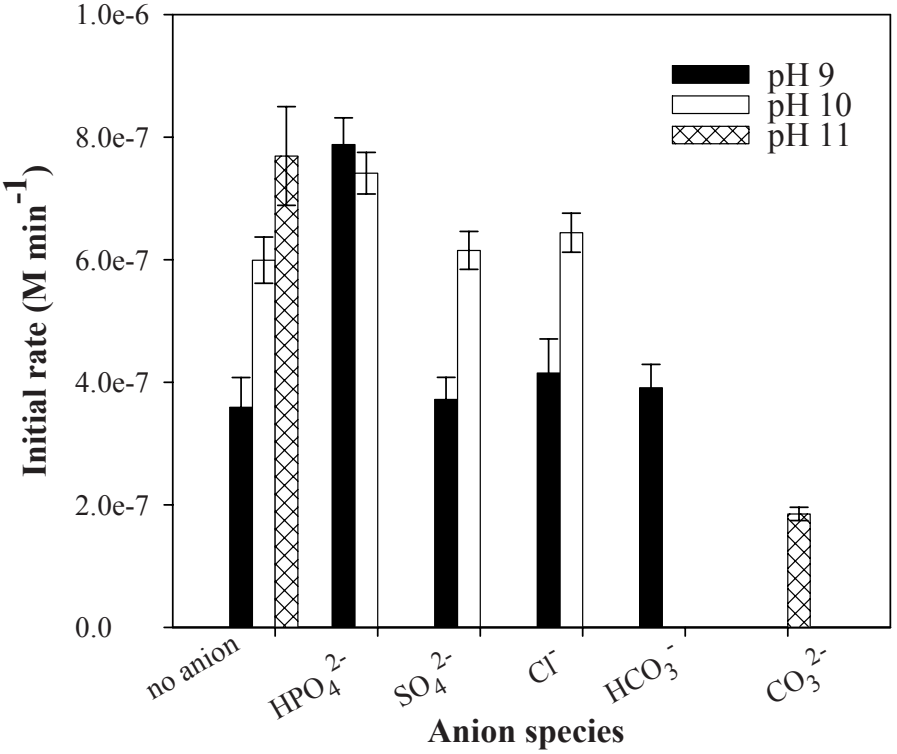


Figure 3.1. Effect of inorganic anions on NH_4^+/NH_3 photocatalytic oxidation at pH ~9 and ~10 (pH ~11 for CO_3^{2-}). $[NH_4^+/NH_3]$: $(9.6 \pm 0.6) \times 10^{-5}$ M; [anion]: 1×10^{-3} M; $[TiO_2]$: 3 g/L; error bars are 95% confidence intervals.

3.3.1.1. Role of ·OH scavenging by anions and/or direct oxidation by anion radicals

To determine whether ·OH scavenging and/or direct oxidation by anion radicals were responsible for rate differences between the different anions, we performed NH_4^+/NH_3 oxidation experiments with UV-illuminated H_2O_2 (UV/H_2O_2) in the presence of Cl^-, SO_4^{2-}, HPO_4^{2-}, and HCO_3^-/CO_3^{2-} at pH ~10, and CO_3^{2-} at pH ~11. In this system, H_2O_2 generates ·OH under UV irradiation (Chu, 2001), which can be scavenged by anions in the solution to form the corresponding anion radicals (e.g., reaction 3.1). A Vycor filter (ACE glass) was used to block wavelengths lower than 220 nm to prevent

possible reactions of aqueous NH_3 with oxidants other than ·OH, including ozone generated from photodissociation of O_2 (Steinfeld et al., 1999). The results of these experiments are shown in Figure 3.2.

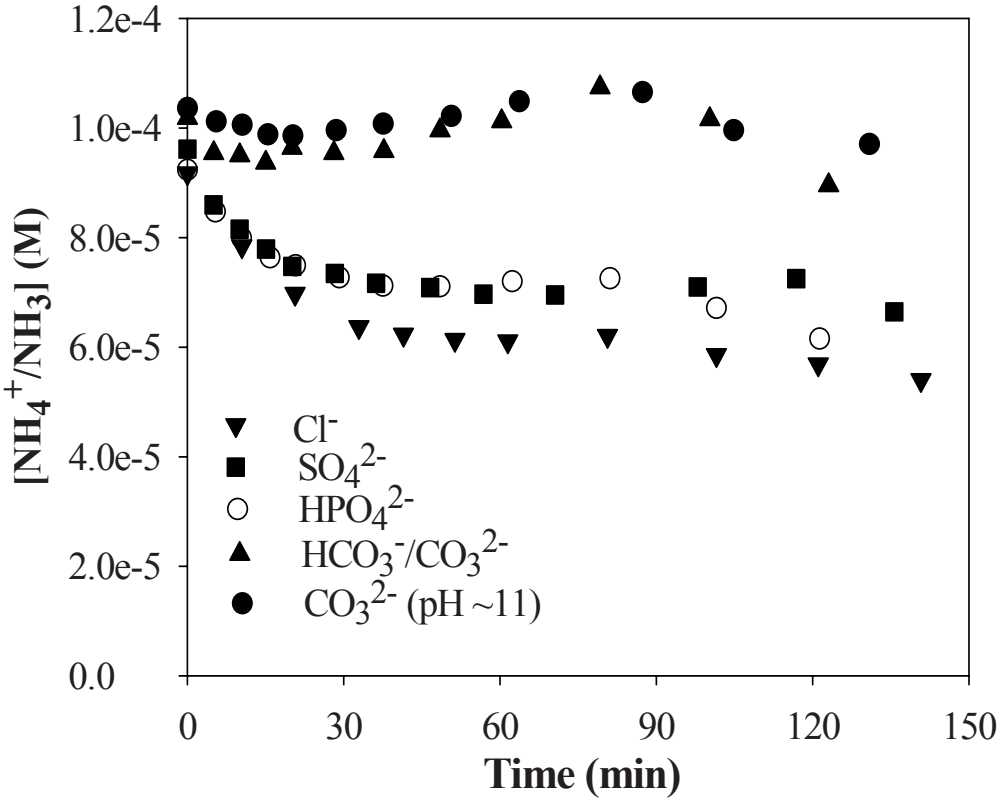


Figure 3.2. Effect of inorganic anions on the homogeneous photochemical oxidation of NH_4^+/NH_3 by UV/H_2O_2 with a Vycor filter at pH ~10, except for the data series labeled CO_3^{2-}, which was done at pH ~11. $[NH_4^+/NH_3]$: $(9.6 \pm 0.6) \times 10^{-5}$ M; $[H_2O_2]$ = 0.001 M; [anion]: 0.005 M.

There was no significant NH_4^+/NH_3 oxidation in the presence of either HCO_3^-/CO_3^{2-} (pH ~10) or CO_3^{2-} (pH ~11), but significant oxidation in the presence of Cl^-, SO_4^{2-}, and HPO_4^{2-} (Figure 3.2), which is evidence that CO_3^{2-} is a better ·OH scavenger than Cl^-, SO_4^{2-}, or HPO_4^{2-}. In the presence of CO_3^{2-} at pH ~11, the initial rate of the

TiO_2-based NH_4^+/NH_3 photocatalytic oxidation was about one third the rate when Cl^-, SO_4^{2-}, or HPO_4^{2-} was present at pH ~10 (Figure 3.1), which is additional evidence of efficient ·OH scavenging by CO_3^{2-} under these conditions. Since approximately 50% of HCO_3^-/CO_3^{2-} is in the form of CO_3^{2-} at pH ~10, our experiments do not provide information on the relative ·OH scavenging efficiency of CO_3^{2-} versus HCO_3^-. However, Buxton et al. (1988) reported that CO_3^{2-} scavenges ·OH more rapidly than HCO_3^- with second order rate constants of 3.9×10^8 M^{-1} s^{-1} for CO_3^{2-} and 8.5×10^6 M^{-1} s^{-1} for HCO_3^-. This can explain why we observed a smaller initial rate of NH_4^+/NH_3 photocatalytic oxidation at pH ~11 (when CO_3^{2-} was the predominant species) than at pH ~9 (when HCO_3^- was the predominant species) (Figure 3.1). As a practical matter, these results suggest that carbonate alkalinity can strongly affect the rates of NH_4^+/NH_3 photocatalytic oxidation at pH values where significant CO_3^{2-} is present.

Figure 3.2 also shows that there was no significant difference in initial rates of NH_4^+/NH_3 oxidation by UV/H_2O_2 in the presence of Cl^-, SO_4^{2-}, or HPO_4^{2-}, unlike the results from TiO_2-based NH_4^+/NH_3 photocatalytic oxidation (Figure 3.1), where HPO_4^{2-} led to faster rates than the other anions. This suggests that, unlike CO_3^{2-} and possibly HCO_3^-, ·OH scavenging by Cl^-, SO_4^{2-}, or HPO_4^{2-} or direct oxidation of NH_4^+/NH_3 by the corresponding anion radicals do not influence reaction rates in the TiO_2 photocatalytic system. If these processes did control reaction rates in the UV/TiO_2 system, we would expect the same trends in reactivity in both the UV/TiO_2 and the UV/H_2O_2 systems, which we did not observe. Based on this, we next examined whether adsorption of anions to the TiO_2 surface was responsible for the differences in TiO_2 photocatalytic oxidation rates when HPO_4^- versus SO_4^{2-}, Cl^-, or HCO_3^- was present (Figure 3.1).

3.3.1.2. Role of anion adsorption

The adsorption of $H_2PO_4^-/HPO_4^{2-}$, SO_4^{2-}, and Cl^- to the TiO_2 surface over the pH range of 3-11 is shown in Figure 3.3.

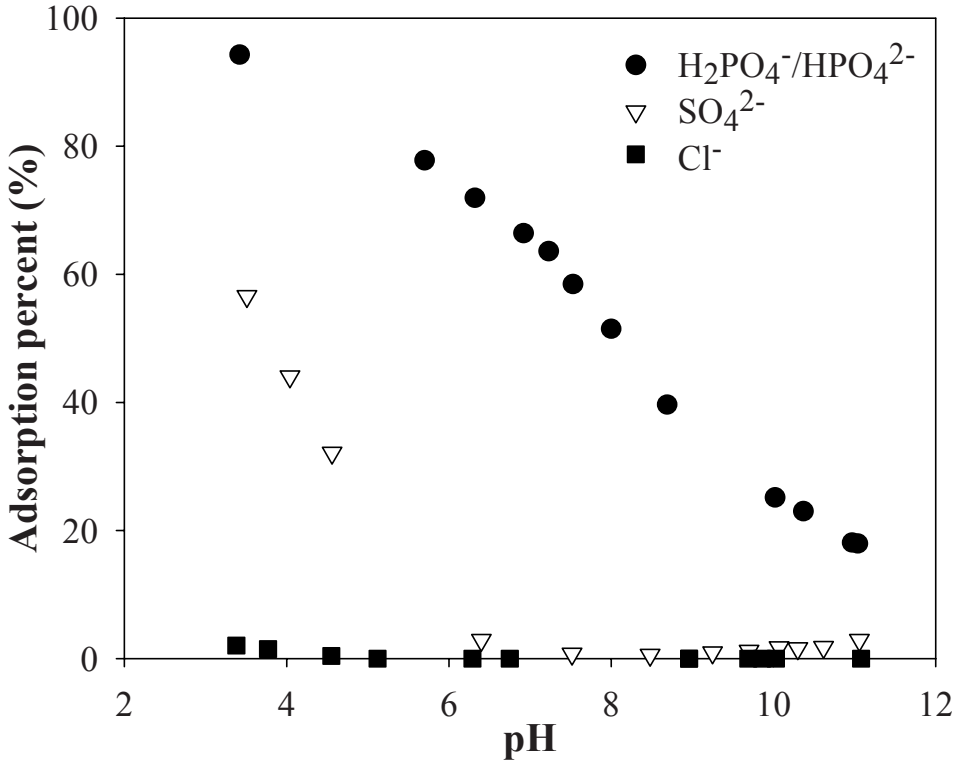


Figure 3.3. Adsorption of chloride (Cl^-), sulfate (SO_4^{2-}) and phosphate ($H_2PO_4^-/HPO_4^{2-}$). [anion]: 2×10^{-4} M; [$NaClO_4$]: 0.01 M; [TiO_2]: 3 g/L; adsorption equilibrium time: 24 hours. pH_{pzc} of the Degussa TiO_2 is 6.2-7.5 (Hoffmann et al., 1995; Fernández-Nieves et al., 1998).

There was significant adsorption of HPO_4^{2-}, but no significant adsorption of Cl^- and SO_4^{2-}, at pH ~9 and ~10. Based on this, as well as the greater rate of NH_4^+/NH_3 photocatalytic oxidation in the presence of HPO_4^{2-} versus Cl^-, SO_4^{2-}, and HCO_3^- (Figure 3.1), we concluded that adsorption of HPO_4^{2-} actually enhanced the initial rate of NH_4^+/NH_3 photocatalytic oxidation. This may be because adsorption of HPO_4^{2-}

increased the negative charge of the TiO_2 surface (Hingston et al., 1967), and this negative charge could transfer to the TiO_2 surface through some pathways, which might neutralize NH_4^+ to NH_3. This would result in a greater initial rate of NH_4^+/NH_3 photocatalytic oxidation, because NH_3 reacts more rapidly with ·OH than does NH_4^+ (Ogata et al., 1981). To make this process possible, the pK_a value of TiO_2 with adsorbed phosphate should be higher than that of NH_4^+ (9.3). However, to the best of our knowledge, there is no reported pK_a value for phosphate-adsorbed TiO_2 in the literature. Therefore, some further research is needed to find the pK_a value to support our speculation.

3.3.2. NO_2^- Photocatalytic Oxidation

Since NO_2^- is an important intermediate in the photocatalytic oxidation of NH_4^+/NH_3 (Wang et al., 1994; Takeda and Fujiwara, 1996; Bonsen et al., 1997; Pollema et al., 1999; Takeda and Fujiwara, 1996, chapter 2), we also studied how inorganic anions affected NO_2^- photocatalytic oxidation. For these experiments, we chose a broad pH range of 4-11 since the different phenomena that could affect reaction rates, such as adsorption, would likely vary significantly over this pH range. Note that we did not study NO_2^- photocatalytic oxidation in the presence of HCO_3^- at acidic pH (< 7.5), because HCO_3^- would be protonated to form dissolved CO_2 and carbonic acid under these conditions. The initial rate of NO_2^- photocatalytic oxidation was also measured when no anions were added (control experiment). Figure 3.4 shows the initial rates of NO_2^- photocatalytic oxidation in the presence of the anions, as well as the control experiment.

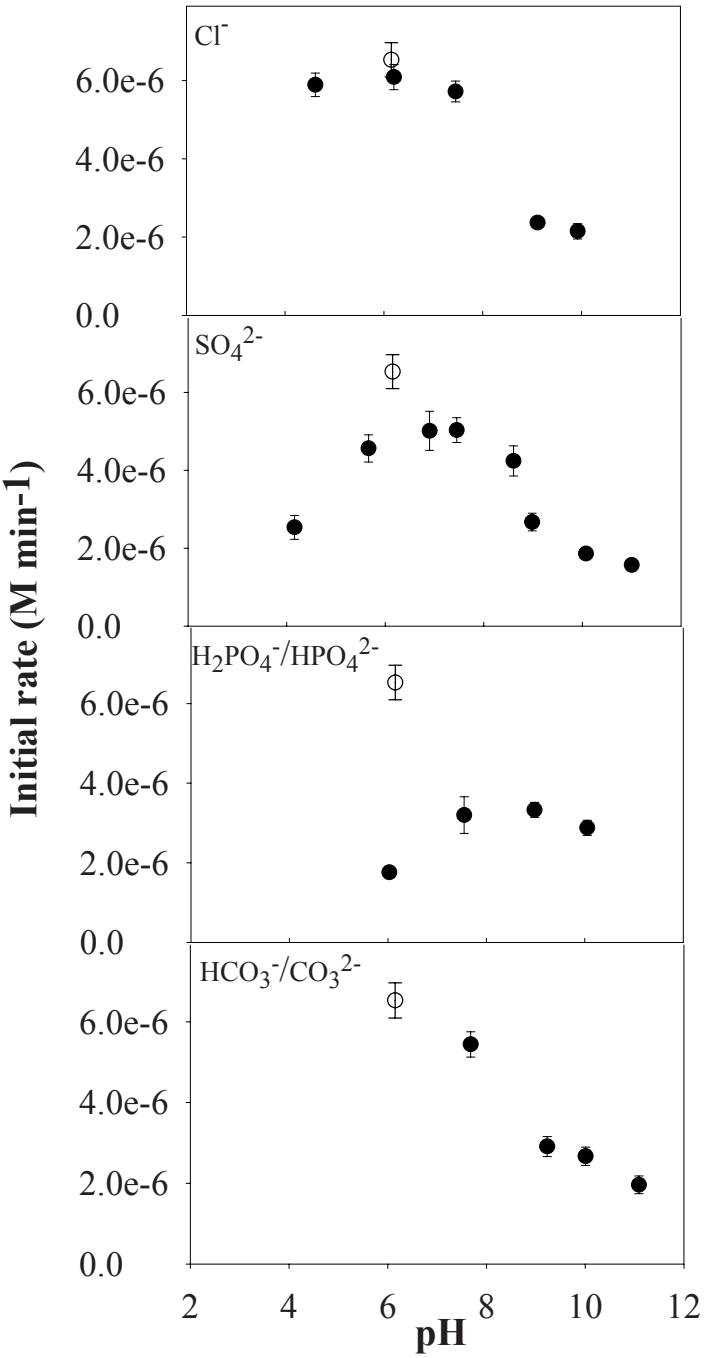


Figure 3.4. Effect of inorganic anions on NO_2^- photocatalytic oxidation between pH 4 and 11. $[NO_2^-]$: $(1.9 \pm 0.1) \times 10^{-4}$ M; [anion]: 1×10^{-3} M; $[TiO_2]$: 3 g/L; error bars are 95% confidence intervals. Some data for the SO_4^{2-} panel were previously reported in chapter 2. Open circles represent the initial rate of NO_2^- photocatalytic oxidation at pH ~ 6 when no anions were added.

A comparison of Figures 3.1 and 3.4 shows that NO_2^- photocatalytic oxidation occurs much faster than NH_4^+/NH_3 photocatalytic oxidation in the presence of common wastewater anions at pH ~9 and ~10 (the pH values below which no significant photocatalytic oxidation of NH_4^+/NH_3 is observed). Thus, photocatalytic oxidation of NH_4^+/NH_3 to NO_2^- is the rate-limiting step in the complete oxidation of NH_4^+/NH_3 to NO_3^- in the presence of these anions.

In alkaline solutions (pH > 7.5), the initial rates of NO_2^- photocatalytic oxidation decreased with increasing pH in the presence of all anions (Figure 3.4). This decrease in rate may be explained by decreasing adsorption of NO_2^- to the TiO_2 surface with increasing pH due to electrostatic repulsion (chapter 2) and/or the involvement of one or more acid-conjugate base pairs of possible intermediates, such as HOONO/$^-$OONO or $HOONO_2/^-OONO_2$, in which the conjugate base acts as a ·OH scavenger or otherwise slows the oxidation of NO_2^- to NO_3^- (chapter 2). Both phenomena could explain the uniform trend of decreasing reaction rates with increasing pH in this pH region.

Compared to the control experiment, SO_4^{2-} and $H_2PO_4^-$, but not Cl^-, inhibited NO_2^- photocatalytic oxidation at pH ~6. In addition, at low to neutral pH in the presence of SO_4^{2-} and $H_2PO_4^-/HPO_4^{2-}$, the initial rate of NO_2^- photocatalytic oxidation increased with increasing pH to a maximum at pH ~7.5 (Figure 3.4). However, nearly constant initial rates were observed for Cl^- in this pH range. All these phenomena are possibly due to different adsorption densities of the anions to the TiO_2 surface. Next we correlated the initial rates of NO_2^- photocatalytic oxidation with adsorption densities of anions at low to neutral pH values.

3.3.2.1. Role of anion adsorption

The negligible adsorption of Cl^- to the TiO_2 surface at low to neutral pH (Figure 3.3) is likely responsible for the nearly constant initial rates for Cl^- in this pH region (i.e., no rate increase with increasing pH). The decrease in adsorption densities of SO_4^{2-} and $H_2PO_4^-/HPO_4^{2-}$ on the TiO_2 surface with increasing pH up to pH ~7.5, as shown in Figure 3.3, can explain the increasing initial rates in the presence of these anions. At low to neutral pH values, greater adsorption of $H_2PO_4^-/HPO_4^{2-}$ to the TiO_2 surface (Figure 3.3) decreased the rate of NO_2^- photocatalytic oxidation more than the other anions, for which adsorption was less significant. This is because greater adsorption of $H_2PO_4^-/HPO_4^{2-}$ would result in competition with NO_2^- for adsorption sites, slowing the NO_2^- oxidation rate. The different kinetic behavior for NO_2^- and NH_4^+/NH_3 photocatalytic oxidation in the presence of $H_2PO_4^-/HPO_4^{2-}$ (i.e., increased reaction rates for NH_4^+/NH_3 photocatalytic oxidation and decreased reaction rates for NO_2^- photocatalytic oxidation) may be due in part to the fact that rates of NO_2^- photocatalytic oxidation are more surface-area -dependent than rates of NH_4^+/NH_3 photocatalytic oxidation (chapter 2), perhaps due to a closer association of NO_2^- with the TiO_2 surface.

Consistent with these observations, Figure 3.4 also illustrates that for any given pH value lower than 7.5, initial rates of NO_2^- photocatalytic oxidation increased in the order $H_2PO_4^-/HPO_4^{2-} < SO_4^{2-} < Cl^-$, which correlates with decreasing extent of adsorption to the TiO_2 surface ($H_2PO_4^-/HPO_4^{2-} > SO_4^{2-} > Cl^-$) (Figure 3.3). Additional evidence that anion adsorption inhibits NO_2^- photocatalytic oxidation below neutral pH comes from experiments at pH ~6 in which the concentration of $H_2PO_4^-/HPO_4^{2-}$ was varied. When the concentration of $H_2PO_4^-/HPO_4^{2-}$ was decreased from 1×10^{-3} M to 1

$\times 10^{-4}$ M, the initial rate increased from $(1.76 \pm 0.1) \times 10^{-6}$ M min^{-1} to $(4.98 \pm 0.27) \times 10^{-6}$ M min^{-1}. Interestingly, despite significant adsorption of $H_2PO_4^-/HPO_4^{2-}$ to the TiO_2 surface over a range of pH values, NO_2^- photocatalytic oxidation was never completely inhibited, which has practical application for treatment of high $H_2PO_4^-/HPO_4^{2-}$ wastewaters.

3.4. Conclusions

In this study, we systematically investigated NH_4^+/NH_3 and NO_2^- photocatalytic oxidation in the presence of common inorganic anions in a bench scale reactor. Neither ·OH scavenging by Cl^-, SO_4^{2-}, or HPO_4^{2-}, nor direct oxidation by the corresponding anion radicals, was significant in TiO_2 photocatalytic oxidation of NH_4^+/NH_3, but CO_3^{2-} significantly inhibited NH_4^+/NH_3 oxidation due to its efficient ·OH scavenging. The presence of Cl^-, SO_4^{2-}, or HCO_3^- did not inhibit photocatalytic oxidation since there was negligible adsorption of these species at the pH values at which NH_4^+/NH_3 oxidation occurs (>9). Adsorption of HPO_4^{2-} resulted in enhanced NH_4^+/NH_3 photocatalytic oxidation.

At pH values lower than ~7.5, Cl^- had no effect on the initial rates of NO_2^- photocatalytic oxidation, while SO_4^{2-} and $H_2PO_4^-/HPO_4^{2-}$ slowed NO_2^- oxidation due to adsorption to the TiO_2 surface. At pH greater than ~7.5 the initial rates of NO_2^- photocatalytic oxidation were similar and independent of the anion present. $H_2PO_4^-/HPO_4^{2-}$ did not dramatically hinder NO_2^- photocatalytic oxidation, despite the fact that there was significant adsorption of HPO_4^{2-} in this pH region.

Our results indicate that photocatalytic oxidation of NH_4^+/NH_3 to NO_2^- is the rate-limiting step in the complete oxidation of NH_4^+/NH_3 to NO_3^- in the presence of common wastewater anions. Therefore, conditions such as alkaline pH should be chosen to maximize the NH_4^+/NH_3 oxidation rate, and not the NO_2^- oxidation rate, in treatment processes designed to remove NH_4^+/NN_3 from water and wastewater. In addition, pretreatment to lower carbonate alkalinity is likely needed for wastewater with high carbonate alkalinity prior to NH_4^+/NH_3 removal by TiO_2 photocatalytic oxidation at pH values above ~9. Typical wastewater concentrations of Cl^-, SO_4^{2-}, and HPO_4^{2-} should not adversely affect NH_4^+/NH_3 removal by TiO_2 photocatalytic oxidation.

CHAPTER 4

The Role of Hydroxyl Radicals in the Photocatalytic Oxidation of Aqueous Ammonia in Model Graywaters

4.1. Introduction

Graywater, or wastewater generated in households from showers, bathtubs, sinks, and washing machines, accounts for more than 50% of domestic wastewater (Roesner et al., 2006). Graywater is a good potential source for water recycling to compensate for the increased water demand in the world because of population growth. Synthetic surfactants are commonly present in graywater due to the use of personal care products (Karsa, 1999; Eriksson et al., 2002). Surfactants could decrease the concentration of dissolved O_2 in graywater due to their biochemical oxygen demand, and low concentrations of surfactant (e.g., 1 ppm) are toxic to certain fish like trout (Rao, 1991). Aqueous ammonia (NH_4^+/NH_3) is another constituent of graywater (Eriksson et al., 2002; Ramon et al., 2004) that could deteriorate water quality due to depletion of dissolved O_2 (Delwiche, 1981). In addition, concentrations of 1 - 4.5 mg/L NH_3 killed 50% of the fish studied after 24-hour exposure (Hued et al., 2006).

A variety of studies have shown that surfactants can be photocatalytically degraded by hydroxyl radical (·OH), a non-selective oxidant produced by UV illuminated TiO_2, with different reaction rates (Hidaka et al., 1990, 1995; Zhao et al., 1992, 1998; Hermann et al., 1997; Prevot et al., 1999; Gelover et al., 2000; Jiménez et al, 2000; Ohtaki et al., 2000; Fabbri et al., 2004, 2006), possibly resulting from different extents of adsorption of surfactants to the TiO_2 surface. For example, Hidaka et al.

(1990) reported that the photodegradation rates of surfactants in acidic solutions decreased in the order of anionic, nonionic, and cationic surfactants. They attributed this to different adsorption affinities to the positively charged TiO_2 surface (Hidaka, 1990). In another work, Zhang et al. (2003) studied the photocatalytic degradation of sodium dodecylbenzene sulfonate (SDBS) and observed different degradation rates at pH 2.6, 5, and 8.4, due to different extents of adsorption to the TiO_2 surface.

Surfactants could compete with other solutes, for example NH_4^+/NH_3, for active sites at the TiO_2 surface (Turchi and Ollis, 1989; Al-Ekabi et al., 1989; Leng et al., 2000), which could influence the photocatalytic degradation of the target compound. For example, Fabbri et al. (2004) showed that when the concentration of sodium dodecylsulfate (SDS) was lower than the critical micelle concentration (CMC) (1×10^{-3} M), SDS significantly decreased the photocatalytic degradation rate of 2,4,5-trichlorophenol (2,4,5-TCP). This was attributed to competitive adsorption between SDS and 2,4,5-TCP for the active sites on the TiO_2 surface (Fabbri et al., 2004).

The byproducts of surfactant photocatalytic degradation are varied. NH_4^+/NH_3 and nitrate (NO_3^-) were detected from the photocatalytic degradation of nitrogen-containing surfactants (Hidaka et al., 1995; Prevot et al., 1999). Carbon dioxide (CO_2) was observed in surfactant degradation including SDBS (Hidaka et al., 1992, 1995). Some other reported products include *p*-phenolsulfonic acid, hydroquinone, and *p*-quinone (Sangchakr et al., 1995), an alcohol, a ketone, a cyclic diketone, carboxylic esters, and a diol (Gelover et al., 2000), aldehydes, and peroxide (Hidaka et al., 1992, 1995) from the photocatalytic degradation of SDBS and other surfactants. Formic acid and acetic acid were detected from the photocatalytic degradation of nonylphenol

polyethoxylate (9) (Horikoshi et al., 2002) and other surfactants including *N*-dodecylpyridinium chloride and dodecanoyl-*N*- (2-hydroxylethyl) amide (Hidaka et al., 1995). All these byproducts could potentially serve as ·OH scavengers by reacting with (and consuming) ·OH. This would, in turn, slow the degradation rates of other solutes such as NH_4^+/NH_3.

Despite the fact that NH_4^+/NH_3 can be successfully photocatalytically degraded by TiO_2 in simple model systems (Wang et al., 1994; Bonsen et al., 1997; Pollema et al., 1999; chapters 2 and 3), no studies have been done on the effect of surfactants and their byproducts on the photocatalytic degradation of NH_4^+/NH_3. Therefore, the overall goal of this research was to investigate the feasibility of using photocatalytic oxidation to remove NH_4^+/NH_3 from graywater, which contains surfactants, and ultimately reuse the treated water. The specific objective of this research was to study how surfactants influenced NH_4^+/NH_3 photocatalytic degradation. We hypothesized that surfactants would decrease the photocatalytic degradation rate of NH_4^+/NH_3 in one of the following ways: (a) competitive adsorption of surfactants with NH_4^+/NH_3 for TiO_2 surface sites, and/or (b) formation of ·OH scavengers during the photocatalytic degradation of surfactants.

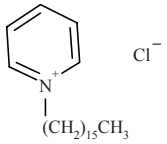
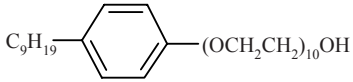
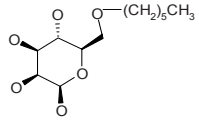
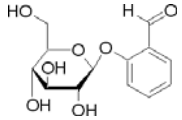
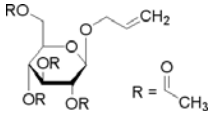
4.2. Experimental Section

4.2.1. Chemicals

Degussa TiO_2 Aeroxide® P 25 (Akron, OH) was used without purification. The manufacturer-reported specific surface area was 50 ± 15 m^2/g. Nanopure water (18.1 $M\Omega \cdot cm$) from an Infinity™ ultrapure water system (model D8961, Barnstead;

Dubuque, IA) was used to prepare solutions. Sodium nitrite ($NaNO_2$), sodium nitrate ($NaNO_3$) (Sigma-Aldrich; Milwaukee, WI), sodium formate (ICN Biomedicals Inc., Aurora, OH), sodium acetate (Merck KcaA, Darmstadt, Germany), and ammonium chloride (Alfa Aesar, Ward Hill, MA), were used as NO_2^-, NO_3^-, formate, acetate, and NH_4^+/NH_3 sources to prepare standard solutions. Sodium chloride (NaCl) (Alfa Aesar) was used to maintain a constant ionic strength (0.001 M). Thirty percent H_2O_2 (Fisher Scientific, Fairlawn, NJ) was used as the ·OH source for the photodegradation of *n*-butyl chloride (*n*-BuCl) (99.5%, Aldrich, Milwaukee, WI). Cetylpyridinium chloride (CPC) (> 99%, Sigma-Aldrich St. Louis, MO), sodium dodecylbenzene sulfonate (SDBS) (~80%, Sigma), Tergitol nonylphenol polyethoxylate (10) (NP10) (Sigma), sodium dodecylsulfate (SDS) (> 99%, Sigma-Aldrich), 1-octanesulfonic acid sodium (OSNa) (~98%, Sigma), dihexyl sulfosuccinate sodium (DSNa) (80% in water, Fluka), cetyltrimethylammonium chloride (CTAC) (25 wt.% in water, Aldrich), Brij® 23 lauryl ether (Brij® 35, Sigma), and hexyl-β-D-glucoside (hexyl glucoside) (75% in water, Akzo Nobel Surface Chemistry LLC, Chicago, IL) were used in this study. Two monosaccarides, helicin (99%, Aldrich) and allyl-tetra-O-acetyl-β-D-glucopyranoside (allyl glucoside) (98%, Aldrich), were also used. The physical/chemical properties of the chemicals are summarized in Table 4.1. All reagents were used as received.

Table 4.1. Physical/chemical properties of surfactants and monosaccharides

Category	Chemicals	Molecular structure	MW (g/mol)	CMC (M) (*ref.*)	Solvent/temperature
Anionic surfactants	Sodium dodecyl sulfate (SDS)	$CH_3(CH_2)_{11}SO_4Na$	288.38	1.62×10^{-3} (*1*)	H_2O/25 ºC
	Sodium dodecylbenzene sulfonate (SDBS)	$CH_3(CH_2)_{11}(C_6H_4)SO_3Na$	348.48	1×10^{-3} (*2*)	0.001 M NaCl/26 ºC
	Dihexyl sulfosuccinate sodium (DSNa)	$CH_3(CH_2)_5COOCH_2CH(SO_3)CH_2COO(CH_2)_5CH_3Na$	388.45	1.4×10^{-2} (*1*)	H_2O/25 ºC
	1-Octanesulfonic acid sodium (OSNa)	$CH_3(CH_2)_7SO_4Na$	216.27	0.16 (*1*)	H_2O /40 ºC
Cationic surfactants	Cetyltrimethylammonium chloride (CTAC)	$CH_3(CH_2)_{15}N(CH_3)_3Cl$	320	1.3×10^{-3} (*1*)	H_2O/30 ºC
	Cetylpyridinium chloride (CPC)		358	8×10^{-4} (*2*)	0.001 M NaCl/26 ºC
Nonionic surfactants	Nonylphenol polyethoxylate (NP10)		660	6.1×10^{-5} (*2*)	0.001 M NaCl/26 ºC
	Brij® 23 lauryl ether (Brij® 35)	$C_{12}H_{25}(OCH_2CH_2)nOH$ n~ 23	1198	9.1×10^{-5} (*3*)	Not available
	Hexyl-β-D-glucoside		264.4	0.25 (*4*)	H_2O
Monosaccharides	Helicin		284.26	Not available	Not available
	Allyl-tetra-O-acetyl-β-D-glucopyranoside		388.37	Not available	Not available

1. Rosen, 2004; 2. Determined by surface tension measurements using a Krüss K-8 interfacial tensiometer by the authors; 3. Sigma website; 4. Provided by Antrace Inc.

4.2.2. Photocatalytic oxidation experiments

We used a photochemical reactor from Ace glass (7841-06, Ace Glass; Vineland, NJ) (chapter 2) that was modified to fit a pH electrode (16 mm in diameter). The reactor had three openings for inserting the pH electrode (Orion, 9802 BN), adding sodium hydroxide (NaOH), and sampling. A step-by-step procedure of kinetic experiments is provided in Appendix A. During the photocatalytic degradation of surfactants, the TiO_2 suspension abruptly becomes acidic after a short time of UV illumination (Hidaka et al., 1986, 1990). Since pH is an important parameter that influences NH_4^+/NH_3 degradation rates, with higher rates at higher pH values (Wang et al., 1994; Bonsen et al., 1997; Pollema et al., 1999; Zhu et al., 2005, Zhu et al., 2007), a pH stat (Radiometer analytical, France) was used to control the suspension pH at ~10.1 (9.8-10.3). At regular time intervals, samples were taken from the reactor using a 30 mL plastic sterile syringe with a leur slip tip, which was attached to an eighteen-inch piece of Teflon tubing (i.d. 3 mm). More details are given in chapter 2. We used a 22500 G force centrifuge (IEC Multi, Thermo Incorporation) to remove TiO_2 particles, and the supernatant was used to quantify surfactant concentrations.

4.2.3. Adsorption experiments

Adsorption experiments were conducted in 30 mL glass vials with Teflon-lined caps. Blank experiments (i.e., surfactant with no TiO_2) showed that adsorption of surfactants to the glass vials was negligible. Sodium chloride (NaCl, 0.001 M) was used as an inert electrolyte for adsorption experiments to maintain a constant ionic strength. To be consistent with kinetic studies, 3 g/L TiO_2 was also used for adsorption

experiments. The solution pH was adjusted to ~10.1 using 1 M NaOH, and vials were then rotated on a shaker for 48 hours in a constant temperature chamber (Sheldon Manufacturing, Model 2020, Cornelius, OR) at 25 ºC. Samples were then centrifuged and the supernatant used to determine the aqueous concentrations of surfactants by UV-vis spectroscopy.

4.2.4. Analytical methods

Aqueous ammonia (NH_4^+/NH_3) was measured using a gas-sensing electrode (model 95-12, Thermo Orion; Beverly, MA); details are given in chapter 2. The concentrations of formate, acetate, NO_2^-, and NO_3^- were determined using a Dionex ion chromatograph (IC) with an Ion Pac® AG 11 guard column (4 × 50 mm), and an Ion Pac® AS 11 anion analytical column (4 × 250 mm), coupled with an ED 50 conductivity detector. The total flow rate was 1 mL/min, which is the sum of three individual solutions (nanopure water, 5 mM NaOH, and 100 mM NaOH). The following gradient program was used to control the flow rates of the three solutions. For the first 2.5 minutes, 1 mM NaOH was used, followed by ramping the NaOH concentration to 2 mM over 2 minutes, then to 5 mM NaOH over 2.5 minutes. The NaOH concentration was then changed to 19.25 mM over 1 minute, and held isocratic for 3.5 minutes. The concentration of *n*-BuCl was monitored by a Tekmar 7000 headspace autosampler/Shimadzu GC 17A /FID with a J&W GS-GASPRO capillary column (30 m × 0.32 mm). The temperatures of the platen, line, and sample loop of the autosampler were all set at 80 ºC. The temperatures of the oven, injector, and detector of the GC were isothermal at 120 ºC, 180 ºC, and 230 ºC, respectively. The total GC run time was 17

minutes. The procedures of preparation of *n*-BuCl stock and standard solutions are presented in Appendix A, and Appendix D provides the principle of the measurement of ·OH.

A UV-vis spectrophotometer (Shimadzu 1601, Columbia, MD) was used to determine the concentrations of SDBS, CPC, and NP10. Concentrations were determined by a multiple wavelength method, for which the details are reported in Workman et al. (1998) and Hari et al. (2005). A Shimadzu Total Organic Carbon Analyzer (TOC 5050A/ASI 5000A) was used to determine the concentration of TOC.

The concentrations of analytes were calculated by five point external standard calibration curves. Standard solutions were prepared daily in duplicate. A blank was analyzed before standard/sample measurements. The data points shown in Figures 4.1, 4.3, 4.6, and 4.7 are mean values of two duplicate analyses of the same sample, and duplicate analyses typically differed by less than 5%. Error bars in Figures 4.2, 4.4, and 4.5 are 95% confidence intervals.

4.3. Results and discussion

To examine the effect of surfactants on NH_4^+/NH_3 photocatalytic degradation, a control experiment (where no surfactants were added) was first conducted to measure the initial rate of NH_4^+/NH_3 degradation at pH ~10.1. A concentration of $(1.06 \pm 0.14) \times 10^{-4}$ M NH_4^+/NH_3 was used throughout this study to be representative of NH_4^+/NH_3 concentrations in graywater (Rose et al., 1991; Eriksson et al., 2002; Ramon et al., 2004). Initial rates were calculated from the slopes of plots of NH_4^+/NH_3 versus time using linear least-squares regression with 95% confidence intervals, using data from the time

period during which approximately 60% of NH_4^+/NH_3 was degraded. In our initial experiments, we chose SDBS, CPC, and NP10 to represent the major categories of surfactants present in graywater, i.e., anionic, cationic, and nonionic surfactants, among which anion surfactant is the predominant category in personal care products and detergents formulations (Karsa, 1999; Gupta et al., 2003). In domestic wastewater, the concentration of anionic surfactants ranges from 1-21 mg/L (Zoller, 1985, 2000; Gupta et al., 2003), or 8.6×10^{-6} - 6×10^{-5} M if an average molecular weight of linear alkyl benzene sulfonates (LAS) is 350 g/mol (calculated from the average alkyl chain length of 12 (Castles et al., 1989). In this study, we chose the median of this reported concentration range, 2×10^{-5} M, which is lower than the critical micelle concentrations of surfactants, as shown in Table 4.1. While we detected inorganic nitrogen species, including NH_4^+/NH_3 and NO_3^-, from the photocatalytic degradation of the cationic surfactant (e.g., CPC), they did not interfere with the measurement of NH_4^+/NH_3 degradation rates since only about 5% of CPC was transformed to inorganic nitrogen-species (NH_4^+/NH_3 and NO_3^-) in 2 hours of UV irradiation.

Although homogeneous degradation of surfactants was insignificant in our photocatalytic kinetic studies due to blocking and scattering of UV light by 3 g/L TiO_2, we still record the homogeneous degradation of the three surfactants, as shown in Figure E1. Photocatalytic degradation of NH_4^+/NH_3 and surfactants (SDBS, CPC, and NP10) was then investigated, and results are presented in Figure 4.1, and the product distribution is shown in Appendix E. Figure 4.1 shows that more than 80% of surfactants were removed in 20 minutes, which was very fast compared to NH_4^+/NH_3 degradation. Consistent with previous studies with NH_4^+/NH_3 alone (Wang et al., 1994; Bonsen et al.,

1997; Pollema et al., 1999; chapters 2 and 3), NO_2^- and NO_3^- were the major intermediates/products of photocatalytic degradation in the presence of surfactants (data not shown).

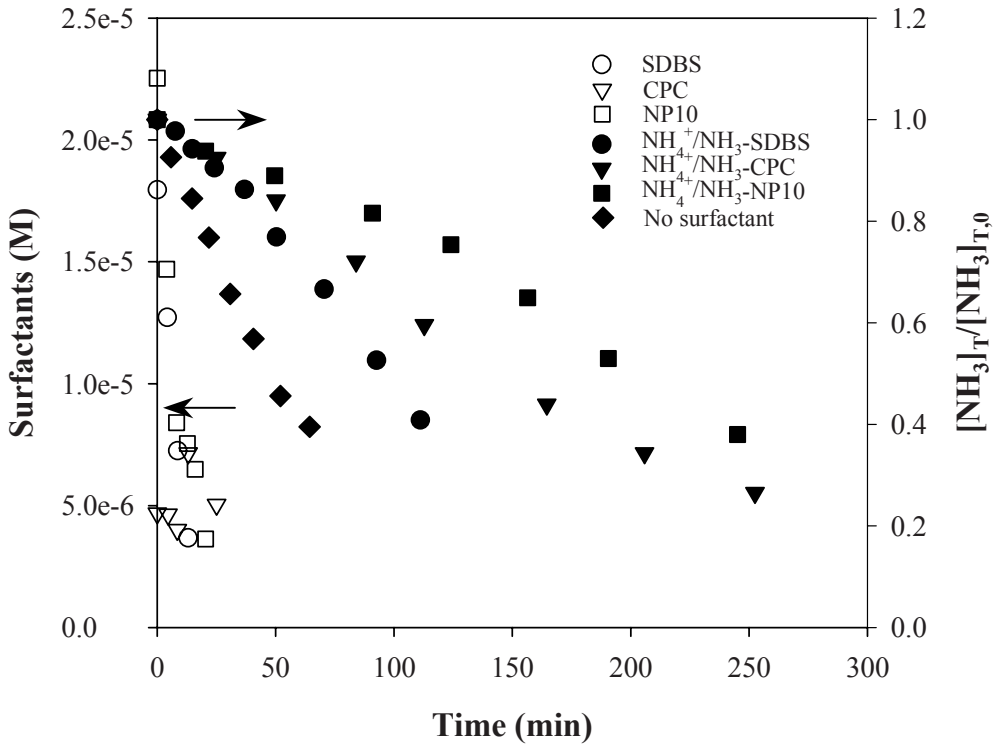


Figure 4.1. Photocatalytic degradation of NH_4^+/NH_3 and surfactants at pH ~ 10.1. Open symbols are for the concentrations of surfactants and closed symbols are for NH_4^+/NH_3 degradation. [Surfactant]: 2×10^{-5} M; [NaCl]: 0.001 M; $[NH_3]_{T,0}$ ($[NH_4^+] + [NH_3]$): $(1.06 \pm 0.14) \times 10^{-4}$ M.

Initial rates of NH_4^+/NH_3 degradation, however, were slowed by surfactants, and decreased in the following order (from fastest to slowest): control (no surfactant) > SDBS > CPC > NP10 (Figure 4.2). Specifically, SDBS, CPC, and NP10 decreased the initial rate of NH_4^+/NH_3 photocatalytic degradation by approximately 50%, 60%, and 80%,

respectively. First we speculated that adsorption of the surfactants at the TiO_2 surface might be responsible for decreased rates of NH_4^+/NH_3, as discussed below.

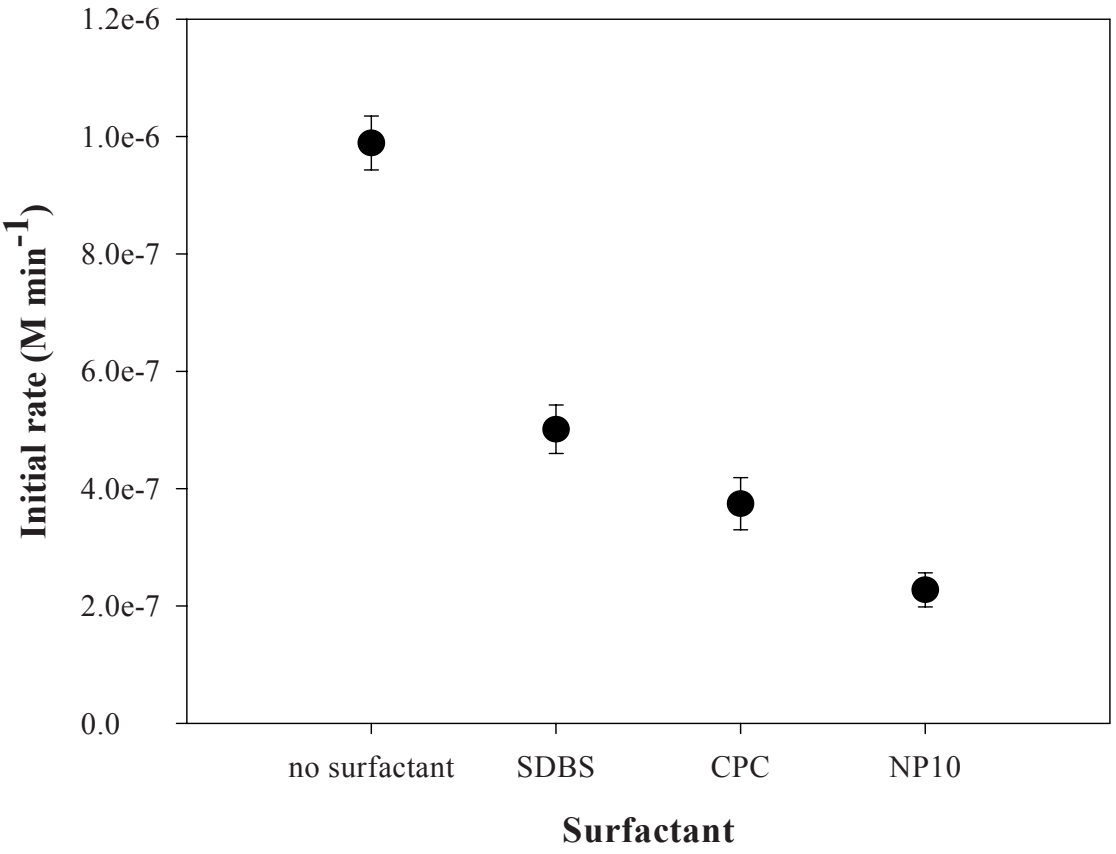


Figure 4.2. Initial rates of NH_4^+/NH_3 photocatalytic degradation in the presence of surfactants at pH ~ 10.1. [Surfactant]: 2×10^{-5} M; [NaCl]: 0.001 M; $[NH_3]_{T,0}$ ($[NH_4^+]$ + $[NH_3]$): $(1.06 \pm 0.14) \times 10^{-4}$ M. Error bars are 95% confidence intervals of initial rates of NH_4^+/NH_3 degradation.

4.3.1. Role of surfactant adsorption

We measured adsorption of SDBS, CPC, and NP10 to the TiO_2 surface at a surfactant concentration of 2×10^{-5} M, which was the same concentration used in kinetic experiments, and found that approximately 12 %, 17 %, and almost 77% of added NP10,

SDBS, and CPC, respectively, were adsorbed to the TiO_2 surface. Adsorption of SDBS was attributed to specific adsorption (Zhao et al., 1993), and adsorption of NP10 may have been via hydrogen bonding between the ether oxygen of the ethylene oxide group and hydroxyl group on the TiO_2 surface (Penfold et al., 2002). Adsorption of CPC was likely due to electrostatic attraction between the cationic surfactant and the negatively charged TiO_2 surface (pH_{pzc} of the Degussa TiO_2 is 6.2-7.5 (Hoffmann et al., 1995; Fernández-Nieves et al., 1998)). The small percent adsorbed values for NP10 and SDBS indicate that disappearance of NP10 and SDBS from aqueous solution (Figure 4.1) was mainly due to photocatalytic degradation. For CPC, however, the initial decrease in concentration was due to both adsorption and degradation. Evidence for CPC degradation includes the appearance of formate and acetate and the eventual decrease in TOC concentration over time (Figure 4.3). The initial increase, then decrease, in TOC (Figure 4.3) may have been due to desorption of products upon degradation of adsorbed CPC.

We also used our adsorption data to calculate the percent of the TiO_2 surface covered by surfactants at the start of the kinetic experiments. First we used the Gibbs adsorption equation (Rosen, 2004) to estimate the minimum surface coverage assuming that only the surfactant head group contacted the surface. Then, we estimated the maximum TiO_2 surface coverage by assuming that the entire surfactant molecule was lying on the TiO_2 surface, which is possible when surfactant concentrations are an order of magnitude below their CMCs (Clint, 1992; Li and Tripp, 2002). Since the NP10 concentration we used (2×10^{-5} M) was only three times lower than its CMC (6×10^{-5} M, Table 4.1), the actual surface coverage by NP10 was likely below the maximum value.

The estimated surfactant coverages (minimum to maximum) were 0.6-4% for NP10, 0.5-5% for SDBS, and 5-27% for CPC. Examination of these numbers shows no relationship between TiO_2 surface coverage and percent decrease in initial rates of NH_4^+/NH_3 removal. For example, while only approximately 0.6% of the TiO_2 surface was covered by NP10, the NH_4^+/NH_3 initial rate decreased by approximately 80% when NP10 was added. From this we concluded that some process other than adsorption was responsible for decreased initial rates of NH_4^+/NH_3 in our system. For higher surfactant loadings and/or lower TiO_2 surface area loadings, however, adsorption of surfactants could be detrimental to cosolute degradation (e.g., Fabbri et al., 2004).

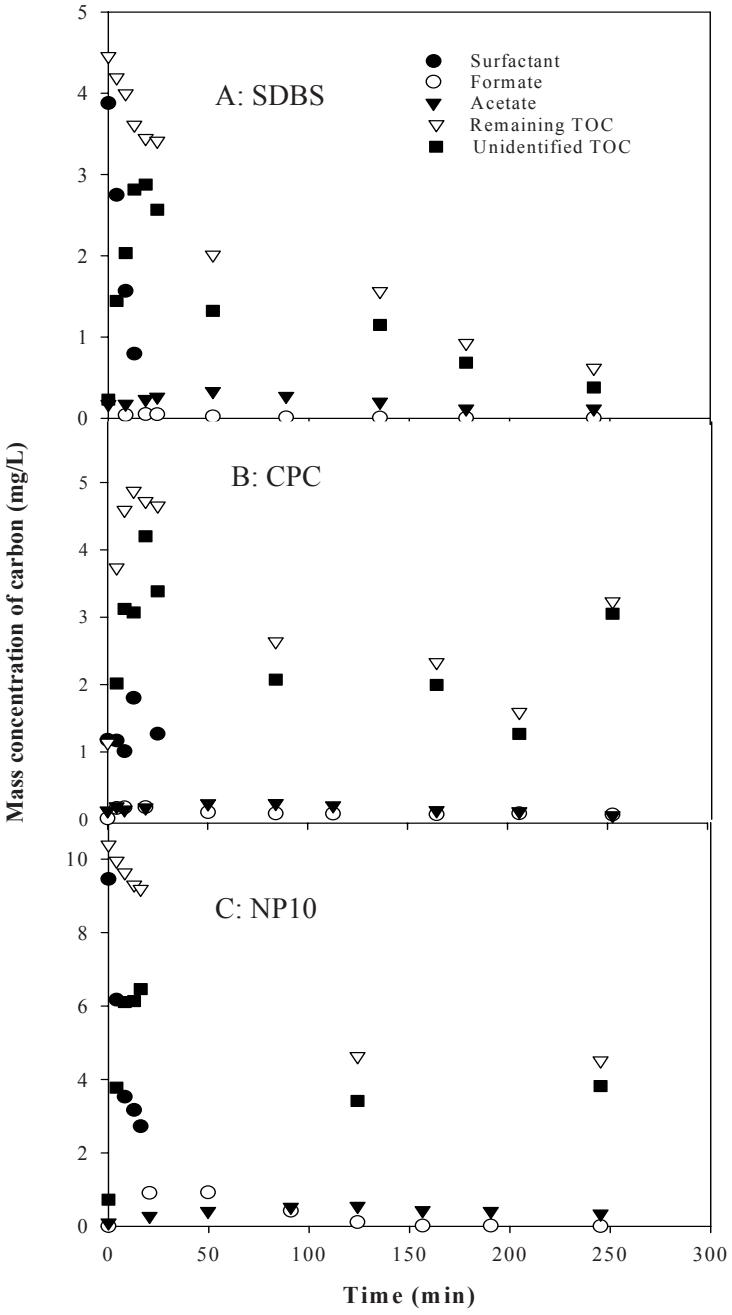


Figure 4.3. Mass concentration of surfactants and selected products during the photocatalytic degradation of NH_4^+/NH_3 and surfactants at pH ~ 10.1. $[NH_3]_{T,0}$: (1.06 ± 0.14) × 10^{-4} M; [surfactant]: 2 × 10^{-5} M. [unidentified TOC] = [Remaining TOC]-$C_{formate}$-$C_{acetate}$-$C_{surfactant}$, where C is the mass concentration of carbon; Data for panel A was obtained from an experiment where $[NH_3]_{T,0}$ was 1.5 × 10^{-4} M.

4.3.2. Role of ·OH scavengers

Next, we investigated whether the products of surfactant photocatalytic degradation acted as ·OH scavengers, thereby slowing initial rates of NH_4^+/NH_3 removal. We performed experiments that were identical in procedure to those illustrated in Figure 4.1 for the first two hours, but that were then modified to facilitate estimation of the steady state ·OH concentration. After UV illumination of the TiO_2 slurry containing the NH_4^+/NH_3-surfactant mixture for two hours, we removed the TiO_2 particles by centrifugation and spiked the remaining supernatant (which contained potential ·OH scavengers) with hydrogen peroxide (H_2O_2) and *n*-BuCl, then illuminated it with UV light. Upon illumination with UV light, H_2O_2 dissociates into ·OH (Chu, 2001). A Vycor filter (Ace glass) was used to block wavelengths lower than 220 nm to prevent possible reactions of aqueous NH_3 with oxidants other than ·OH, including ozone generated from photodissociation of O_2 (Steinfeld, 1993). The steady state concentration of ·OH was then calculated from the pseudo-first-order rate constant for *n*-BuCl decay, which we determined by monitoring [*n*-BuCl] over time (Liao et al., 2001). Lower steady state concentrations of ·OH corresponded to higher concentrations of ·OH scavengers, due to reaction with and consumption of ·OH by the scavengers.

We quantified the concentration of ·OH after two hours because at that time there was complete surfactant removal (Figure 4.1) but still significant surfactant byproducts remaining (as evidenced by TOC measurements) that could serve as potential ·OH scavengers. While we measured the steady state ·OH concentration in the H_2O_2/UV system (no TiO_2), the relative effect of ·OH scavengers on NH_4^+/NH_3 degradation rates was expected to be the same in the TiO_2/UV and H_2O_2/UV systems.

Examples of the photodegradation of *n*-BuCl under these conditions are illustrated in Figure 4.4. About 90% of *n*-BuCl was degraded in 10 minutes for SDBS, and in 20 minutes for NP10. This indicates that less ·OH scavengers were formed during the photocatalytic degradation of SDBS than NP10, which can explain why we obtained a faster initial rate of NH_4^+/NH_3 photocatalytic degradation in the presence of SDBS than NP10 (Figure 4.2).

.

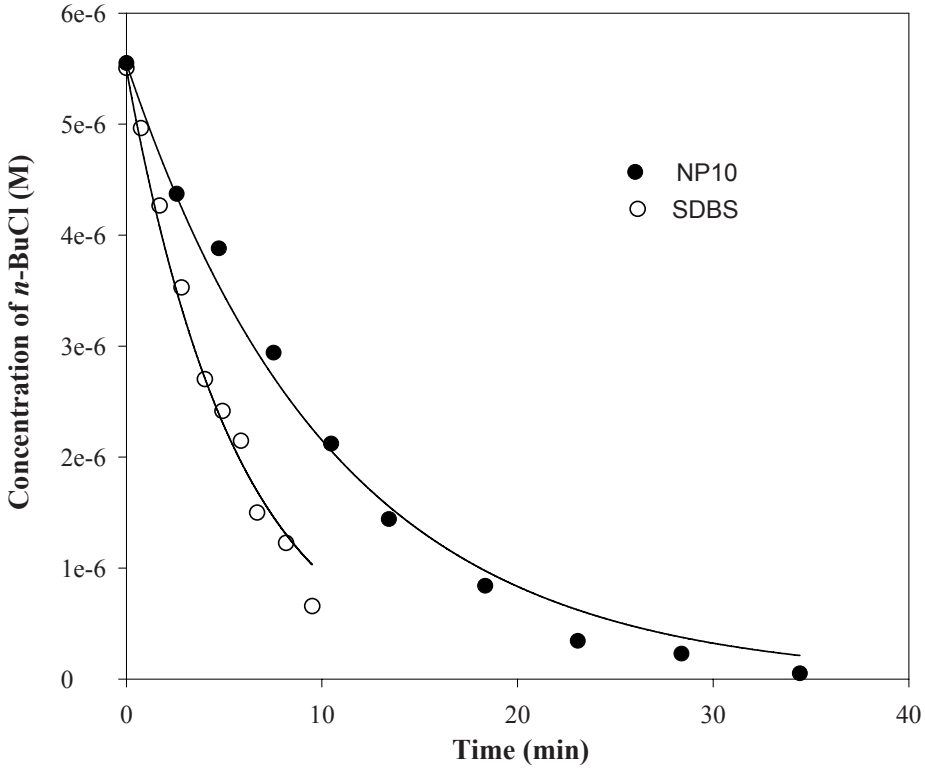


Figure 4.4. Photodegradation of *n*-BuCl by UV/H_2O_2 at pH ~10.1 with initial addition of surfactants. A Vycor filter was used; [Surfactant]: 2×10^{-5} M; $[NH_3]_{T,0}$ ($[NH_4^+] + [NH_3]$): $(1.06 \pm 0.14) \times 10^{-4}$ M; [NaCl]: 0.001 M; lines are pseudo-first order reaction model fits of the concentration of *n*-BuCl versus time.

We also expanded our study to include other surfactants because preliminary experiments with CPC, NP10, and SDBS showed a good correlation between initial rates

of NH_4^+/NH_3 degradation and [·OH]. Additional surfactants were chosen to identify the effects of different functional groups on the formation of ·OH scavengers and ultimately on NH_4^+/NH_3 reaction rates. We chose sodium dodecyl sulfate (SDS), cetyltrimethylammonium chloride (CTAC), and Brij® 35 because these surfactants are similar in structure to SDBS, CPC, and NP10, respectively, but don't contain aromatic rings. 1-Octanesulfonic acid sodium (OSNa) is similar in structure to SDS, but with a shorter linear alkyl chain (OSNa). Unlike SDS, dihexyl sulfosuccinate sodium (DSNa) has a branched alkyl chain. Hexyl-β-D-glucoside (hexyl glucoside) is similar to NP10 and Brij® 35, but with a different head group. We also chose two monosaccharides, helicin and allyl-tetra-O-acetyl-β-D-glucopyranoside (allyl glucoside) (Table 4.1) that are present in graywater (Konopka, 1997) and have similar structures as surfactants, to determine their effect on NH_4^+/NH_3 photocatalytic degradation. Except for Brij® 35, we used a concentration of 2×10^{-5} M surfactant or monosaccharide. A lower concentration of Brij® 35 (1.2×10^{-5} M) was used to get a measurable initial rate of NH_4^+/NH_3 photocatalytic degradation. Photodegradation of *n*-BuCl with initial addition of these compounds are shown in Appendix D. Profiles of the photocatalytic degradation of NH_4^+/NH_3 and surfactants and their product distribution are illustrated in Appendix E.

The relationship between the relative initial rate of NH_4^+/NH_3 photocatalytic degradation and the relative steady-state concentration of ·OH (both are relative to the control experiment) is illustrated in Figure 4.5. Specifically, the *x*- and *y*-axes represent the steady-state concentration of ·OH in the presence of UV/H_2O_2 and byproducts from surfactant photocatalytic degradation and initial rate of NH_4^+/NH_3 photocatalytic degradation with addition of surfactant or monosaccharide divided by the same

parameters for the control experiment (i.e., NH_4^+/NH_3 + UV/ TiO_2; no surfactants or monosaccharides). Figure 4.5 shows a positive correlation between relative initial rates of NH_4^+/NH_3 degradation and relative steady-state concentrations of ·OH. In other words, higher concentrations of ·OH, resulting from lower concentrations of ·OH scavengers, led to higher initial rates of NH_4^+/NH_3 degradation. There are no clear exceptions to this trend that can be attributed to molecule type (i.e., surfactant or monosaccharide), surfactant type (i.e., nonionic, anionic, or cationic), functional group (i.e., branched versus linear or aromatic versus nonaromatic), or head group.

The coefficient of determination (R^2) from least-squares linear regression was 0.81. From a statistical point of view, R^2 represents the fraction of variability in *y* that can be explained by the variability in *x* (Taylor and Cihon, 2004). Accordingly, a R^2 value of 0.81 means that the steady-state ·OH concentration (*x*), and correspondingly the concentration of ·OH scavengers, can explain about 81% of the variance in initial rates of NH_4^+/NH_3 degradation (*y*). This suggests that the formation of ·OH scavengers is the main reason for decreasing initial rates of NH_4^+/NH_3 degradation in the presence of surfactants. Some other factors such as adsorption of byproducts to the TiO_2 surface could account for the other 19% of the variance in initial rates of NH_4^+/NH_3 degradation. Adsorption could also be more important at higher surfactant loadings and/or lower TiO_2 surface area loadings, as discussed earlier.

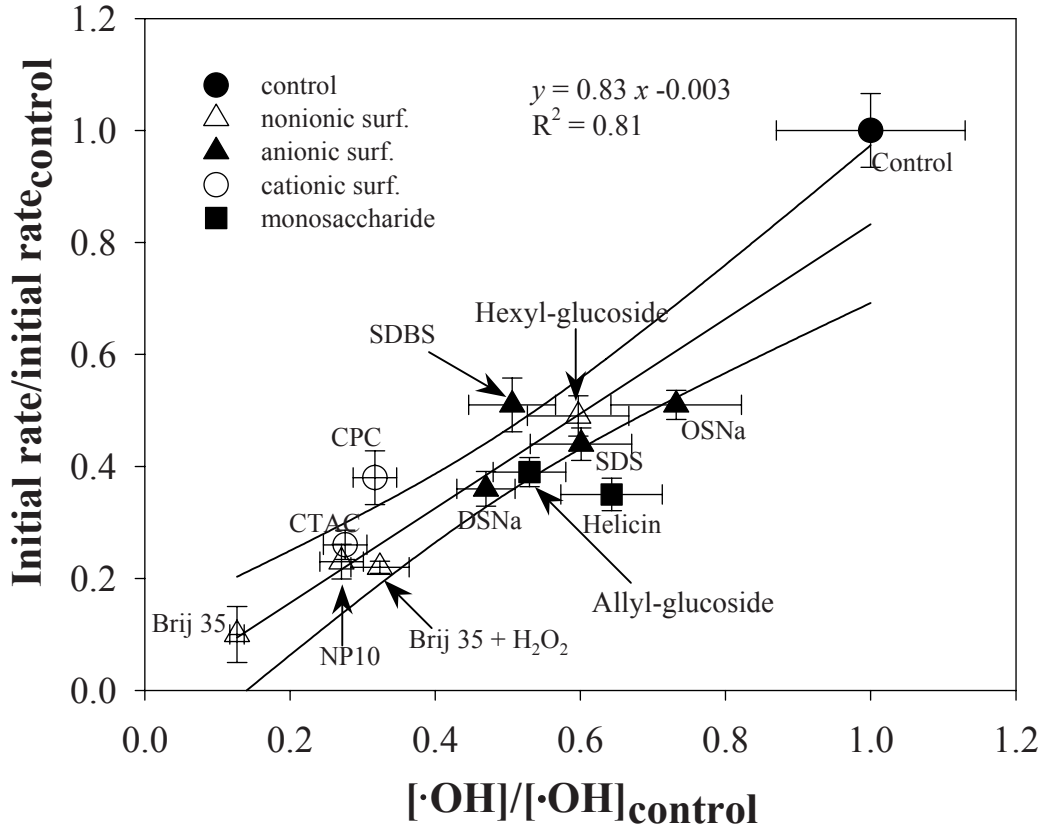


Figure 4.5. Relative initial rate of NH_4^+/NH_3 degradation versus relative concentration of ·OH in the presence of surfactants/monosaccharides. $[NH_3]_{T,0}$: $(1.06 \pm 0.14) \times 10^{-4}$ M, [surfactants/monosaccharides]: 2×10^{-5} M except for Brij® 35 (1.2×10^{-5} M); pH: ~10.1 Error bars are 95% confidence intervals of initial rates of NH_4^+/NH_3 degradation and [·OH] (calculated from propagation of error, as described in Appendix D). The straight line is the linear regression line. The curved lines represent upper and lower bounds of the 95% confidence interval.

Next we tested whether the detrimental effects of ·OH scavengers could be counteracted by increasing the steady-state ·OH concentration by adding 0.01 M H_2O_2 (an additional ·OH source when illuminated by UV light) and measuring the initial rate of NH_4^+/NH_3 photocatalytic degradation in the presence of 1.2×10^{-5} M Brij® 35. We chose 1.2×10^{-5} M Brij® 35 for this experiment because it decreased the initial rate of NH_4^+/NH_3 degradation the most (90%) compared to the control (Figure 4.2). We found that addition of 0.01 M H_2O_2 to a solution containing 1.2×10^{-5} M Brij® 35 increased the

initial rate of NH_4^+/NH_3 photocatalytic degradation by a factor of approximately 2.3, and increased the concentration of ·OH by a factor of approximately 2.5, compared to 1.2×10^{-5} M Brij® 35 alone. This indicates that an additional ·OH source can partly compensate for detrimental effects of ·OH scavengers. Our results also provide further evidence that ·OH scavenging is the mechanism by which rates of NH_4^+/NH_3 are decreased in the presence of surfactants, since the data points for Brij® 35 with and without added H_2O_2 both fall along the same line of relative initial rate versus relative [·OH] (Figure 4.5).

Since ·OH scavengers were responsible for decreased initial rates of NH_4^+/NH_3 degradation, we tried to identify species that could possibly act as ·OH scavengers. Of the acid/conjugate base pair NH_4^+/NH_3, only NH_3 is reactive in TiO_2 photocatalysis (Chapter 2); therefore the second order rate constant for reaction of NH_3 with ·OH is shown in Table 4.1. Figure 4.3 shows that the TOC remaining decreased during the photocatalytic degradation of NH_4^+/NH_3 and surfactants, indicating organic carbon mineralization and production of carbonate. At our experimental pH (~10.1), carbonate is present as both HCO_3^- and CO_3^{2-}, but only CO_3^{2-} reacts with ·OH faster than does NH_3 (Table 4.2), so only CO_3^{2-} is a possible ·OH scavenger in our system. Our previous study (Zhu et al. 2007) also concluded that CO_3^{2-} slowed rates of NH_4^+/NH_3 photocatalytic oxidation, probably by ·OH scavenging.

Table 4.2. Second order rate constants (*k*) of ·OH with organic/inorganic compounds

Compounds (*ref.*)[1]	***k* (M^{-1} s^{-1}) (*ref.*)[2]**
NH_3	1.0×10^8 (*6*)
HCO_3^-/CO_3^{2-} (*1,2*)	8.5×10^6 (*7*)/3.9×10^8 (*7*)
Acetate (*3*)/acetic acid (*1,4*)	7×10^7 (*8*)/ 1.7×10^7 (*8*)
Formate (*3*)/formic acid (*1,4*)	2.4×10^9 (*8*)/ 1.0×10^8 (*8*)
Formaldehyde (*1,2*)	2.3×10^{10} (*8*)
p-phenolsulfonic acid (*5*)	6.5×10^9 (*9*)
Hydroquinone (*5*)	2.1×10^{10} (*10*)
p-quinone (*5*)	6.6×10^9 (*11*)

[1]Reference(s) showing that this compound is formed via surfactant degradation. [2]Reference(s) for the second order rate constant of this compound with ·OH. [3]N/A means not applicable. (*1*). Hidaka et al. (1995); (*2*). Hidaka et al. (1992); (*3*). This work; (*4*). Horikoshi et al. (2002); (*5*). Sangchakr et al. (1995); (*6*). Neta et al., (1978); (*7*). Buxton et al. (1988); (*8)* Ervens et al. (2003); (*9*). Pramanick et al. (2000); (*10*). Ross (1977); (*11*). Schuchmann et al. (1998).

As shown in Figure 4.3, we fortuitously detected formate and acetate as organic products of surfactant photocatalysis, which we next assessed as possible ·OH scavengers. While there was no relationship between acetate concentration and rates of NH_4^+/NH_3 degradation, there did, however, appear to be a correlation between formate concentration and NH_4^+/NH_3 degradation rates, as illustrated in Figures 4.6A and 4.6B. For instance, in the presence of Brij® 35 or NP10 (numbered 1 and 2 in Figure 4.6), there was a slower degradation rate of NH_4^+/NH_3 as the concentration of formate increased, followed by a faster rate as the concentration of formate decreased. The degradation rates of NH_4^+/NH_3 in the presence of several other surfactants also followed this trend.

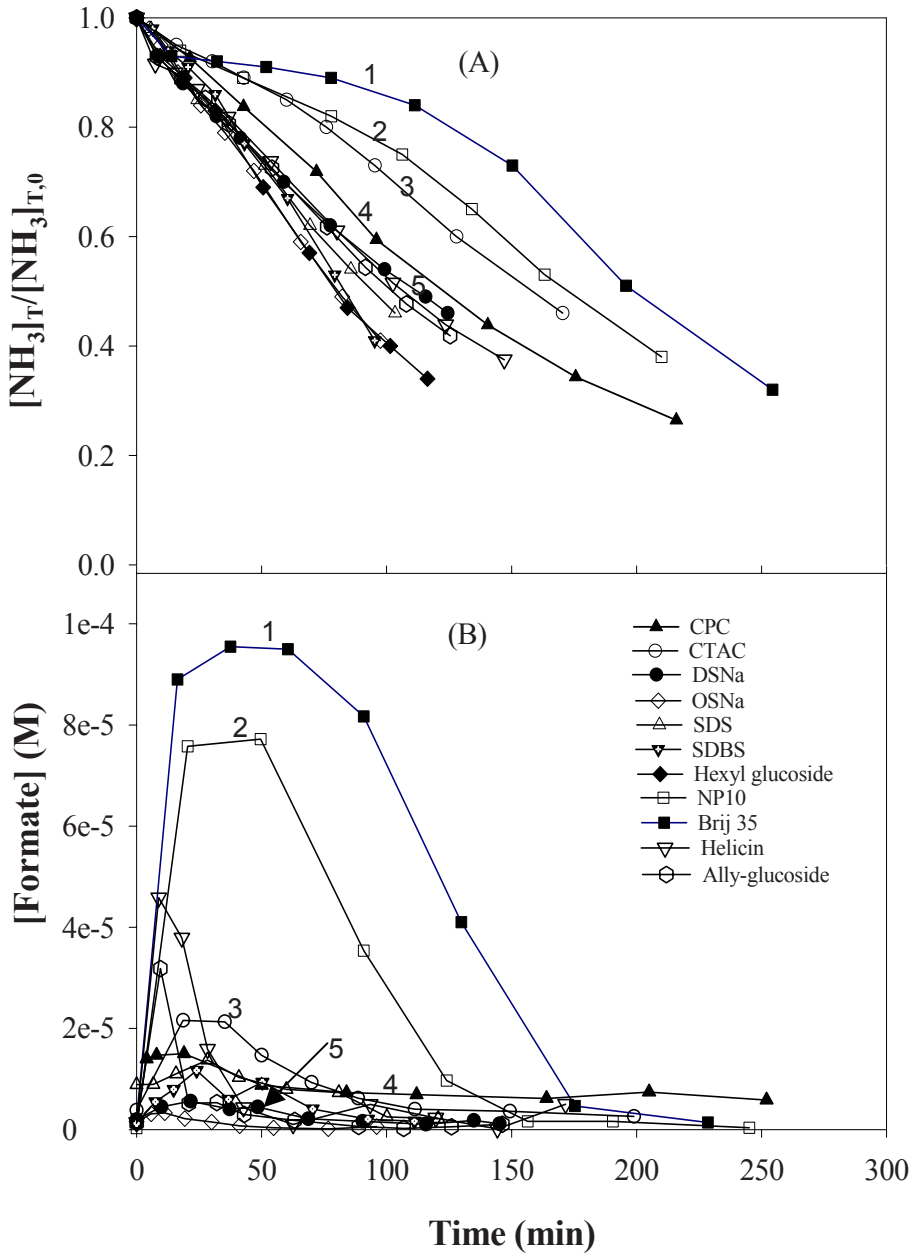


Figure 4.6. NH_4^+/NH_3 photocatalytic degradation (A) and formate formation (B) at pH ~ 10.1. $[NH_3]_{T,0}$: (1.06 ± 0.14) × 10^{-4} M, [surfactant]/[monosaccharides]: 2 × 10^{-5} M, except for Brij® 35 (1.2 × 10^{-5} M); pH: ~10.1; [NaCl]: 0.001 M; the numbers on the figures represent NH_4^+/NH_3 and formate concentrations in the presence of Brij® 35 (1), NP10 (2), CTAC (3); CPC (4), and DSNa (5).

Specifically, NH_4^+/NH_3 rates increased in the following order: Brij® 35 < NP10 < CTAC < CPC < DSNa (Figure 4.6A), while the maximum concentration of formate decreased in the same order, i.e., Brij® 35 > NP10 > CTAC > CPC > DSNa (Figure 4.6B) (follow numbers 1 to 5 in sequence in both figures). The degradation rates of NH_4^+/NH_3 in the presence of other surfactants and the monosaccharides (unnumbered data series in Figure 4.6) were too close to correlate. Table 4.1 shows that acetate has a smaller second order rate constant with ·OH than does NH_3, which explains why acetate did not act as a ·OH scavenger. Formate, on the other hand, reacts faster with ·OH than does NH_3 (Table 4.1); thus it was an effective ·OH scavenger in our experiments.

Formate account for a small fraction of the total organic carbon (TOC), and the majority of TOC from surfactant photocatalytic degradation was unidentified (Figure 4.3). It is likely that the unidentified TOC consists of species such as aldehydes and aromatic- and quinone-related compounds that have previously been identified in surfactant photodegradation (Hidaka et al., 1992, 1995; Zhao et al., 2003; Sangchakr et al., 1995). Of these compounds, only those with second order rate constants with ·OH that are similar to or greater than that for NH_3 (10^8 M^{-1} s^{-1}) (Neta et al., 1978; Ross, 1977; Pramanick et al., 2000; Schuchmann et al., 1998; Ervens et al., 2003) have the potential to react with ·OH faster than NH_3, thus "scavenging" and lowering the steady state concentration of ·OH available for reaction with NH_3. Further research is needed to identify the role of different surfactant byproducts in ·OH scavenging. Despite slowed rates of NH_4^+/NH_3 degradation, both surfactants/monosaccharides and NH_4^+/NH_3 were removed by TiO_2 photocatalysis, indicating that this process can effectively treat both

carbonaceous biochemical oxygen demand (CBOD) and nitrogenous BOD (NBOD) in graywater.

We also tested for a correlation between initial rates of NH_4^+/NH_3 degradation and the mass concentration of carbon in the TiO_2 suspensions. Figure 4.7 shows a correlation with a R^2 of 0.59, meaning that approximately 59% of the variance in initial rates of NH_4^+/NH_3 degradation (y) can be explained by the mass concentration of carbon (x) (Taylor and Cihon, 2004). The practical application of this is that one could measure the mass concentration of carbon (directly via TOC or indirectly via chemical oxygen demand (COD)) and estimate the initial rate of NH_4^+/NH_3 degradation to determine the feasibility of using photocatalysis to remove NH_4^+/NH_3 from graywater. Again, factors like adsorption of byproducts from surfactant photocatalysis to the TiO_2 surface could explain the remaining variance in initial rates of NH_4^+/NH_3 degradation.

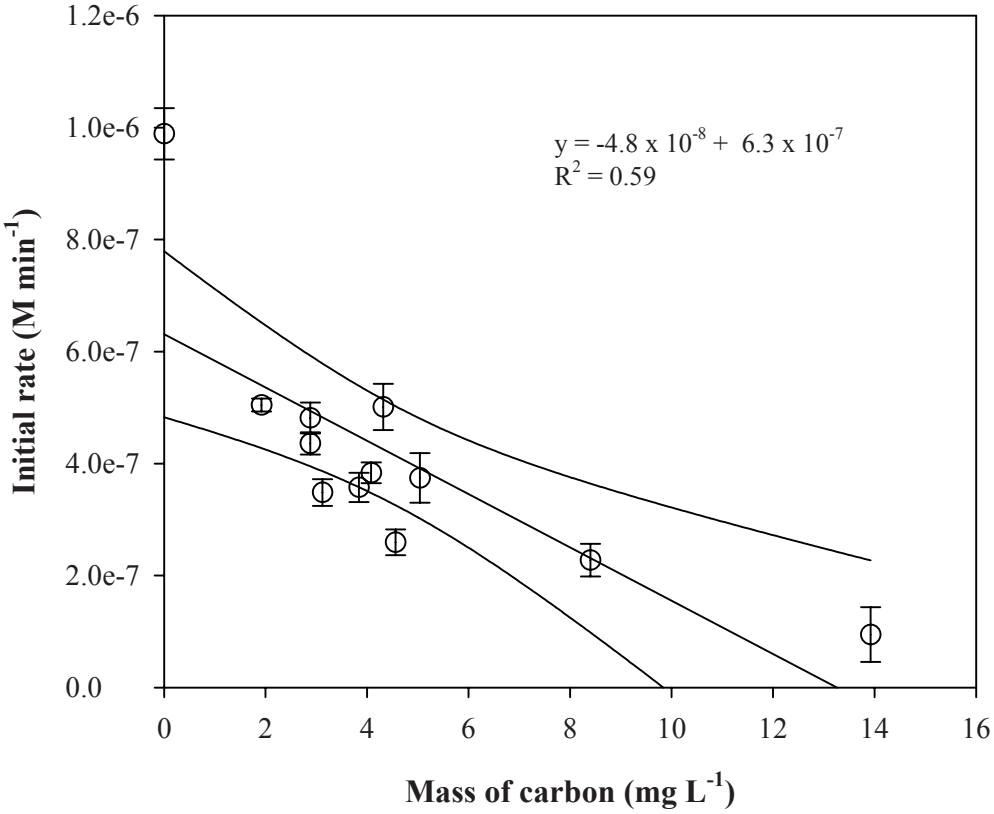


Figure 4.7. Initial rate of NH_4^+/NH_3 degradation at pH 10.1 vs. the mass concentration of carbon. $[NH_3]_{T,0}$: $(1.06 \pm 0.14) \times 10^{-4}$ M, [surfactant]/[monosaccharide]: 2×10^{-5} M, except for Brij® 35 (1.2×10^{-5} M). Error bars are 95% confidence intervals of initial rates of NH_4^+/NH_3 degradation. The straight line is the linear regression line. The curved lines represent upper and lower bounds of the 95% confidence interval.

4.4 Conclusions

Photocatalytic degradation of NH_4^+/NH_3 in the presence of surfactants was studied. Photocatalytic degradation of surfactant was very fast compared to NH_4^+/NH_3 degradation. Initial rates of NH_4^+/NH_3 photocatalytic degradation was decreased approximately by 50-90% in the presence of chosen surfactants or monosaccharides. Decreased initial rates of NH_4^+/NH_3 in the presence of 2×10^{-5} M surfactants were not due to adsorption of surfactants to the TiO_2 surface. Formation of ·OH scavengers, including formate and carbonate, was mainly responsible for decreasing initial rates of

NH_4^+/NH_3 photocatalytic degradation in the presence of surfactants or monosaccharides. A negative correlation ($R^2 = 0.59$) was observed between the initial rate of NH_4^+/NH_3 degradation and the mass concentration of carbon. For practical purposes, one could roughly determine the feasibility of using photocatalytic oxidation to remove NH_4^+/NH_3 from graywater by measuring the concentration of TOC or COD in the system. While surfactants decreased initial rates of NH_4^+/NH_3 degradation, the photocatalysis process can effectively remove both surfactants and NH_4^+/NH_3 from wastewater. This indicates that photocatalysis can be used to remove both carbonaceous and nitrogenous BOD from graywater.

CHAPTER 5

Conclusions and Recommendations

5.1. Conclusions

In this work, effects of the concentration of TiO_2, pH, inorganic anions, and surfactants on NH_4^+/NH_3 photocatalytic degradation were investigated. Some major findings are listed below:

- Without sufficient TiO_2, complete oxidation of NH_4^+/NH_3 to NO_3^- will not occur because TiO_2 is required to oxide NO_2^- to NO_3^- during NH_4^+/NH_3 oxidation to NO_2^-. For TiO_2 concentrations ≥ 1 g/L,
- Initial rates of NH_4^+/NH_3 photocatalytic oxidation are proportional to the initial concentrations of neutral NH_3, and not total NH_3 (i.e., $[NH_4^+] + [NH_3]$). Thus, the pH-dependent equilibrium between NH_4^+ and NH_3, and not the pH-dependent electrostatic attraction between NH_4^+ and the TiO_2 surface, is responsible for the increase in rates of NH_4^+/NH_3 photocatalytic oxidation with increasing pH.
- Photocatalytic oxidation of NH_4^+/NH_3 to NO_2^- is the rate-limiting step in the complete oxidation of NH_4^+/NH_3 to NO_3^- in the presence of common wastewater inorganic anions at pH > 9.
- Different inorganic anions have different influences on NH_4^+/NH_3 and NO_2^- photocatalytic oxidation. Except for CO_3^{2-}, which decreased the homogeneous oxidation rate of NH_4^+/NH_3 by UV-illuminated hydrogen peroxide, ·OH scavenging by inorganic anions (Cl^-, SO_4^{2-}, $H_2PO_4^-/HPO_4^{2-}$,

and HCO_3^-) and/or direct oxidation of NH_4^+/NH_3 and NO_2^- by anion radicals ($Cl\cdot$, $SO_4\cdot^-$, $HPO_4\cdot^-$, and $HCO_3\cdot$) did not affect initial rates of TiO_2 photocatalytic oxidation.

- Adsorption of HPO_4^{2-} enhanced NH_4^+/NH_3 photocatalytic oxidation at pH ~9 and ~10, but it inhibited NO_2^- oxidation at low to neutral pH values. The presence of Cl^-, SO_4^{2-}, and HCO_3^- had no effect on NH_4^+/NH_3 and NO_2^- photocatalytic oxidation at pH ~9 and ~10, whereas CO_3^{2-} slowed NH_4^+/NH_3 but not NO_2^- photocatalytic oxidation at pH ~11.
- Photocatalysis can remove both surfactants and NH_4^+/NH_3 from graywater. While surfactants dramatically decreased the initial rates of NH_4^+/NH_3 photocatalytic degradation by approximately50-90% in the presence of chosen surfactants or monosaccharides, more than 50% of NH_4^+/NH_3 can be removed after 4 hours of UV illumination. Adsorption of surfactants was not responsible for the decrease in initial rates of NH_4^+/NH_3 degradation when a concentration of 2×10^{-5} M surfactants was applied.
- Formation of hydroxyl radical ($\cdot OH$) scavengers, including formate, from the photocatalytic degradation of surfactants, is the main reason for decreasing initial rates of NH_4^+/NH_3 degradation.

5.2. Recommendations for graywater recycling

- pH is a very important parameter in NH_4^+/NH_3 photocatalytic oxidation. We should choose high pH values (> 9) to increase the fraction of total NH_4^+/NH_3

in the form of NH_3, in order to obtain a faster initial rate of NH_4^+/NH_3 photocatalytic degradation in graywater recycling.

- TiO_2 photocatalysis can remove both surfactants and NH_4^+/NH_3 in graywater. This has practical applications in graywater recycling in that, different from the biological wastewater treatment, TiO_2 photocatalysis only need one reactor for carbonaceous and nitrogenous biochemical oxygen demand (CBOD and NBOD) and NH_4^+/NH_3 removal.

5.3. Recommendations for future work

- Since NO_3^- was detected as the final product of TiO_2-based NH_4^+/NH_3 photocatalytic degradation in our study, it would be beneficial to develop an effective catalyst to directly convert NH_4^+/NH_3 to N_2. To achieve this, some transition metals including Fe and Ru could be doped to the TiO_2 catalyst to change the reaction mechanisms of NH_4^+/NH_3 oxidation.
- We used the TiO_2 suspension to treat NH_4^+/NH_3, which needs to have a post-treatment step to remove the TiO_2 particles after photocatalysis. To overcome this step, to develop an immobilized catalyst (e.g., thin film) and test the efficiency of NH_4^+/NH_3 removal would be very helpful. This can also easily reuse the catalyst, which would decrease treatment cost.
- Investigate possible reasons to cause the points that deviate from the regression line of the initial rates of NH_4^+/NH_3 degradation as a function of [·OH] and the mass concentration of carbon. Different adsorption affinities of intermediates from the photocatalytic degradation of surfactants could be

one of the reasons. To identify the byproduct distribution of the photocatalytic degradation of surfactants using GC/MS or HPLC/MS and study the adsorption of these byproducts to the TiO_2 surface could help get insights.

- Precipitation would be occurring due to the presence of the mixed surfactants (e.g., anionic + cationic) in graywater. To examine the effect of precipitation of surfactants on the TiO_2 surface on the photocatalytic degradation of NH_4^+/NH_3 can provide practical suggestions on graywater recycling.
- Since graywater contains some other constituents such as urea and amino acids, it would be interesting to evaluate how these constituents influence NH_4^+/NH_3 photocatalytic degradation in graywater recycling.
- It will be useful to investigate complicated systems such as the combination of two or more parameters (e.g., amino acids + surfactants) and check overall removal efficiency of organic and inorganic contaminants in real graywater recycling.

LITERATURE CITED

Abdullah, M., Low, G. K. C.; Matthews, R. W. Effects of common inorganic anions on rates of photocatalytic oxidation of organic carbon over illuminated titanium dioxide, *J. Phys. Chem.* **1990**, 94, 6820-6825.

Al-Ekabi, H.; Serpone, N.; Pelizzetti, E.; Minero, C.; Fox, M. A.; Draper, R. B. Kinetic studies in heterogeneous photocatalysis. 2. Titania-mediated degradation of 4-chlorophenol alone and in a three-component mixture of 4-chlorophenol, 2,4-dichlorophenol, and 2,4,5-trichlorophenol in air-equilibrated aqueous media. *Langmuir* **1989**, 5(1), 250-255.

Alif A.; Boule, P. Photochemistry and environment Part XIV. Phototransformation of nitrophenols induced by excitation of nitrite and nitrate ions. *J. Photochem. Photobiol. A: Chem.* **1991**, 59, 357-367.

Benson, J.; Caplan, I.; Jacobs, R. Blackwater and graywater on U.S. Navy ships; technical challenges and solutions. *Navel Eng. J.* **1999**, 111(3), 293-305.

Bhatkhance, D. S.; Pangarkar, V. G.; Beenackers A. ACM. Photocatalytic degradation for environmental applications-a review. *J. Chem. Technol. and Biotechnol.* **2001**, 77, 102-116.

Bielski, B. H. J.; Cabelli, D. E.; Arudi, R. L.; Ross, A. B. Reactivity of perhydroxyl/ superoxide radicals in aqueous solution. *J. Phys. Chem. Ref. Data* **1985**, 14(4), 1041-1051.

Bonsen, E. M.; Schroeter, S.; Jacobs, H.; Broekaert, J. A. C. Photocatalytic degradation of ammonia with TiO_2 as photocatalyst in the laboratory and under the use of solar radiation. *Chemosphere* **1997**, 35(7), 1431-1445.

Bourikas, K.; Vakros, J.; Kordulis, C.; Lycourghiotis, A. Potentiometric mass titrations: experimental and theoretical establishment of a new technique for determining the point of zero charge (PZC) of metal (hydr) oxides. *J. Phys. Chem. B.* **2003**, 107, 9441-9451.

Braida, W.; Ong, S. K. Decomposition of nitrite under various pH and aeration conditions. *Wat, Air, Soil Pollu.* **2000**, 118, 13-26.

Bravo, A.; Garcia, J.; Domènech, X.; Peral, J. Some aspects of the photocatalytic oxidation of ammonium ion by titanium dioxide. *J. Chem. Res.* **1993**, 376-377.

Brusa, M. A.; Grela, M. A. Experimental upper bound on phosphate radical production in TiO_2 photocatalytic transformations in the presence of phosphate ions. *Phys. Chem. Chem. Phys.* **2003**, 5, 3294-3298.

Butler, D.; Friedler, E.; Gatt, K. Characterizing the quantity and quality of domestic wastewater inflows. *Water Sci.Technol.* **1995**, 31(7), 13-24.

Buxton, G.V., Greenstock, C. L.; Helman, W P.; Ross, A. B. Rate constants for reactions of radicals in aqueous solution. *J. Phys. Chem. Ref. Data* **1988**, 17, 514-525.

Calza, P.; Pelizzetti, W. Photocatalytic transformation of organic compounds in the presence of inorganic ions. *Pure Appl. Chem.* **2001**, *73*, 1839-1848.

Castles, M. A.; Moore, B. L.; and Ward, S. R. Measurement of linear alkylbenzenesulfonates in aqueous environmental matrixes by liquid chromatography with fluorescence detection. *Anal. Chem. (Wash.)* **1989,** 61(22), 2534-2340.

Chen, H.; Zahraa, O.; Bouchy, M. A. Inhibition of the adsorption and photocatalytic degradation of an organic contaminant in an aqueous suspension of TiO_2 by inorganic ions. *J. Photochem. Photobiol.* **1997**, 108, 37-44.

Chen, S.; Cao, G. Photocatalytic oxidation nitrite by sunlight using TiO_2 supported on hollow glass microbeads. *Solar Energy*, **2002**, 73(1), 15-21.

Chen, F.; Zhao, J.; Hidaka, H. Adsorption factor and photocatalytic degradation of dye-constituent aromatics on the surface of TiO_2 in the presence of phosphate anions. *Res. Chem. Intermed.* **2003**, 29(7-9), 733-748.

Chu, W. Modeling the quantum yields of herbicide 2,4-D decay in UV/H_2O_2 process. *Chemosphere*, **2001**, 44, 935-941.

Christensen, M. H; Harremoes, P. Nitrification and denitrification in wastewater treatment. *Wat. Pollut. & Microbiol.* **1978**, 2, 391-414.

Connor, P. A.; McQuillan, A. J. Phosphate adsorption onto TiO_2 from aqueous solutions: an in situ internal reflection infrared spectroscopic study. *Langmuir*, **1999**, 15, 2916-2921.

Daniels, M.; Meyers, R. V.; Belardo, E. V. Photochemistry of the aqueous nitrate system. I. Excitation in the 300-mμ band. *J. Phys. Chem.* **1968**, 72, 389-399.

Degussa Website, **https://www1.sivento.com/wps/portal/p3/aerosil/productsearch,** accessed on March 4, 2004**.**

Delwiche, C. C. *Denitrification, Nitrification, and Atmosphere Nitrous Oxide*, John Wiley & Sons: New York, **1981**, pp107-108.

Eriksson, E.; Auffarth K.; Henze, M.; Ledin, A. Characteristics of grey water. *Urban Water* **2002**, 4, 85-104.

Ervens, B.; Gligorovski, S.; Herrmann, H. Temperature-dependent rate constants for hydroxyl radical reactions with organic compounds in aqueous solutions. *Phys. Chem. Chem. Phys.* **2003**, 5(9), 1811-1824.

Europe Union (EU) drinking water standards, http://www.lenntech.com/EU's-drinking-water-standards.htm, accessed on February 13, **1998**.

Fabbri, D.; Prevot, A. B.; Pramauro, E. Kinetic effects of SDS on the photocatalytic degradation of 2,4,5-trichlorophenol. *Appl. Catal. B: Environ.* **2004,** 49, 233-238.

Fabbri, D.; Prevot, A. B.; Pramauro, E. Effect of surfactant microstructures on photocatalytic degradation of phenol and chlorophenols. *Appl. Catal. B:Environ.* **2006***,* 62, 21-27.

Fang, H.; Chuo, M.; Huang, C. Nitrification of ammonia-nitrogen in refinery wastewater, *Water Res.* **1993**, 27, 1761-1765.

Fernández-Nieves, A.; Richter, C. N.; De las Nieves, F. J. Point of zero charge estimation for a TiO_2/water interface. *Prog. Coll. Poly. Sci.* **1998**, 110, 21-24.

Focht, D. D.; Chang, A. C. Nitrification and denitrification processes related to waste water treatment. *Adv. in Appl. Microbiol.* **1975**, 19, 153-186.

Fox M. A., and Dulay M. T., 1993, Heterogeneous photocatalysis, *Chem. Rev.* **1993**, 93, 341-357.

Gelover, S.; Leal, T.; Bandala, E. R.; Román, A.; Jimenez, A.; Estrada, C. Catalytic photodegradation of alkyl surfactants. *Water Sci. Technol.* **2000**, 42(5-6), 101-106.

[a] Gopalarao, G; Murty, K. S. Photosensitisation by solids. Part II. Photosensitized oxidation of ammonia in aqueous solution with titania as the photosensitiser. *J. Indian Chem. Soc.* **1941**, 18, 127-137; [b]Gopalarao G.; Varadanam, C. I. Photosensitization

by solids. Part III. Photosensitized oxidation of ammonia in aqueous solution with colloidal titania as the photosensitiser. *J. Indian Chem. Soc.* **1941**, 18, 361-370.

Goldstein, S.; Czapski, G.; Lind, J.; Merenyi, G. Mechanism of decomposition of peroxynitric ion (O_2NOO^-): evidence for the formation of $O_2^{\bullet-}$ and $^{\bullet}NO_2$ radicals. *Inorg. Chem.* **1998**, 37, 3943-3947.

Gupta, S.; Pal, A.; Gosh, P. K. Bandyopadhyay, M. Performance of waste activated carbon as a low-cost adsorbent for the removal of anionic surfactant from aquatic environment *J. Environ. Sci. Health, Part A* **2003**, 38, 381- 397.

Hermann, R.; Gerke, J.; Ziechmann, W. Photodegradation of the surfactants Na-dodecylbenzendsulfonate and dodecylpyridinium-chloride as affected by humic substances. *Water, Air, Soil Pollut*. **1997**, 98, 43-55.

Herrmann, J. Heterogeneous photocatalysis: fundamentals and applications to the removal of various types of aqueous pollutants. *Catal. Today* **1999**, 53, 115-129.

Hidaka, H.; Kubota, H.; Graetzel, M.; Pelizzetti, E.; Serpone, N. Photodegradation of surfactants. II: degradation of sodium dodecylbenzenesulfonate catalyzed by titanium dioxide particles. *J. Photochem.* **1986**, 35(2), 219-30.

Hidaka, H.; Yamada, S.; Suenaga, S.; Zhao, J. Photodegradation of surfactants part VI complete photocatalytic degradation of anionic cationic and nonionic surfactants in aqueous semiconductor dispersions. *J. Mol. Catal.* **1990**, 59, 279-290.

Hidaka, H.; Zhao, J.; Pelizzetti, E.; Serpone, N. Photodegradation of surfactants. 8. Comparison of photocatalytic processes between anionic sodium dodecylbenzenesulfonate and cationic benzyldodecyldimethylammonium chloride on the TiO_2 surface. *J. Phys. Chem.* **1992**, 96, 2226-2230.

Hidaka, H.; Nohara, K.; Zhao, J.; Pelizzetti, E.; Serpone, N. Photodegradation of surfactants XIV. Formation of NH_4^+ and NO_3^- ions for the photocatalyzed mineralization of nitrogen-containing cationic, non-ionic and amphoteric surfactants. *J. Photochem. Photobiol. A: Chem.* **1995**, 91, 145-152.

Hingston, F. J.;. Atkinson, R. J; Posner, A. M.; Quirk, J. P. Specific adsorption of anions. *Nature*, **1967**, 215, 1459-1461.

Hoffmann, M. R.; Martin, S. T.; Choi, W. Y.; Bahnemann, D. W. Environmental applications of semiconductor photocatalysis. *Chem. Rev.* **1995**, 95(1), 69-96.

Horikoshi, S.; Watanabe, N.; Onishi, H.; Hidaka, H.; Serpone, N. Photodecomposition of a nonylphenol polyethoxylate surfactants in a cylindrical photoreactor with TiO_2 immobilized fiberglass cloth. *Appl. Catal. B: Environ.* **2002**, 37, 117-129.

Hu, C.; Yu, J.; Hao, Z.; Wong, P. K. Effects of acidity and inorganic ions on the photocatalytic degradation of different azo dyes. *Appl. Catal. B: Environ.* **2003**, 46, 35-47.

Hu, C.; Tang, Y.; Lin, L.; Hao, Z.; Wang, Y.; Tang, H. Effect of inorganic anions on photoactivity of various photocatalysts under different conditions. *J. Chem. Technol. Biotech.* **2004**, 79, 247-252.

Hued, A. C.; Caruso, M. N.; Wunderlin, D. A.; Bistoni, M. A. Field and in vitro evaluation of ammonia toxicity on native fish species of the central region of Argentina. *B. Environ. Contam. and Tox.* **2006**, 76(6), 984-991.

Hurse, T.; Connor, M. Nitrogen removal from wastewater treatment lagoons. *Water Sci. Technol.* **1999**, 39, 191-198.

Jayson, G. G.; Parsons, B. J.; Swallow, A. J. Some simple, highly reactive, inorganic chlorine derivatives in aqueous solution. *J. Chem.Soc., Faraday Trans. 1: Phys. Chem. Condensed Phases* **1973**, 69(9), 1597-1607.

Jenkins, D.; Snoeyink, V. L.; Ferguson, J. F.; Leckie, J. O. *Water Chemistry Laboratory Manual,* Third Edition, John Wiley & Sons: New York, 1980.

Jiménez, A. E.; Estrada, C. A.; Cota, A. D.; Román, A. Photocatalytic degradation of DBSNa using solar energy. *Sol. Energy Mater. & Sol. Cells* **2000**, 60, 85-95.

Jøergensen, S. E.; Libor, O.; Graber, K. Lea; Barkacs, K.; Copenhagen, Den. Ammonia removal by use of clinoptilolite**.** *Water Res.* **1976**, 10(3), 213-24.

Karsa, D. R.; Bailey, R. M.; Shelmerdine, B.; McCann, S. A. *Overview: a decade of change in the surfactant industry. In Industrial Applications of Surfactants* IV, edited by Karsa, D. R., Akcros Chemical Lts: Manchester, UK, **1999**.

Kochany, J.; Lipczynska-Kochany, E. Application of the EPR spin-trapping technique for the investigation of the reactions of carbonate, bicarbonate, and phosphate anions with hydroxyl radicals generated by the photolysis of H_2O_2. *Chemosphere*, **1992**, 25 (12), 1769-1782.

Konopka, A.; Zakharova, T.; Oliver, L.; Turco, R. F. Microbial biodegradation of organic wastes containing surfactants in a continuous-flow. *J. Ind. Microbiol. & Biot.* **1997**, 18(4), 235-240.

Kosmulski, M. pH-dependent surface charging and point of zero charge II. update. *J. Coll. Inter. Sci.* **2004***,* 275, 214-224.

Kudo, A., Domen, K., Maruya, K., Onishi, T. Photocatalytic reduction of NO_3^- to form NH_3 over Pt-TiO_2, *Chem. Let.* **1987**, 1019-1022.

Kuo, C. H.; Yuan, F.; Hill, D. O. Kinetics of oxidation of ammonia in solutions containing ozone with or without hydrogen peroxide. *Ind. Eng. Chem. Res.* **1997**, 36(10), 4108-4113.

Lard, E. W.; Birnbaum, B. H.; Deane, T. N. Shipboard laundry wastewater treatment systems. *Am. Soc. Mech. Eng.* **1976**, 76, 1-8.

Larson, R. A.; Zepp, R. G. Reactivity of the carbonate radical with aniline derivatives. *Environ. Toxicol. Chem.* **1988**, 7(4), 265-274.

Lee, J.; Park, H.; Choi, W. Selective photocatalytic oxidation of NH_3 to N_2 on platinized TiO_2 in water. *Environ. Sci. Technol.* **2002**, 36(24), 5462-5468.

Leng, W.; Liu, H.; Cheng, S.; Zhang, J.; Cao, C. Kinetics of photocatalytic degradation of aniline in water over TiO_2 supported on porous nickel. *J. Photochem. Photobiol. A: Chem.* **2000**, 131, 125-132.

Letterman, R. D. *Water quality and treatment: a handbook of community water supplies,* AWWA, Fifth Edition, McGraw-Hill, **1999**, Chapter 6.

Li, Q.; Xie, R.; Shang, J. Mintz, E. Effect of precursor ratio of synthesis and optical absorption of TiON photocatalytic nanoparticles. J. Am. Ceram. Soc., **2007**, 90(4), 1045-1050.

Li, Y. X.; Wasgestian, F., Photocatalytic reduction of nitrate ions on TiO_2 by oxalic acid, *J. Photochem. and Photobiol. A: Chem.* **1998**, 112, 255-259.

Li, H. Y.; Tripp, C. P. Spectroscopic identification and dynamics of adsorbed cetyltrimethylammonium bromide structures on TiO_2 surfaces. Lanmuir, **2002**, 18, 9441-9446.

Liao, C.H.; Kang, S.F.; Wu, F.A. Hydroxyl radical scavenging role of chloride and bicarbonate ions in the H_2O_2/UV process. *Chemosphere*, **2001**, 44, 1193-1200.

Litter, M. I. Heterogeneous photocatalysis: transition metal ions in photocatalytic systems. *Appl. Cataly. B: Environ*. **1999**, 23(2-3), 89-114.

Low, G. K. C.; McEvoy, S. R.; Matthews, R. W. Formation of nitrate and ammonium ions in titanium dioxide mediated photocatalytic degradation of organic compounds containing nitrogen atoms. *Environ. Sci. Technol.* **1991**, 25, 460-467.

Løgager, T.; Sehested, K. Formation and decay of peroxynitrous acid: a pulse radiolysis study. *J. Phys. Chem*. **1993**, 97(25), 6664-6669.

Lyndon, B. Advanced Life Support Program Requirements Definition and Design Considerations. NASA CTSD-ADV-245 (Rev A). Johnson Space Center, Houston, TX, **1996**.

Mack, J.; Bolton, J. R. Photochemistry of nitrite and nitrate in aqueous solution: a review. *J. Photochem. Photobiol. A: Chem.* **1999**, 128, 1-13.

Mark, G.; Korth, H. G.; Schuchmann, H. P.; von Sonntah, C. The photochemistry of aqueous nitrate ion revisited. *J. Photochem. Photobiol. A: Chem.* **1996**, 101, 89-103.

Maruthamuthu, P.; Neta, P. Phosphate radicals. spectra, acid-base equilibria, and reaction with inorganic compounds. *J. Phys. Chem.* **1978**, 82(6), 710-713.

Miller, J. C.; Miller, J. N. *Statistics for Analytical Chemistry*, second Edition, Chichester, England : E. Horwood ; New York: Halsted Press, **1988**, pp.33-50.

Milis, A.; Domènech, X. Photoassisted oxidation of nitrite and nitrate over different semiconducting oxides. *J. Photochem. Photobiol. A: Chem.* **1993**, 72, 55-59.

Milis, A.; Peral, J.; Domènech, X.; Navío, J. A. Heterogeneous photocatalytic oxidation of nitrite over iron-doped TiO_2 samples. *J. Mol. Cataly., A: Chem.* **1994**, 87(1), 67-74.

Mills, A.; Davies, R. H.; Worsley, D. Water purification by semiconductor photocatalysis. *Chem. Soc. Rev.* **1993**, 22(6) 417-425.

Nagarajan, R.; Wang, C. Solution behavior of surfactants in ethylene glycol: probing the existence of a CMC and of micellar aggregates. *J. Colloid Interf. Sci.* **1996**, 178, 471-482.

Nagaveni, K.; Sivalingam, G.; Hegde, M. S.; Madras, G. Solar photocatalytic degradation of dyes: high activity of combustion synthesized nano TiO_2. *Applied Cataly. B: Environ.* **2004**, 48(2), 83-93.

Neta, P.; Maruthamuthu, P.; Carton, P.M.; Fessenden, R.W. Formation and reactivity of the amino radical. *J. Phys. Chem.* **1978**, 82, 1875-1878.

Neta, P., Huie, R. E., Ross, A. B.Rate constants for reactions of inorganic radicals in aqueous solution. *J. Phys. and Chem. Ref. Data*, **1988**, 17, 1027-1262.

Ogata, Y.; Tomizawa, K.; Adachi, K. Photo-oxidation of ammonia with aqueous hydrogen peroxide. *Mem. Fac. Eng., Nagoya Univ.* **1981**, 3(1), 58-65.

Ohtaki, M.; Sato, H.; Fujii, H.; Eguchi, K. (2000) Intermolecularly selective decomposition of surfactant molecules on photocatalytic oxidative degradation over TiO_2 photocatalyst. *J. Mol. Catal. A: Chem.* **2000**, 155, 121-129.

O'Shea, K. E.; Cardona, C. The reactivity of phenol in irradiated aqueous suspensions of TiO_2 mechanistic changes as a function of solution pH. *J. Photochem. Photobiol. A: Chem.* **1995**, 91(1), 67-72.

O'Shea, K. E.; Pernas, E.; Saiers J. The influence of mineralization products on the coagulation of TiO_2 photocatalyst. *Langmuir* **1999**, 15(6), 2071-2076.

Őzkan, A.; Őzkan, M. H.; Gűrkan, R.; Akcay, M.; Sőkmen, M. Photocatalytic degradation of a textile azo dye, Sirius Gelb GC on TiO_2 or Ag-TiO_2 particles in the absence and presence of UV irradiation: the effect of some inorganic anions on the photocatalysis. *J. Photochem. Photobiol. A: Chem.* **2004**, 163, 29-35.

Pagsberg, P. B. Investigation of the NH_2 radical produced by pulse radiolysis of ammonia in aqueous solution. *Ris Report*, **1972**, 256, 209-221.

Pelizzetti, E.; Serpone, N. *Photocatalysis, Fundamental and Applications*, John Wiley & Sons: New York, **1989**, pp 218-223.

Pirkanniemi, K.; Sillanpää, M. Heterogeneous water phase catalysis as an environmental application: a review. *Chemosphere* **2002**, 48(10), 1047-1060.

Pollema, Cy H.; Milosavljević, E. B.; Hendrix, J. L.; Solujić, L.; Nelson, J. H. Photocatalytic oxidation of aqueous ammonia (ammonium ion) to nitrite or nitrate at TiO_2 particles. *Monatsh. Chem.* **1992**, 123, 333-339.

Penfold, J.; Staples, E.; Tucker, I. On the consequences of surface treatment on the adsorption of nonionic surfactants at the hydrophilic silica-solution interface. *Langmuir* **2002**, 18, 2967-2970.

Pramanick, D.; Sarkar, J. Studies on some radical transfer reactions by entrapping the radicals as polymer endgroups. Part V. Reaction of OH radical with sulfonated and sulfated substrates. *J. Polym. Mater.* **2000**, 17(2), 127-132.

Prevot, A. B.; Pramauro, E.; Guardia, M de la (1999) Photocatalytic degradation of carbaryl in aqueous TiO_2 suspensions containing surfactants. *Chemosphere* **1999**, 39(3), 493-502.

Ramon, G.; Green, M.; Semiat, R; Dosoretz, C. Low strength graywater characterization and treatment by direct membrane filtration. *Desalination* **2004**, 170(3), 241-250.

Randall, D. J.; Tsui, T. K. N. Ammonia toxicity in fish. *Marine Pollution Bulletin* **2002**, 45, 17-23.

Rao, C. S. Sources and classification of water pollutants. *Environmental pollution control engineering*, Third Edition, Wiley Eastern Ltd: New York, **1995**, pp 301-302.

Rose, J. B.; Sun, G.; Gerba, C. P.; Sinclair, N. A. Microbial quality and persistence of enteric pathogens in graywater from various household sources. *Water Res.* **1991**, 25(1), 37-42.

Rosen, M. J. *Surfactants and interfacial phenomena*. Third Edition, John Wiley & Sons, Inc.: New Jersey, **2004,** pp, 46-49; 121-148.

Roesner, L.; Qian, Y.; Criswell, M.; Stromberger, M.; and Klein, S. *Long-term effects of landscape irrigation using household graywater-literature review and synthesis*; Water Environment Researc Foundation (WERF) and the Soap and Detergent Association (SDA): Fort Collins, **2006**; pp 1-82.

Ross, F.; Ross, A. B. *Selected specific rates of reactions of transients from water in aqueous solution. III. Hydroxyl radical and perhydroxyl radical and their radical ions*, Report, National Bureau of Standards, NSRDS-NBS 59, **1977**.

Sangchakr, B; Hisanaga, T.; Tanaka, K. Photocatalytic degradation of sulfonated aromatics in aqueous TiO_2 suspension. *J. Photochem. Photobiol. A: Chem.* **1995**, 85, 187-190.

Schuchmann, M. N.; Bothe, E.; von Sonntag, J.; von Sonntag, C. Reaction of OH radicals with benzoquinone in aqueous solutions. A pulse radiolysis study. *J. Chem. Soc., Perkin Trans. 2: Phys. Org. Chem.* **1998**, (4), 791-796.

Senn, P. Numerical computation of surface areas of molecules. *J. Math. Chem.* **1991**, 6, 351-358.

Sharpless, C. M.; Linden, K. G. UV photolysis of nitrate: effects of natural organic matter and dissolved inorganic carbon and implications for UV water disinfection. *Environ. Sci. Technol.* **2001**, 35, 2949-2955.

Sigma website: http://www.sigmaaldrich.com/catalog/search/ProductDetail/SIAL/P1254, accessed on December 12, 2006.

Skoog, D. A.; West, D. M.; Holler, F. J. *Fundamentals of Analytical Chemistry*, Thomson Learning, Inc., **1996**, pp 33-39.

Sökmen, M.; and Özkan, A., Decolourising textile wastewater with modified titania: the effect of inorganic anions on the photocatlysis. *J. Photochem. Photobio. A: Chem.* **2002**, 147, 77-81.

Staehelin, J.; Hoigné, J. Decomposition of ozone in water: rate of initiation by hydroxide ions and hydrogen peroxide. *Environ. Sci. Technol.* **1982**, 16, 676-681.

Steinfeld, J. I.; Francisco, J. S.; Hase, W. L. *Chemical Kinetics and Dynamics*, Second Edition, Upper Saddle River: New Jersey, **1999**, pp 25-27.

Stumm, W.; Morgan, J. J. *Aquatic Chemistry*: *Chemical Equilibria and Rates in Natural Waters*, Third Edition, John Wiley & Sons: New York, **1996**, pp120-129, 152.

Sun, C. C.; Chou, T. C. Detoxification of nitrite ion in suspension TiO_2 aerobic aqueous solution. *J. Chin. Inst. Chem. Engrs.* **1999**, 30(1), 59-69.

Takeda, K.; Fujiwara, K. Characteristics on the determination of dissolved organic nitrogen compounds in natural waters using titanium dioxide and platinized titanium dioxide mediated photocatalytic degradation. *Wat. Res.* **1996**, 30(2), 323-330.

Taylor, J. K.; Cihon, C. *Statistical techniques for data analysis*, Second Edition, Chapman and Hall/CRC: New York, **2004**, p 208.

Tchobanoglous, G.; Burton, F. L.; Stensel, H. D. *Wastewater Engineering: Treatment and Reuse*, Third Edition, McGraw-Hill: Boston **2003**, p.109.

Tilak, K. S.; Lakshmi, S. J.; Susan T. A. The toxicity of ammonia, nitrite and nitrate to the fish, *Catla catlat* (Hamilton). *J. Environ. Biol.* **2002**, 23(2), 147-149.

Turchi, C. S.; Ollis, D. F. Mixed reactant photocatalysis: intermediates and mutual rate inhibition. *J. Catal.* **1989**, 119, 483-496.

United States Environmental Protection Agency (US EPA), Wastewater technology fact sheet-ammonia stripping, Washington, D. C. EPA 832-F-00-019, September **2000**.

United Nation, Population Fund, UN FPA, 2001, http://www.unfpa.org/swp/2001/english/ch02.html.

Yoon, Y.; Lueptow, R. M. Reverse osmosis membrane rejection for ersatz space mission wastewaters. *Water Res.* **2005**, 39, 3298-3308.

Wang, A. H. *Photoassisted oxidation of aqueous ammonia with or without iron-doped titanium dioxide*. Master's Thesis. The University of Toledo, USA, **1991**.

Wang, A. H.; Edwards, J. G.; Davies, J. A. Photooxidation of aqueous ammonia with titania-based heterogeneous catalysis. *Solar Energy* **1994**, 52(6), 459-466.

Wang, K.; Hsieh,Y.; Chou, M.; Chang, C. Photocatalytic degradation of 2-chloro and 2-nitrophenol by titanium dioxide suspensions in aqueous solution. *Appl. Catal. B: Environ.* **1999**, 21, 1-8.

Wu, G.; Katsumura, Y.; Muroya, Y.; Lin, M.; Morioka, T. Temperature Dependence of Carbonate Radical in $NaHCO_3$ and Na_2CO_3 Solutions: Is the Radical a Single Anion? *J. Phys. Chem*. *A* **2002**, 106, 2430-2437.

Xia, X. H.; Xu, J. L.; Yun, Y. Effects of common inorganic anions on the rates photocatalytic degradation of sodium dodecylbenzenesulfonate over illuminated titanium dioxide. *J. Environ. Sci.* **2002**, 14, 188-194.

Zafra, A.; Garcia, J.; Milis, A.; Domènech, X. Kinetics of the catalytic oxidation of nitrite over illuminated aqueous suspensions of TiO_2. *J. Mol. Catal. A: Chem.* **1991**, 70, 343-349.

Zhang, T.; Oyama, T.; Horikoshi, S.; Zhao, J.; Serpone, N.; Hidaka, H. Photocatalytic decomposition of the sodium dodecylbenzene sulfonate surfactant in aqueous titania suspensions exposed to highly concentrated solar radiation and effects of additives. *Appl. Catal. B: Environ.* **2003**, 42, 13-24.

Zhang, W.; An, T.; Cui, M.; Sheng, G.; Fu, J. Effects of anions on the photocatalytic and photoelectrocatalytic degradation of reactive dye in a packed-bed reactor. *J. Chem. Technol. Biotechnol.* **2005**, 80, 223-229.

Zhao, J.; Oota, H; Hidaka, H.; Pelizzetti, E.; Serpone, N. Photodegradation of surfactants X. Comparison of the photo-oxidation of the aromatic moieties in sodium

dodecylbenzene sulfonate and in sodium phenyldodecyl sulfonate at TiO_2-H_2O interfaces. *J. Photochem. Photobiol. A: Chem.* **1992**, 69(2), 251-256.

Zhao, J.; Hidaka, H.; Takamura, A.; Pelizzetti, E.; Serpone, N. Photodegradation of surfactants. 11. ξ -Potential measurements in the photocatalytic oxidation of surfactants in aqueous titania dispersions. *Langmuir* **1993**, 9(7), 1646-1650.

Zhao, J.; Wu, K.; Wu, T.; Hidaka, H.; Serpone, N. (1998) Photodegradation of dyes with poor solubility in an aqueous surfactant/TiO_2 dispersion under visible light irradiation. *J. Chem. Soc., Faraday Trans.* **1998**, 94(5), 673-676.

Zoller, U. The "hard" and "soft" surfactant profile of Israel municipal wastewaters. *J. Am. Oil Chem. Soc.* **1985**, 62(6), 1006-1009.

Zoller, U. The surfactant profile of municipal wastewater: influents and effluents. *Water Sci. Technol.* **1985**, 17(8), 1451-1452.

Zoller, U.; Hushan, M. The nonionic surfactant pollution profile of Israel's Mediterranean Sea coastal water. *Water Sci. Technol.* **2000**, 42(1-2), 429-435.

APPENDIX A

Detailed Experimental Procedures

Preparation of stock solutions for kinetic batch experiments

0.01 M NH_4Cl stock solution. Weigh 0.107 g ammonium chloride into a 200 mL volumetric flask and fill it to the marked line with nanopure water.

0.1 M NaCl stock solution. Weigh 0.5844 g sodium chloride into a 100 mL volumetric flask and fill it to the marked line with nanopure water. Also weigh a certain amount of other inorganic anions (SO_4^{2-}, $H_2PO_4^-/HPO_4^{2-}$, and HCO_3^-/CO_3^{2-}) for the effect of inorganic anions on the photocatalytic degradation of NH_4^+/NH_3 and NO_2^-.

0.002 M surfactant stock solution. Weigh a certain amount of a surfactant into a 500 mL volumetric flask and fill it to the marked line with nanopure water.

Step by step procedures to conduct a typical kinetic batch experiment of $NH_4^+NH_3$ photocatalytic degradation

1. Add 13 mL 0.01 M NH_4Cl and 0.1 M NaCl into a 1350 mL canning jar to obtain 1×10^{-3} M NaCl and 1×10^{-4} M NH_4Cl.
2. Add 13 mL 0.002 M surfactant stock solution (when the effect of surfactants on the photocatalytic degradation of NH_4^+/NH_3 is investigated) to obtain 2×10^{-5} M surfactant. Otherwise, skip this step.
3. Add 1274 mL nanopure water (or 1261 mL when a surfactant is present) into the canning jar so that the total volume of the solution is 1300 mL.

4. Put a stir bar into the jar and place the jar on the top of a magnetic stirrer, a piece of cardboard is placed between the stir plate and the jar to reduce heat transferring from the stirrer to the solution.
5. Weigh 3.9 g Degussa P25 TiO_2 into the solution to obtain 3 g/L TiO_2.
6. Use 0.5 M NaOH to adjust the suspension pH to ~10.
7. The solution is covered with a piece of aluminum foil and a black plastic bag to keep the suspension in the dark for 24 hours to reach adsorption equilibrium. If the suspension contains a surfactant, 48 hours is required instead.
8. The suspension is then transferred to a Pyrex reactor from Ace glass
9. A quartz cooling water jacket is inserted into the reactor, and a UV lamp is placed inside of the cooling water jacket.
10. Put a Ross pH electrode (Orion) and NaOH transferring tip into the reactor to control the reaction pH around 10.1 when studying the effect of surfactants on the photocatalytic degradation of NH_4^+/NH_3. Otherwise go to next step.
11. Turn on the tap water and let water flow through the cooling water jacket to remove the heat that is produced from the UV lamp, to maintain the suspension temperature around 25-32 ºC.
12. Take about 35 mL TiO_2 suspension before the light is turned on. The suspension is filtered through a piece of 0.1 μm membrane to remove TiO_2 particles for the measurement of NH_4^+/NH_3, NO_2^-, and NO_3^-. When surfactants (hexadecylpyridinium chloride (CPC), sodium dodecylbenzene sulfonate (SDBS), and nonylphenol polyethoxylate (10) (NP10)) are present in the suspension,

another 10 mL suspension is withdrawn to measure the concentration of surfactants and total organic carbon (TOC).

13. Turn on the UV lamp and start the photocatalytic degradation of NH_4^+/NH_3 and surfactants (when surfactants are present in some instances).
14. Take suspensions at certain time intervals until about 60% of the initial concentration of NH_4^+/NH_3 is degraded. The suspensions are treated the same way as described in Step 12.

Preparation of IC stock solution and standards

1. *Prepare a 0.02 M stock solution of formate, acetate, NO_2^-, NO_3^-, SO_4^{2-}, and HPO_4^{2-}.* Add 0.136 g sodium formate, 0.2722 g sodium acetate, 0.138 g sodium nitrite, 0.17 g sodium nitrate, 0.284 g sodium sulfate, and 0.356 g disodium hydrogen phosphate dihydrate to a 100 mL volumetric flask. Fill the flask to the marked line with nanopure water.
2. *Prepare calibration standards by diluting the stock solution (0.02 M).* For example, to prepare a 1×10^{-5} M of anions mentioned in step 1, add 50 μL of 0.02 M stock solution to a 100 mL volumetric flask and fill the flask to the marked line with nanopure water. The following table provides the volumes of stock solution to prepare standards at given concentrations.

Table A1. Calibration standards for IC analysis (100 mL in total)

[Anion], M	$V_{stock\ soln}$ (μL)
2.5×10^{-6}	12.5
5×10^{-6}	25
1×10^{-5}	50
5×10^{-5}	250
1×10^{-4}	500
2×10^{-4}	1000

Preparation of GC/FID stock solution and standards

A headspace method was used to determine the concentration of *n*-BuCl during homogeneous photodegradation of *n*-BuCl. Two stock solutions are first prepared and then the standards are prepared from the second stock solution.

1. *Preparation of n-BuCl stock solution 1 (2.42×10^{-3} M).* Add 15 μl 99% *n*-BuCl into a serum bottle with actual volume of 59 mL. The bottle is rapidly capped with a Teflon-lined rubber septum and crimp-seal it. The solution is then put on a shaker in a constant temperature chamber and shake for 24 hours to ensure that the dissolution of *n*-BuCl into nanopure water is completed.
2. *Preparation of n-BuCl stock solution 2 (1.01×10^{-5} M).* Add 245 μL stock solution 1 into another serum bottle (59 mL). The bottle is rapidly capped with a Teflon-lined rubber septum and crimp-seal it. The solution is then put on a shaker in a constant temperature chamber and shake for 24 hours.
3. *Preparation of n-BuCl calibration standards.* Calibration standards of *n*-BuCl are prepared by diluting the stock solution 2 of *n*-BuCl. For example, to prepare a

concentration of 6.28×10^{-8} M *n*-BuCl standard, a 25 μL of *n*-BuCl stock solution 2 and 3.975 mL nanopure water are added into a 22 mL vial and crimp-sealed with a Teflon-lined rubber septum. The following table A2 summarizes the volumes of water and stock solution 2 to prepare given concentrations of standards.

Table A2. Calibration standards for GC/FID analysis (4 mL solution in 22 mL vials)

[*n*-BuCl], M	V_{water} (mL)	$V_{stock\ soln}$ (mL)
6.28×10^{-8}	3.975	0.025
1.26×10^{-7}	3.95	0.05
2.51×10^{-7}	3.9	0.1
5.03×10^{-7}	3.8	0.2
1.26×10^{-6}	3.5	0.5
2.51×10^{-6}	3	1
6.28×10^{-6}	1.5	2.5

Procedures for determination of NH_4^+/NH_3

1. Prepare a series of calibration standards (the lowest concentration should be at or higher than 5×10^{-6} M) from a 0.01 M NH_4Cl stock solution.
2. Rinse the electrode with nanopure water and blot the water off (do not touch membrane).
3. Connect the ammonia electrode to the pH meter, and choose mV mode by pressing "**Mode"** on the pH meter until "mV" appears.
4. Immerse the electrode into 10 mL a pH 4 buffer solution until the number on the meter is around 130.

5. Rinse the electrode with nanopure water and immerse the electrode into the lower standard solution (10 mL), attention should be paid that there is no bubbles on the membrane.
6. Add 0.2 mL ionic strength adjustment (ISA) solution and press "**Measure**" button on the meter.
7. Wait until the meter says "**ready**" and record the number shown on the screen of the pH meter.
8. Remove the electrode from the solution and rinse it with nanopure water.
9. Follow step 5 to step 8 and measure higher concentrations.
10. After finishing the standards measurement, measure unknown samples using the same procedure. All standards and samples are measured in duplicates. One blank is measured before the first standard and sample.
11. When all samples are measured, rinse the electrode with nanopure water and soak it in a 0.1 M NH_4Cl solution without adding ISA.

Note: if the electrode will not be used for more than one week, dissemble completely and rinse the inner body, out body and bottom cap with nanopure water. Dry and reassemble electrode without filling solution or membrane.

Procedure for determination of power output of the UV lamp

1. Unplug two connectors (black and white) in the middle of the cords of the lamp.
2. Put a red connector on each disconnected cord of the lamp.
3. Turn on the Radioshack Digital Multimeter by pressing "SELECT" and switch it to the "V" function.
4. Double press "SELECT" until a sign of AC current "~" appears on the screen. The red and black cords are connected to the positive (V.mA.Ω) pole and negative pole (COM), respectively.
5. Plug both red and black leads of the multimeter across little red flakes in Step 2, and then turn on the lamp and record the reading of the voltage on the screen of the meter. Usually it will take 2-3 minutes to get a stable reading after the lamp is turned on.

6. Switch the red cord of the multimeter from positive pole to current measurement (10A MAX).
7. Switch the function from V to 10A for the measurement of current.
8. Disconnect one of the connector of the lamp (either white or black).
9. Use a piece of wire clamps on both ends to connect the multimeter to both ends of the connecter.
10. Turn on the lamp and record the reading of current.
11. Turn off the multimeter by pressing HOLD/ZERO and “RANGE” buttons.
12. Calculate the power output by multiplying current and voltage, if the output decreased 10% of the initial value, indicating that the lamp is attenuated. A new lamp should be replaced at this point.

APPENDIX B

Estimation of Illuminated Water Volume as a Function of TiO_2 Concentration

This appendix is related to chapter 2, providing details to estimate the illuminated water volume at a TiO_2 concentration range of 0-3 g/L.

First, a UV spectrum of TiO_2 suspension (0.025 g/L) was obtained by a Shimadzu 1601 UV-vis spectrophotometer, which is shown in Figure B1.

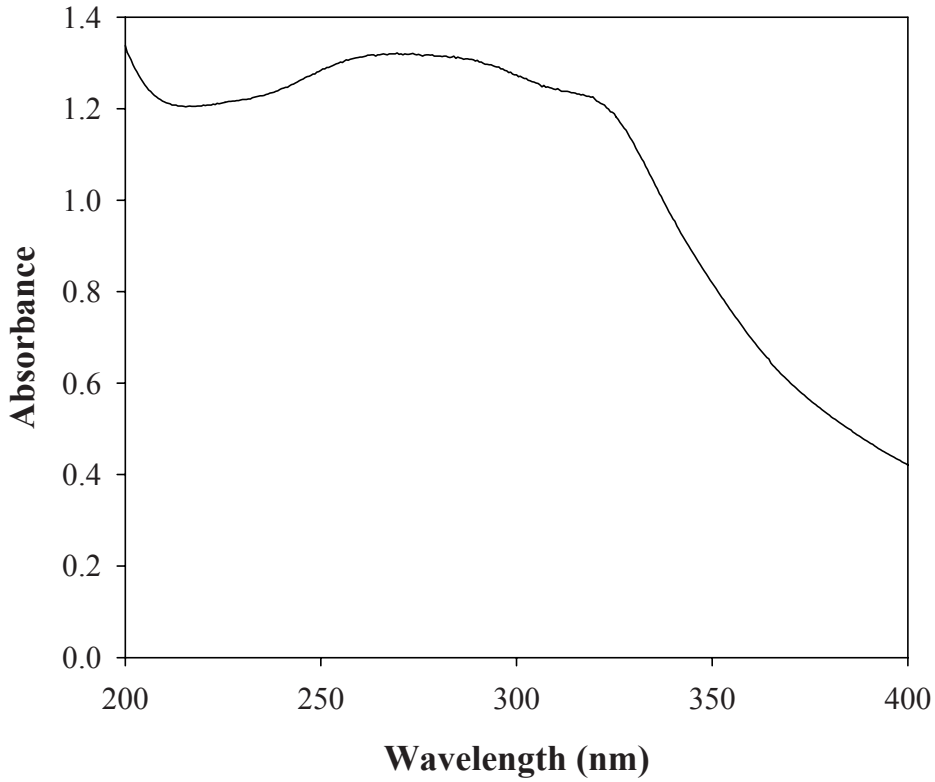


Figure B1. UV spectrum of 0.025 g/L TiO_2 suspension at pH 9.9.

It is known that the band-gap of the Degussa P25 TiO2 is ~3.2 eV (Li et al., 2007), which corresponds to a wavelength of 388 nm. From Figure B1, the absorbance (A) of the TiO_2 suspension at 388 nm is 0.482. We then applied the Beer-Lambert law

$$A = -\log T = -\log (I/I_0) = abc \qquad (B1)$$

Where A is UV absorbance; T is UV transmittance; I_0 and I represent for the initial light intensity before and after passing the suspension; a is the absorbance coefficient; b is the path length of the sample (cm); and c is the concentration of TiO_2 suspension in this case. Equation B1 was reorganized as:

$$a = A/bc \qquad (B2)$$

We calculated the absorbance coefficient with a value of 19.28 L g^{-1} cm^{-1} by plugging the values of A, b, and c. Since the coefficient "a" is only dependent on the nature of the solution at a certain wavelength, it is a constant at different concentration of TiO_2 at a wavelength of 388 nm.

Equation B1 was reorganized as

$$I/I_0 = 10^{-abc} \qquad (B3)$$

We defined r_1 as the distance between the center of the UV lamp and outside of the cooling water jacket (r_1 = 2.65 cm), r_2 as the radius of the photoreactor as described in chapter 2 (r_2 = 4.5 cm), and b as the distance that the UV light can pass through the water. We used an excel spreadsheet to calculate I/I_0 at a certain b and c. Then we sorted out b values at which I/I_0 = 0.01 for each TiO_2 concentration. The reason to choose I/I_0 = 0.01 is because 99% of the UV light was absorbed/scattered by the TiO_2 particles and the other 1% of the UV light would also be attenuated at a little further distance.

Furthermore, the value from the UV-vis spectrophotometer is not reliable UV transmittance is lower than 1%, i.e., $I/I_0 = 10^{-2} = 0.01$.

According to the b value, percentage of illuminated water volume (V/V_0) was calculated by dividing the illuminated water volume (V) by the total water volume in the reactor (V_0), according to the following equation:

$$\frac{V}{V_0} = \frac{\pi h((r_1 + b)^2 - r_1^2)}{\pi h(r_2^2 - r_1^2)} \qquad \text{(B4)}$$

Where h is the height of the suspension in the reactor. The illuminated water volume versus the TiO_2 concentration was then plotted, as shown in Figure B2. The actual values of the percentage of illuminated water volume vary with the chosen wavelength and the light intensity during the calculation, but the trend will be the same. After comparing the percentage of illuminated water volume as TiO_2 concentration increased, the extent to absorbing and scattering of the UV light by TiO_2 particles is obvious. In other words, homogeneous degradation of ammonia is insignificant when the TiO_2 concentration if at 3 g/L.

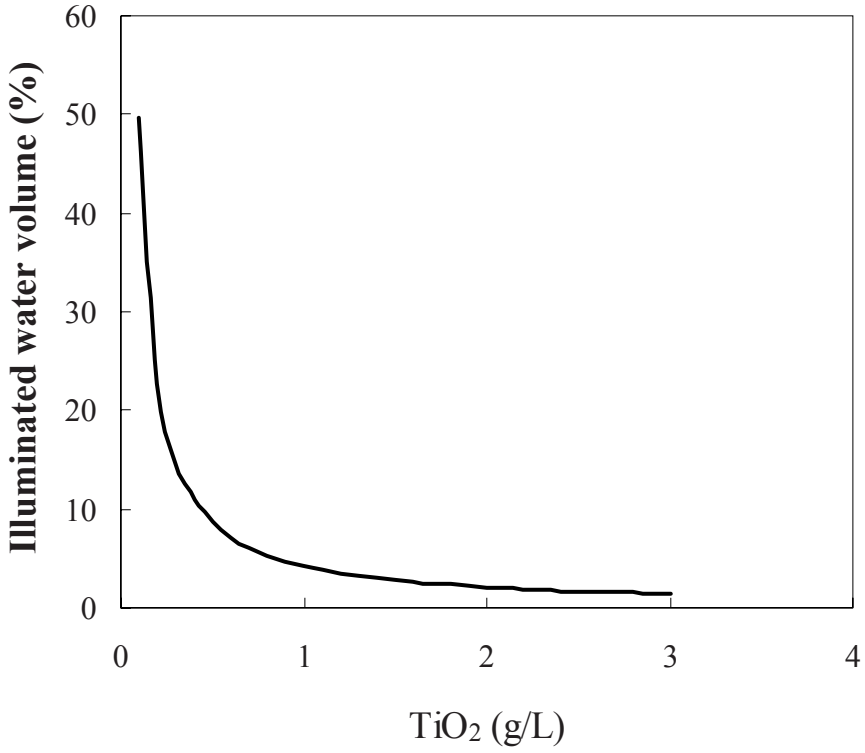


Figure B2. Percentage of illuminated water volume versus TiO_2 concentration at the light intensity (I/I_0) of 0.01 at a wavelength of 388 nm.

APPENDIX C

Sequential First Order Reaction Rate Law

The integrated differential equations corresponding to reaction 1.2 in chapter 2 are shown in equations C1-3 (Steinfeld et al., 1999).

$$[NH_3]_{T,\,t} = [NH_3]_{T,0}\, e^{-k_1 t} \qquad \text{(C1)}$$

$$[NO_2^-]_t = [NH_3]_{T,0}\, \frac{k_1}{k_2 - k_1}(e^{-k_1 t} - e^{-k_2 t}) \qquad \text{(C2)}$$

$$[NO_3^-]_t = [NH_3]_{T,0}\left[1 - \frac{k_2}{k_2 - k_1} e^{-k_1 t} + \frac{k_1}{k_2 - k_1} e^{-k_2 t}\right] \qquad \text{(C3)}$$

In these equations, $[NH_3]_{T,0}$ is the initial concentration of total NH_3 (i.e., $[NH_4^+]$ + $[NH_3]$), and $[NH_3]_{T,t}$, $[NO_2^-]_t$, and $[NO_3^-]_t$ are the concentrations of total NH_3, NO_2^-, and NO_3^- at a given time t, respectively. Equation C1 is the integrated rate law for total NH_3 disappearance and equations C2 and C3 are the integrated rate laws for NO_2^- and NO_3^- formation.

Sigma Plot (version 2001) was used to calculate k_1 and k_2 by non-linear regression of the experimental concentrations of total NH_3, NO_2^-, and NO_3^- versus time using equations C1–C3. These k_1 and k_2 values were plugged into equations C1–C3, and the concentration of each species was calculated as functions of time, then plotted as solid lines in Figures 2.3d.

APPENDIX D

Measurement of the Concentration of ·OH in UV/H_2O_2 System

This appendix provides details on the principle of measurement of the concentration of ·OH in UV/H_2O_2 system after UV-illumination of NH_4^+/NH_3-surfactant mixture for 2 hours. Photocatalytic degradation of *n*-chloro-butane (*n*-BuCl) in H_2O_2/UV is then provided, followed by the summary of pseudo first order rate constants of *n*-BuCl photodegradation and the steady state concentration ·OH. All the information belongs to chapter 4.

Basically, a microprobe compound *n*-BuCl was used to determine the concentration of ·OH in the UV/H_2O_2 system. It was assumed that the degradation of *n*-BuCl is proportional to the concentrations of *n*-BuCl and ·OH (Hagg and Hoigné, 1985), and the differential equation of the reaction rate was written as (Liao et al., 2002):

$$\frac{d[\text{BuCl}]}{d\text{t}} = -k[\text{BuCl}][\cdot\text{OH}] \qquad \text{(D1)}$$

where k is the second order rate constant of *n*-BuCl photodegradation. If some ·OH scavengers (e.g., HCO_3^-/CO_3^{2-} and formate) were present in the solution, they would compete with *n*-BuCl for ·OH. Then the consumption of ·OH would be due to the combination of *n*-BuCl and ·OH scavengers, which was expressed as the following equation (Hagg and Hoigné, 1985):

$$\frac{d[\cdot\mathrm{OH}]}{d\mathrm{t}} = -k[\mathrm{BuCl}][\cdot\mathrm{OH}] - \sum k_i[S_i][\cdot OH] \qquad \text{(D2)}$$

where S_i is the ·OH scavenger, and k_i is the second order rate constant of the reaction of ·OH with ·OH scavengers. If the concentration of S_i is significantly greater than *n*-BuCl, we assumed that (Hagg and Hoigné, 1985):

$$k[\mathrm{BuCl}] << k_i[\mathrm{S_i}] \qquad \text{(D3)}$$

So the consumption rate of ·OH was controlled by the sum of the rates of the reactions of ·OH scavengers with ·OH (Hagg and Hoigné, 1985):

$$\frac{d[\cdot\mathrm{OH}]}{d\mathrm{t}} = -\sum k_i[\mathrm{S_i}][\cdot\mathrm{OH}] \qquad \text{(D4)}$$

During the reactions, ·OH is so reactive that it does not accumulate to any significant amount. In other words, the formation rate of ·OH is equal to the destruction rate of ·OH. At this point, we assumed [·OH] was at a steady state concentration, called $[\cdot\mathrm{OH}]_{ss}$. So the equation D1 was written as equation D5 (Hagg and Hoigné, 1985):

$$\frac{d[\mathrm{BuCl}]}{d\mathrm{t}} = -k[\mathrm{BuCl}][\cdot\mathrm{OH}]_{ss} \qquad \text{(D5)}$$

Assume

$$k' = k[\cdot\mathrm{OH}]_{ss} \qquad \text{(D6)}$$

$$\therefore \frac{d[\text{BuCl}]}{d\text{t}} = -k'[\text{BuCl}] \qquad \text{(D7)}$$

The value k in equation D4 was reported in the literature, 3×10^9 M^{-1} s^{-1} (Haag and Hoigné, 1985). We plotted the concentration of *n*-BuCl as function of the irradiation time; the experimental data were then fit to the pseudo-first order reaction model (equation D7), and the value k' was obtained from non-linear least-squares regression. The steady-state concentration of ·OH was then calculated from equation D6.

The following figures (Figures D1-D11) illustrate the photodegradation of *n*-BuCl by UV/H_2O_2 after the photocatalytic degradation of NH_4^+/NH_3 and surfactants/monosaccharides for two hours at pH ~10.1. Table D1 summarizes pseudo first order rate constants of *n*-BuCl degradation and steady-state concentrations of ·OH in the presence of surfactants/monosaccharides at pH ~10.1.

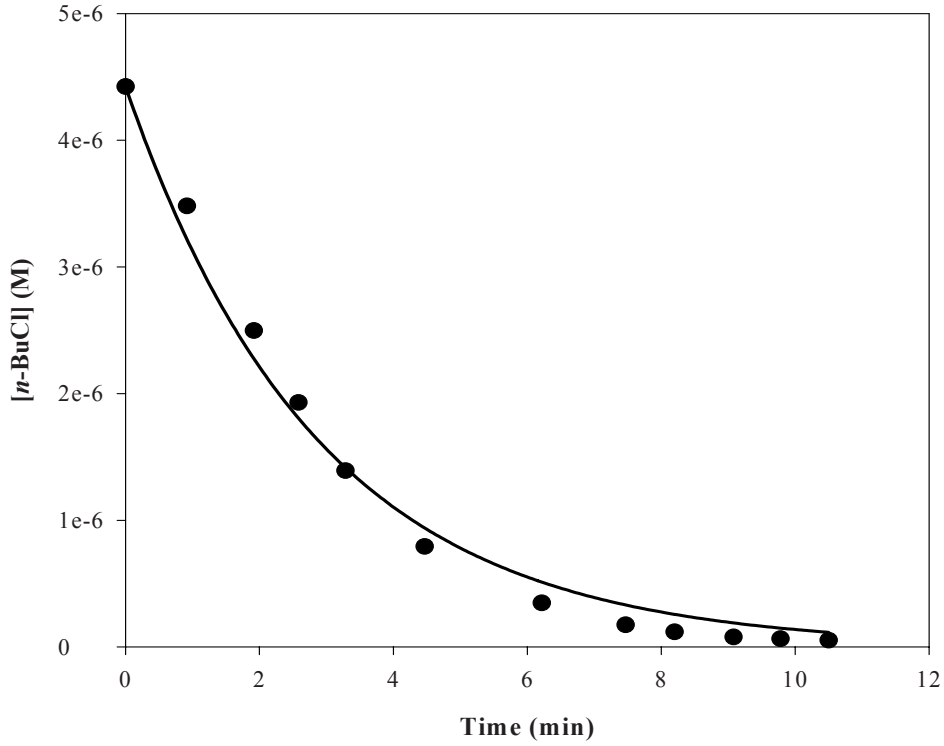


Figure D1. Photodegradation of *n*-BuCl without surfactants (control)

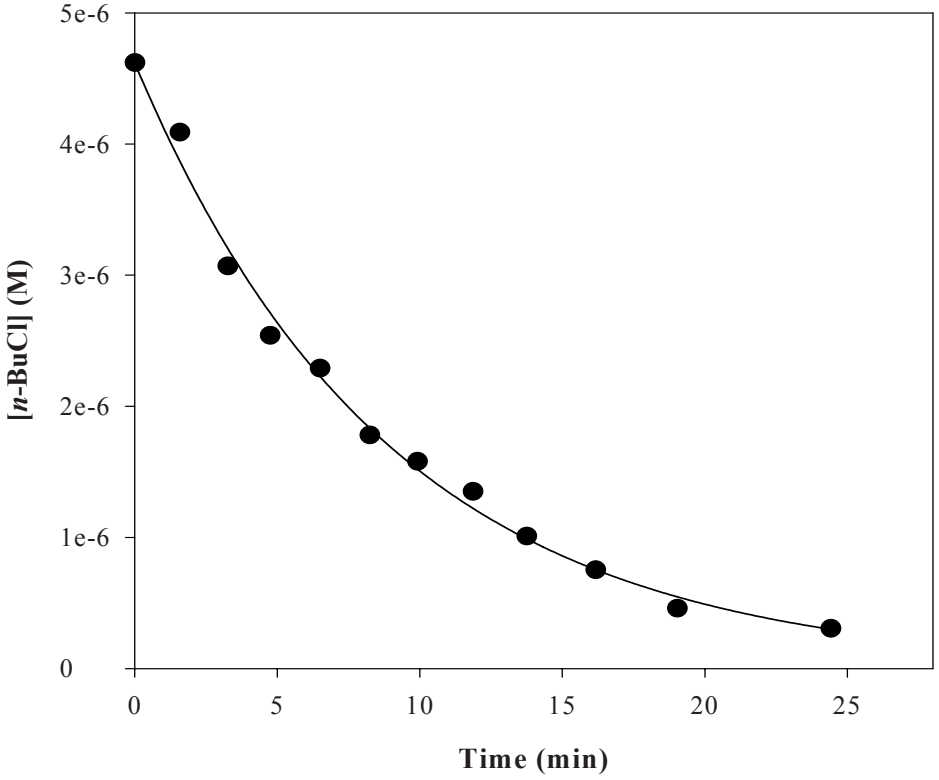


Figure D2. Photodegradation of *n*-BuCl with 2 ×10^{-5} M cetylpyridinium chloride

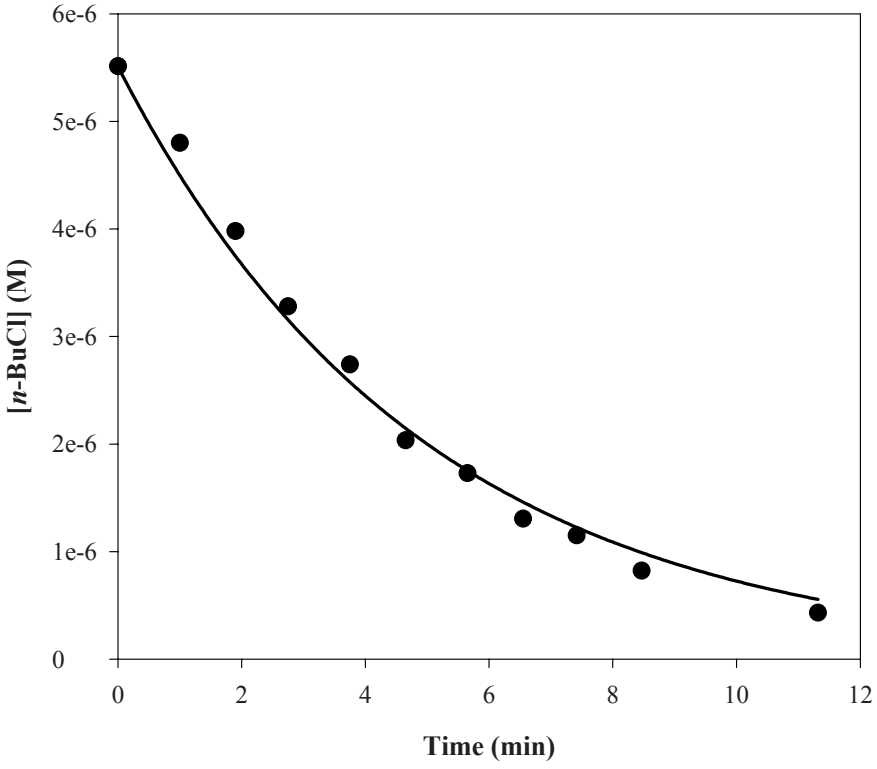


Figure D3. Photodegradation of *n*-BuCl with 2 ×10^{-5} M hexyl-β-D-glucoside

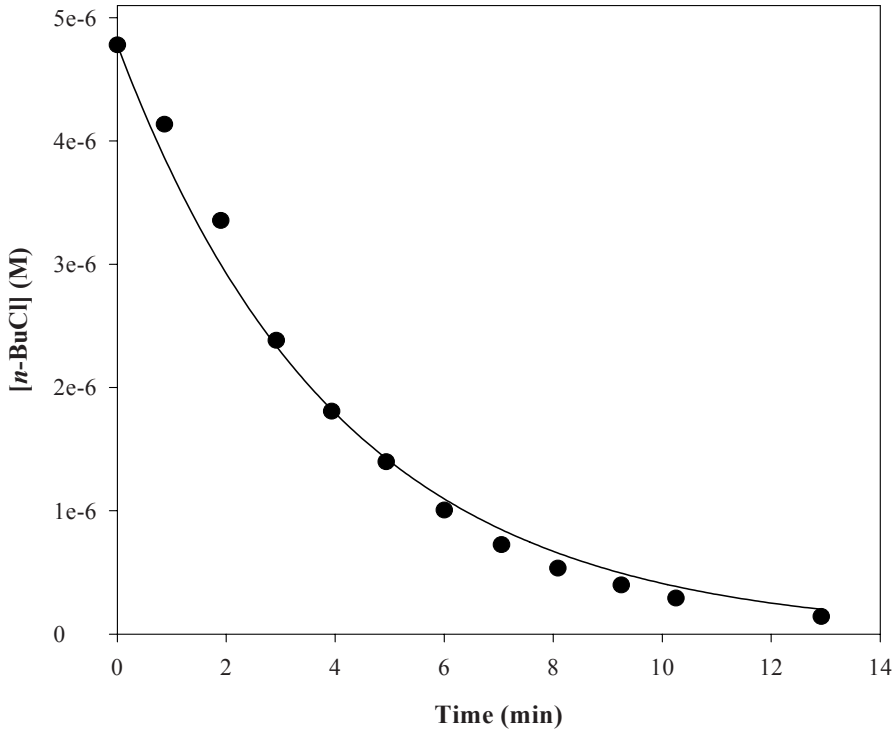


Figure D4. Photodegradation of *n*-BuCl with 2 ×10^{-5} M 1-octanesulfonic acid sodium

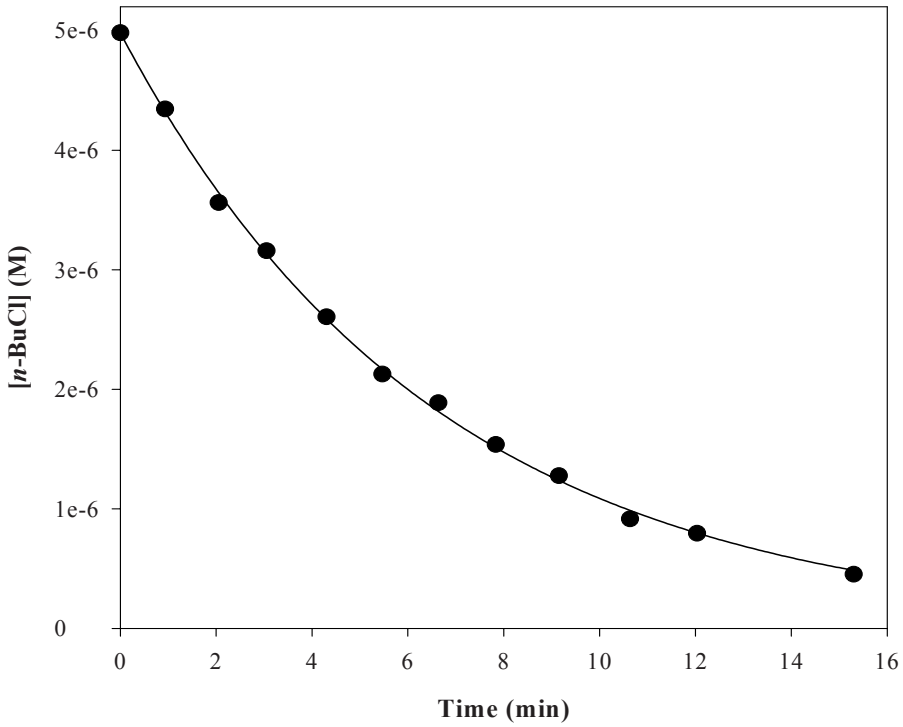


Figure D5. Photodegradation of *n*-BuCl with 2 ×10^{-5} M dihexyl sulfosuccinate sodium

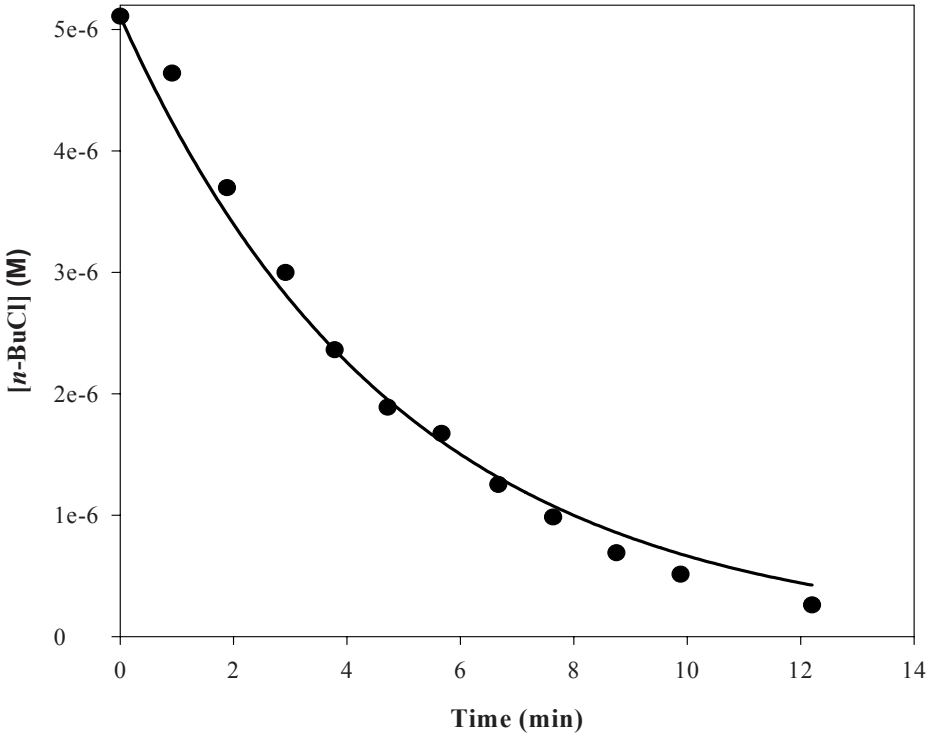


Figure D6. Photodegradation of *n*-BuCl with 2 ×10^{-5} M sodium dodecylsulfate

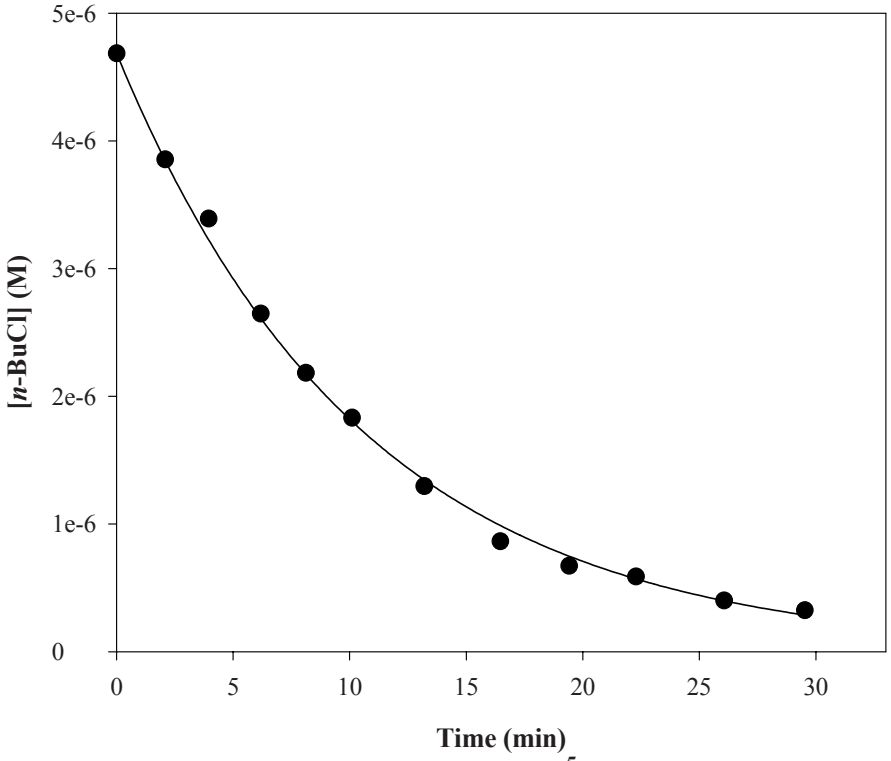


Figure D7. Photodegradation of *n*-BuCl with 2 ×10^{-5} M cetyltrimethylammonium chloride

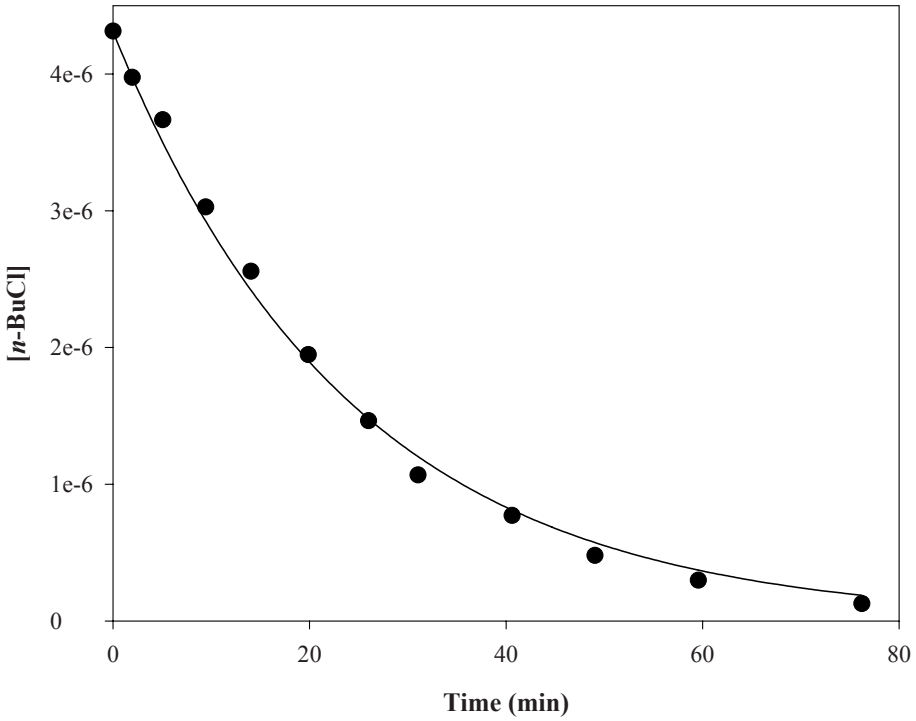


Figure D8. Photodegradation of *n*-BuCl with 1.2 ×10^{-5} M Brij® 23 lauryl ether

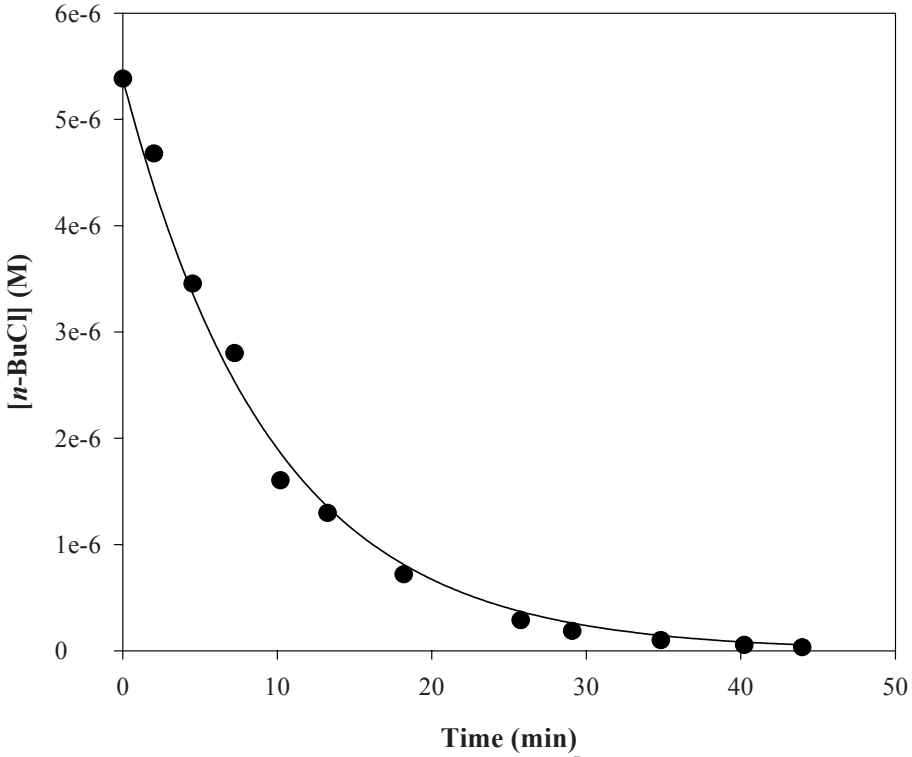


Figure D9. Photodegradation of *n*-BuCl with 1.2 ×10^{-5} M Brij® 23 lauryl ether and 0.01 M H_2O_2

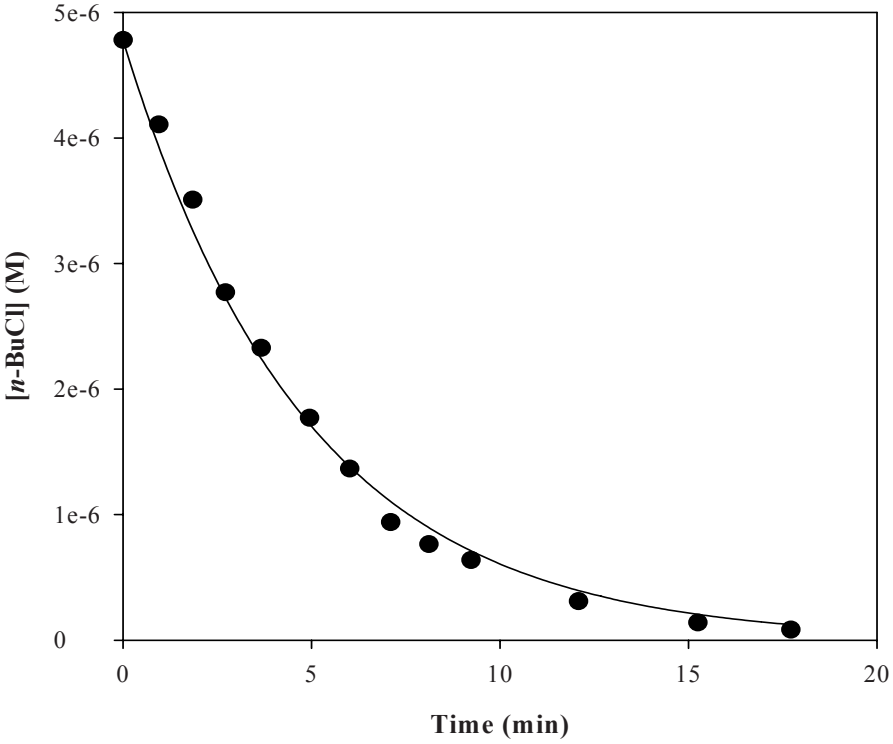


Figure D10. Photodegradation of *n*-BuCl with 2 ×10^{-5} helicin

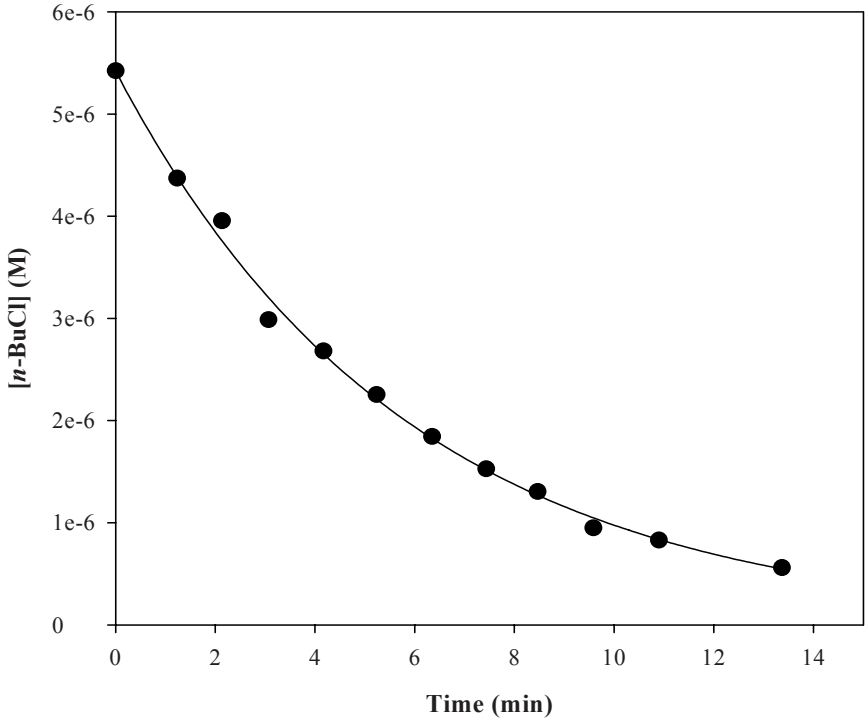


Figure D11. Photodegradation of *n*-BuCl with 2 ×10^{-5} ally-tetra-O-acetyl -β-D-glucopyranoside

Table D1. Pseudo first order rate constants of *n*-BuCl degradation and steady-state concentration of ·OH in the presence of surfactant/monosaccharide at pH ~ 10.1

Surfactant	k' (min^{-1}) [1]	$[\cdot OH]_{ss} \times 10^{12}$ (M) [2]
No surfactant (control)	0.254 ± 0.0140	1.41 ± 0.17
Nonylphenol polyethoxylate (10)	0.0688 ± 0.00390	0.382 ± 0.0490
Sodium dodecylbenzene sulfonate	0.128 ± 0.00640	0.713 ±0.080
Cetylpyridinium chloride	0.0804 ± 0.00270	0.447 ± 0.0330
Sodium dodecylsulfate	0.152 ± 0.00700	0.856 ± 0.0856
Brij® 23 lauryl ether	0.0323 ± 0.00100	0.180 ± 0.0122
Hexyl-β-D-glucoside	0.151 ± 0.00620	0.841 ± 0.0767
Cetyltrimethylammonium chloride	0.0699 ± 0.00150	0.389 ± 0.0183
1-Octanesulfonic acid sodium	0.186 ± 0.00840	1.03 ± 0.010
Dihexyl sulfosuccinate	0.119 ± 0.00140	0.662 ± 0.0171
Helicin	0.163 ± 0.00520	0.907 ± 0.0629
Allyl-tetra-O-acetyl-β-D-glucopyranoside	0.134 ± 0.00290	0.747 ± 0.0355
Brij® 23 lauryl ether with 0.01 M H_2O_2	0.0822 ± 0.00380	0.456 ± 0.0465

[1]: errors are standard errors from the nonlinear regression output; [2]errors are 95% confidence intervals of $[\cdot OH]_{ss,}$ which are determined from standard errors and t values from a student *t* distribution table as shown below.

Error propagation method was used to estimate the standard error of $[\cdot OH]_{ss}$, $SE([\cdot OH]_{ss}$, which is expressed as (Skoog et al., 1996):

$$SE([\cdot OH]_{ss}) = [\cdot OH] \times \left(\frac{SE(k')}{k'} \right) \quad \text{(D8)}$$

95% confidence interval of $[\cdot OH]_{ss}$ were then determined from their standard errors and t-values from a student *t* distribution table (Miller and Miller, 1988):

$$[\cdot OH]_{ss} = [\cdot OH]_{ss} \pm SE[\cdot OH]_{ss}) \times t_{(\alpha/2),\,(n-1)} \quad \text{(D9)}$$

where $\alpha = 0.05$(95% confidence interval), n is the number of experimental data points used in this regression, and n-1 is the degrees of freedom.

An example calculation of standard error of the $[\cdot OH]_{ss}$ for the control experiment is shown below.

First the steady state concentration of ·OH was calculated based on equation D6:

$$[\cdot OH]_{ss} = \frac{0.254\,\text{min}^{-1}}{3\times10^{9}\,\text{M}^{-1}\text{s}^{-1}} \times \frac{1\,\text{min}}{60\text{s}} = 1.41\times10^{-12}\,\text{M} \qquad \text{(D10)}$$

Then the standard error of the $[\cdot OH]_{ss,}$ $SE([\cdot OH]_{ss})$ was calculated according to equation D8:

$$SE([\cdot OH]_{ss} = 1.41\times10^{-12} \times \left(\frac{0.014}{0.254}\right) = 7.77\times10^{-14} \qquad \text{(D11)}$$

Then 95% confidence interval of $[\cdot OH]_{ss}$ was then calculated from equation D9:

$$[OH]_{ss} = 1.41 \times 10^{-12}\,\text{M} \pm (7.77 \times 10^{-14} \times 2.201)$$

$$= (1.41 \pm 0.17) \times 10^{-12}\,\text{M} \qquad \text{(D12)}$$

Appendix E

Profiles of the Photocatalytic Degradation of Ammonia in the Presence of Surfactants/monosaccharides

This appendix provides the profiles of homogeneous degradation of SDBS, CPC, and NP10 and ammonia degradation with/without surfactants/ monosaccharide and their byproduct distribution at pH ~10.1. All these figures are related to chapter 4.

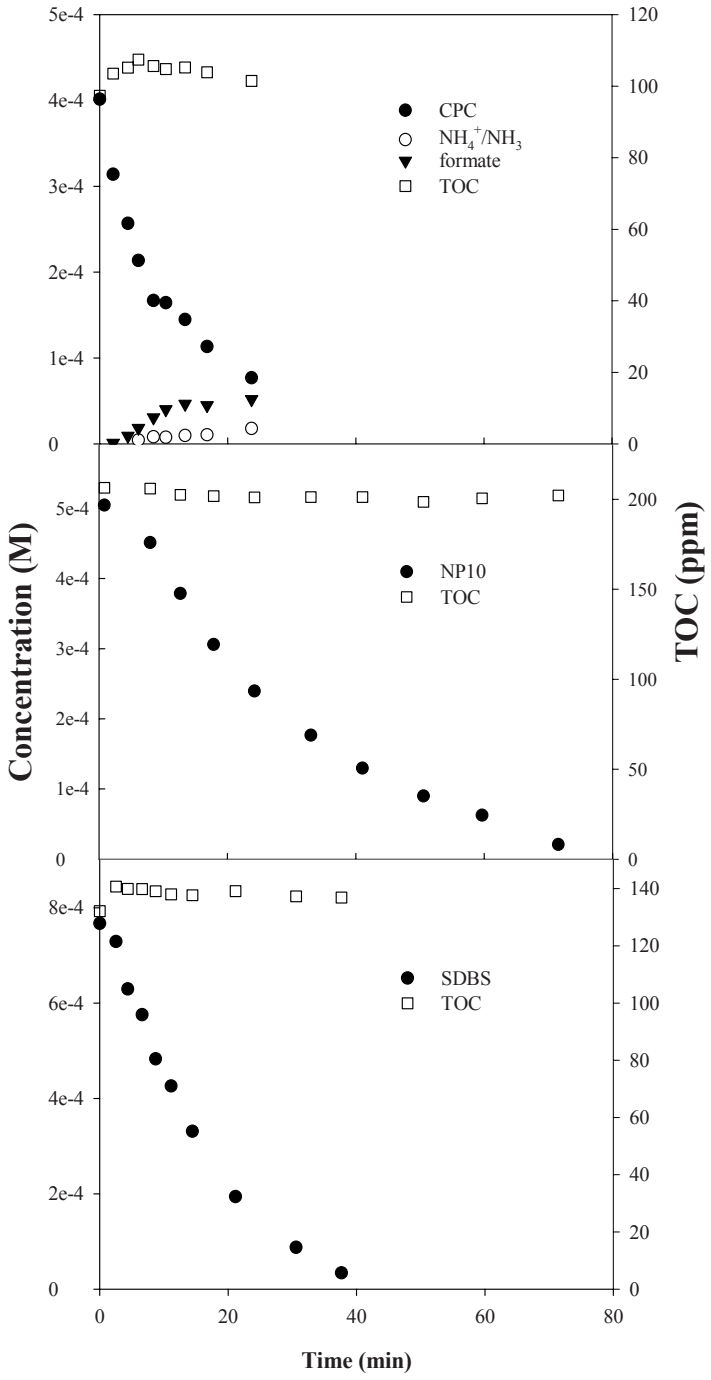


Figure E1. Homogeneous degradation of CPC, NP10, and SDBS at pH ~10.1. [NaCl]: 0.001 M.

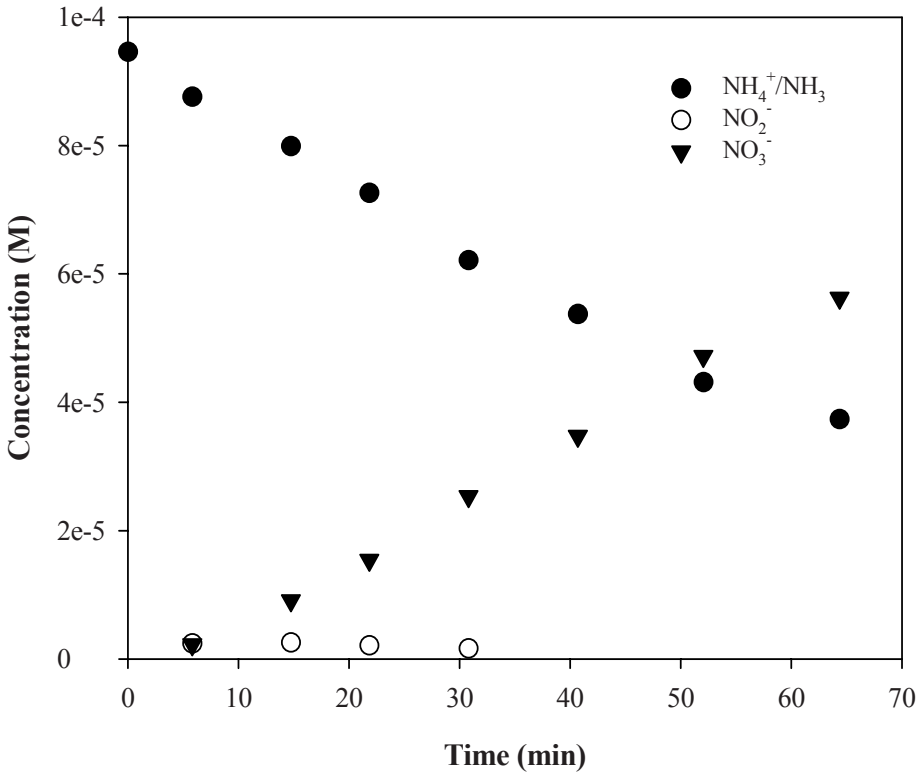


Figure E2. Photocatalytic degradation of NH_4^+/NH_3 without surfactants (control)

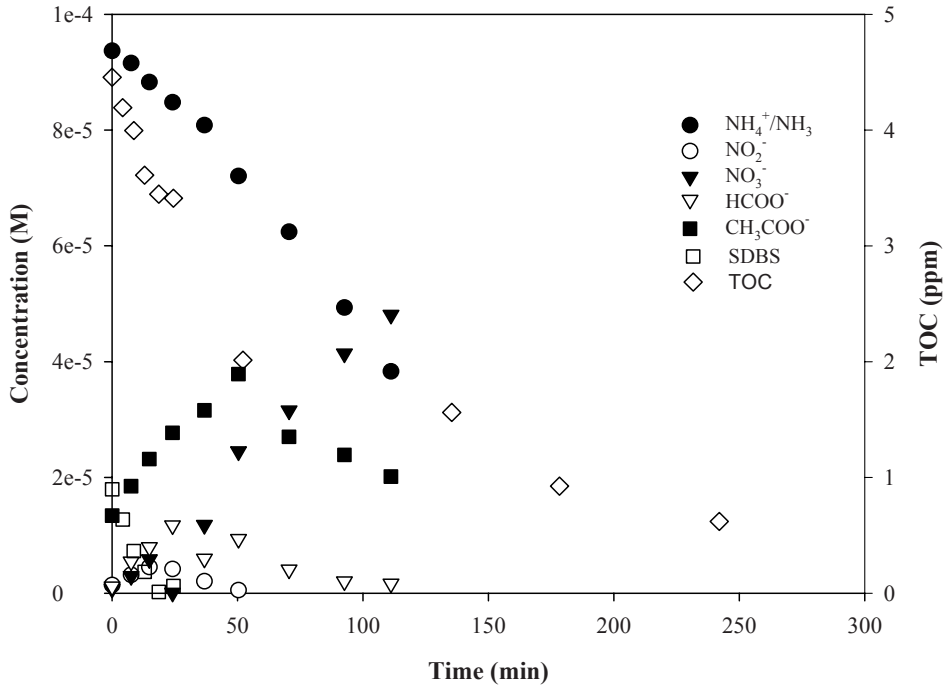


Figure E3. NH_4^+/NH_3 degradation with 2×10^{-5} M sodium dodecylbenzene sulfonate

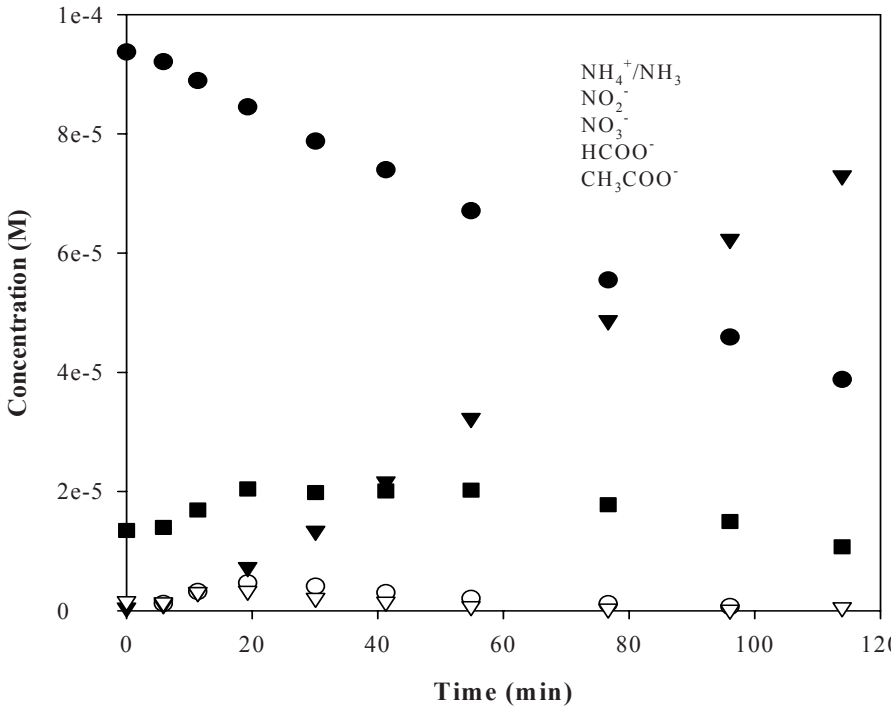


Figure E4. NH_4^+/NH_3 degradation with 2×10^{-5} M 1-octanesulfonic acid sodium

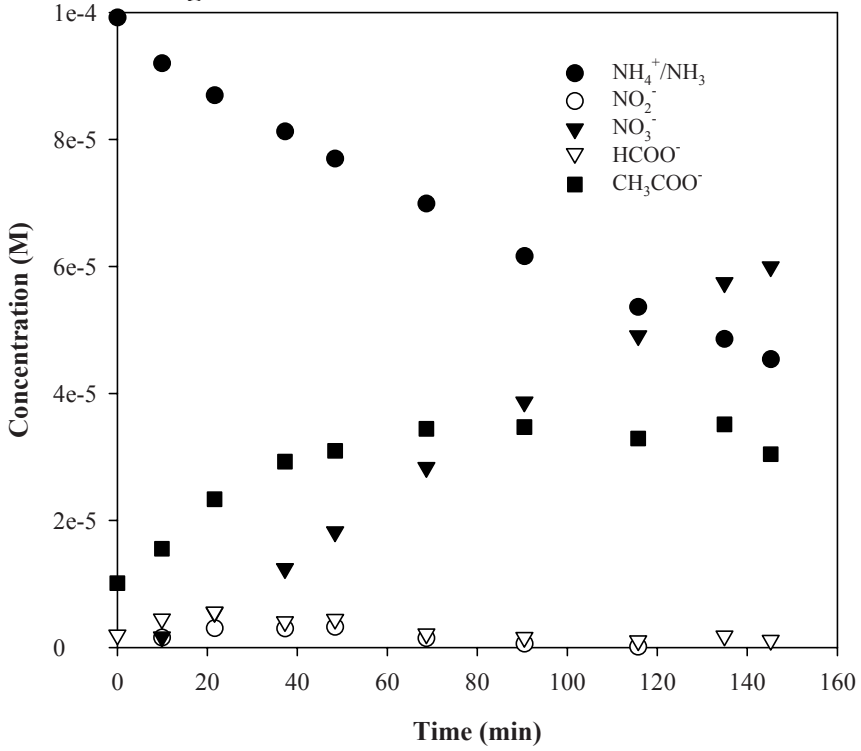


Figure E5. NH_4^+/NH_3 degradation with 2×10^{-5} M dihexyl sulfosuccinate sodium

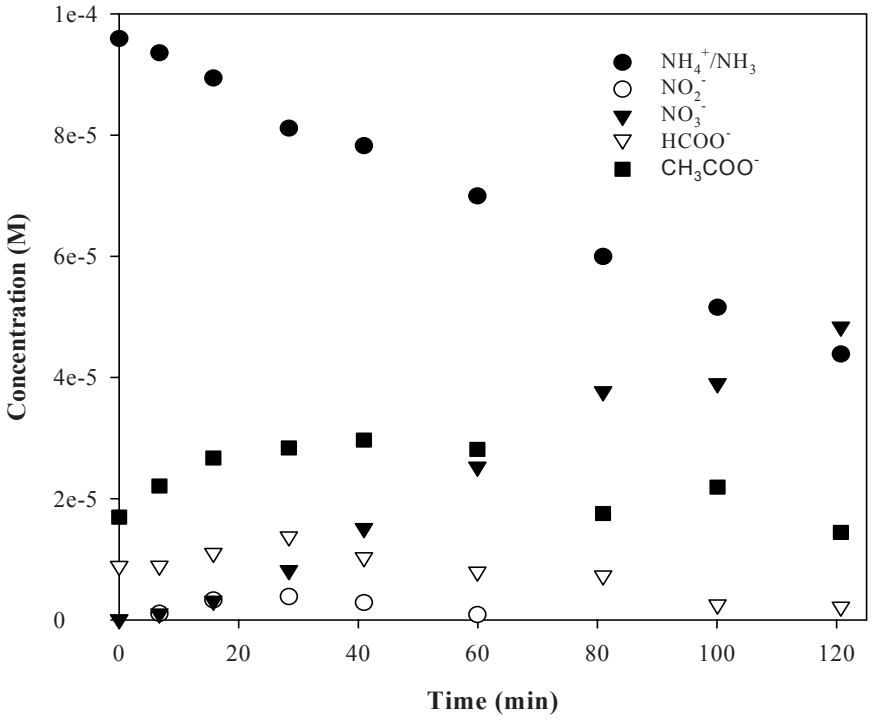


Figure E6. NH_4^+/NH_3 degradation with 2×10^{-5} M sodium dodecylsulfate

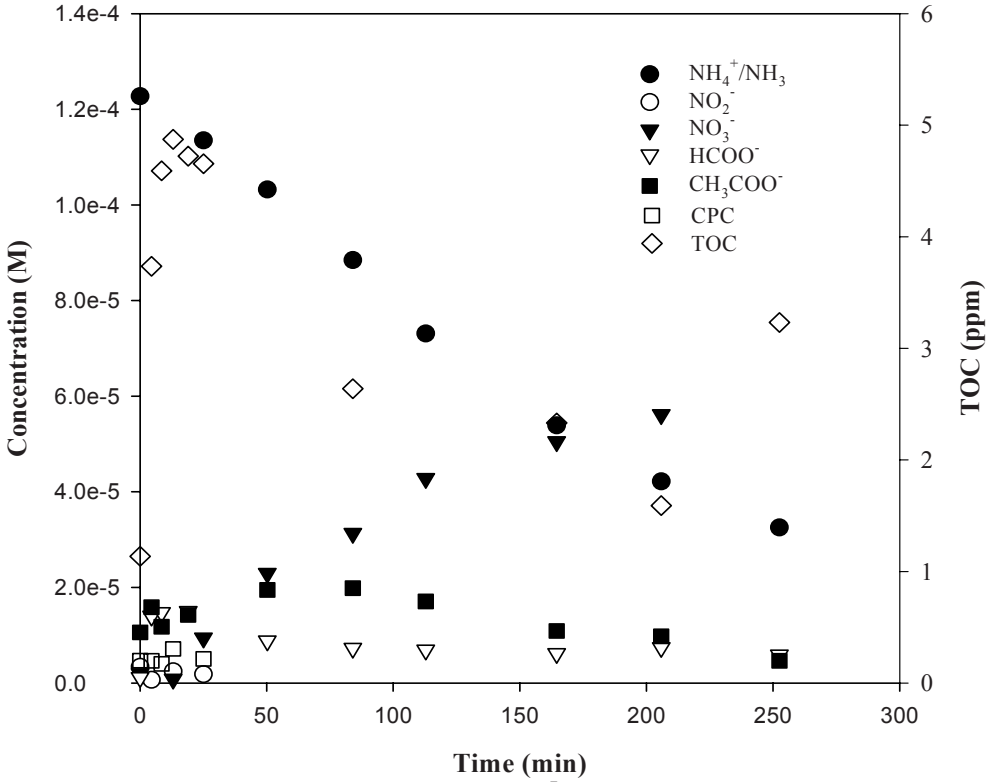


Figure E7. NH_4^+/NH_3 degradation with 2×10^{-5} M cetylpyridinium chloride

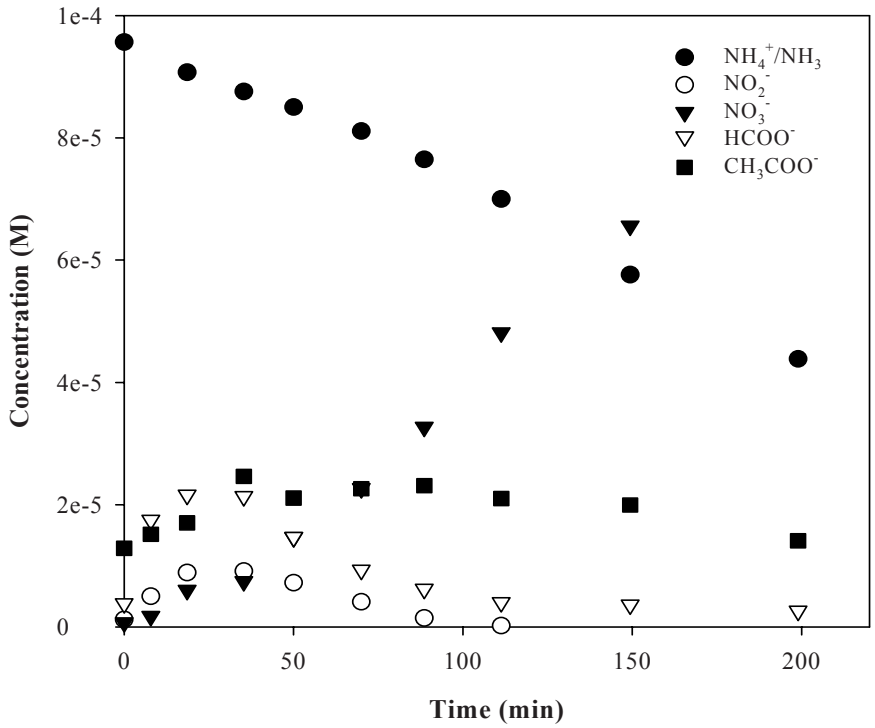


Figure E8. NH_4^+/NH_3 degradation with 2×10^{-5} M cetyltrimethylammonium chloride

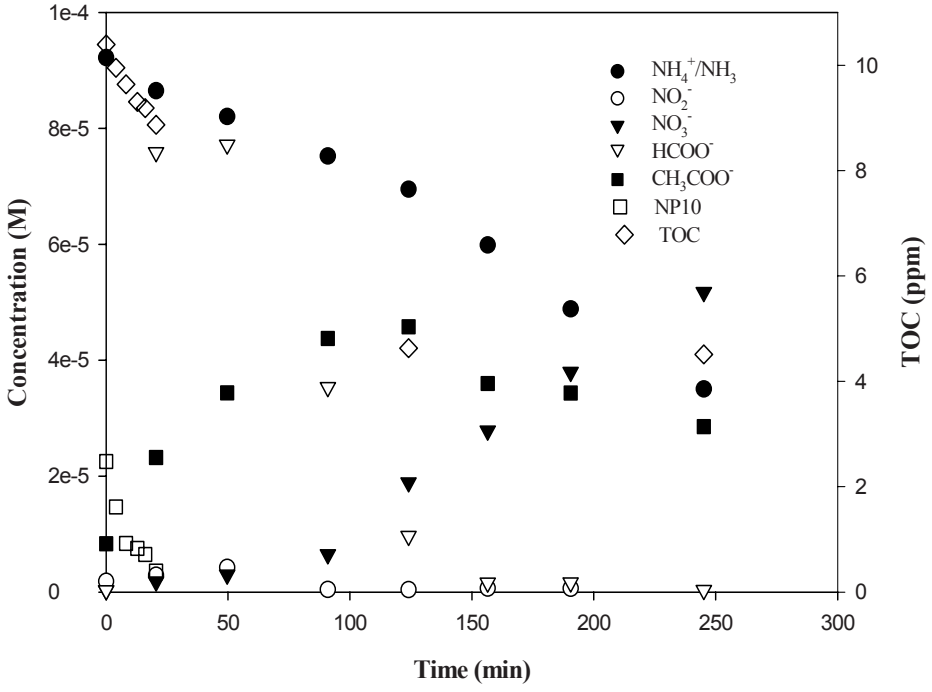


Figure E9. NH_4^+/NH_3 degradation with 2×10^{-5} M NP10

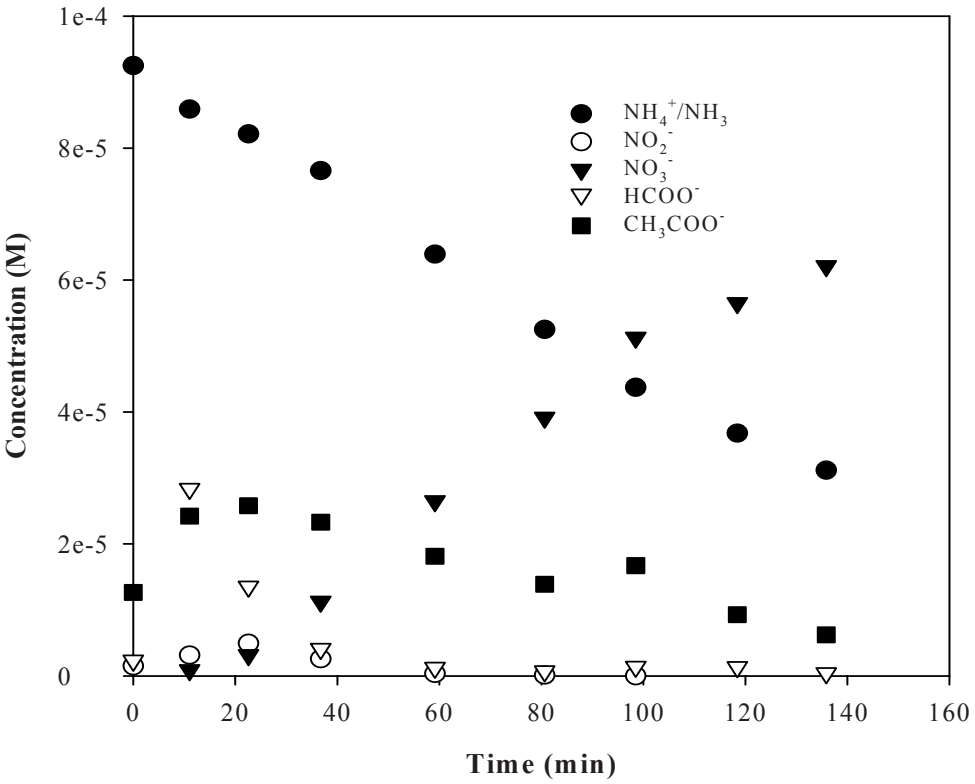


Figure E10. NH_4^+/NH_3 degradation with 2×10^{-5} M hexyl-β-D-glucoside

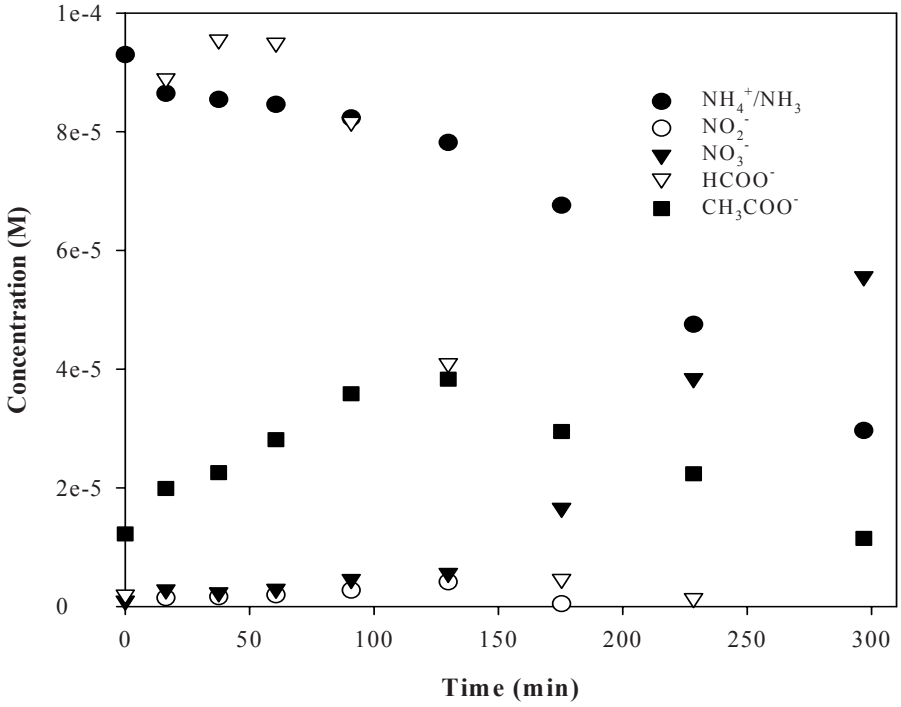


Figure E11. NH_4^+/NH_3 degradation with 1.2×10^{-5} M Brij®35

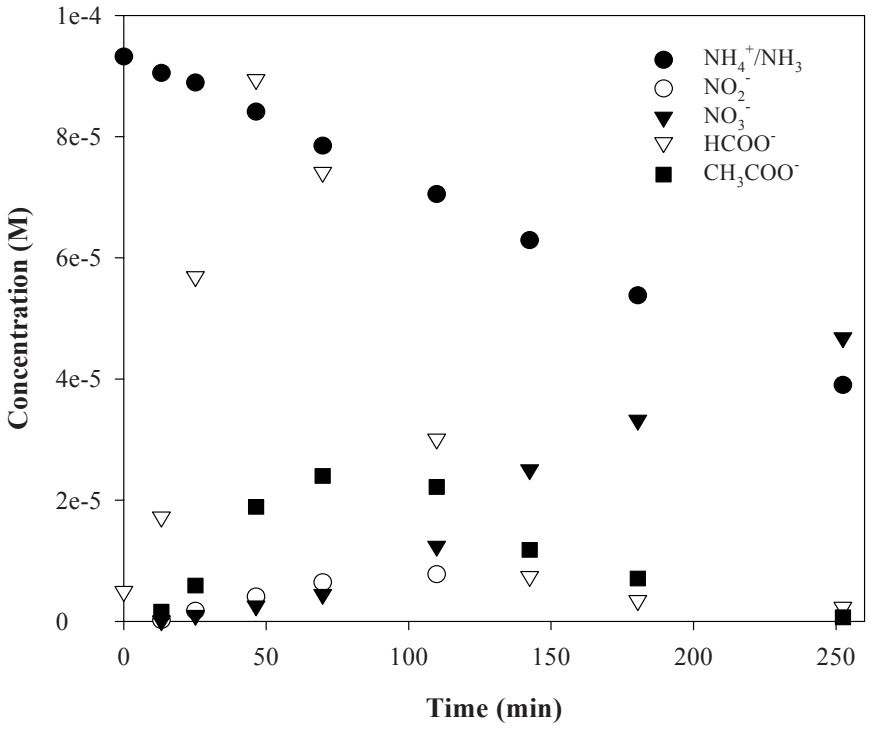


Figure E12. NH_4^+/NH_3 degradation with 1.2×10^{-5} M Brij® 35 and 0.01 M H_2O_2

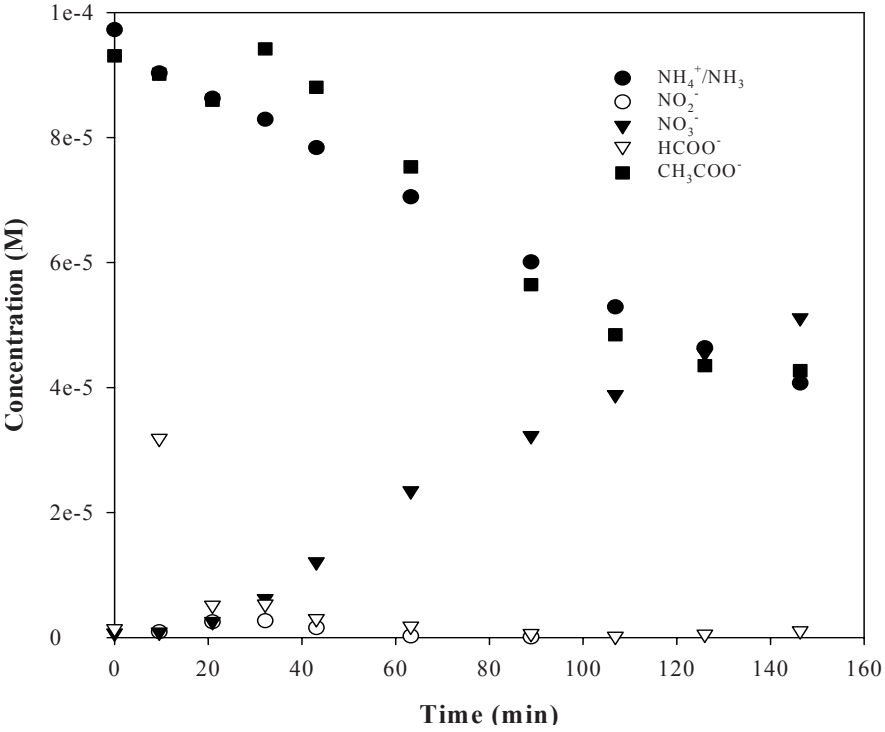


Figure E13. NH_4^+/NH_3 degradation with 2×10^{-5} M ally-tetra-O-acetyl-β-D-glucopyranoside

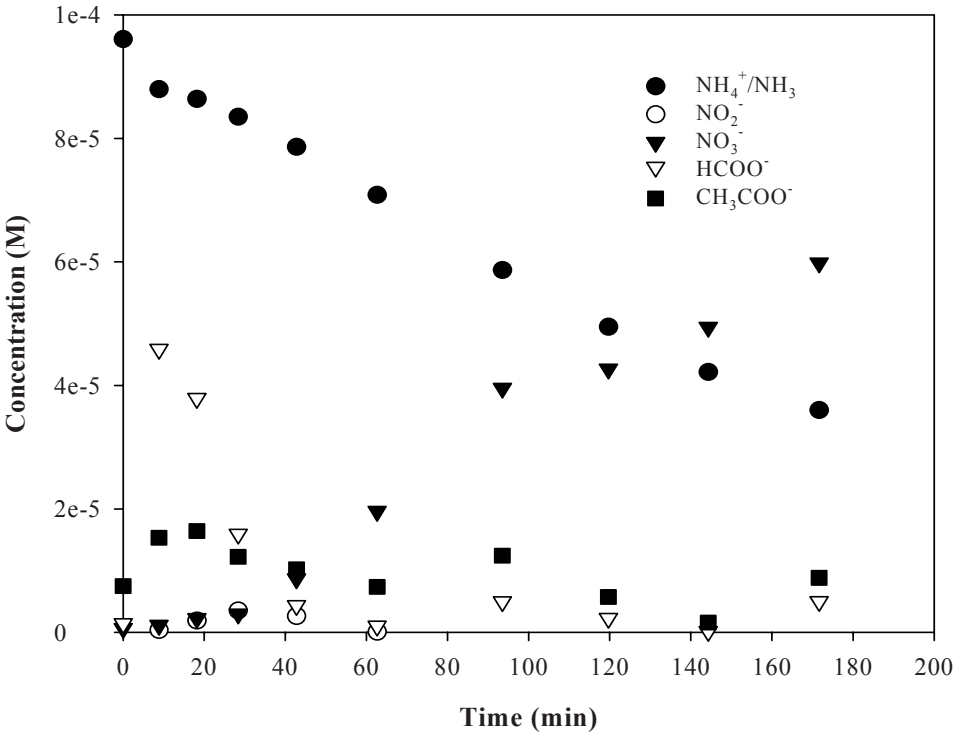


Figure E14. NH_4^+/NH_3 degradation with 2×10^{-5} M helicin

APPENDIX F

Determination of Critical Micelle Concentration of Surfactants and Surface Coverage of Surfactants on the TiO_2 Surface

This appendix provides details on critical micelle concentration (CMC) measurement and how to calculate surface coverage by surfactants (SDBS, CPC, and NP10) on TiO_2, which are related to chapter 4. Surfactant CMCs were determined by surface tension measurements using a Krüss K-8 interfacial tensiometer (Hamburg, Germany). This instrument operates on the DuNouy principle, in which a platinum–iridium ring is suspended from a torsion balance, and the force (in mN/m) need to pull the ring free from the surface film (surface tension) is measured. By plotting the surface tension as a function of logarithm a surfactant concentration, the concentration where the surface tension starts to level off is the CMC. All the CMCs measurements were conducted in 0.001 M NaCl at 26 ºC, which were also used in kinetic studies. Figures F1-F3 are the CMCs of SDBS, CPC, and NP10, respectively.

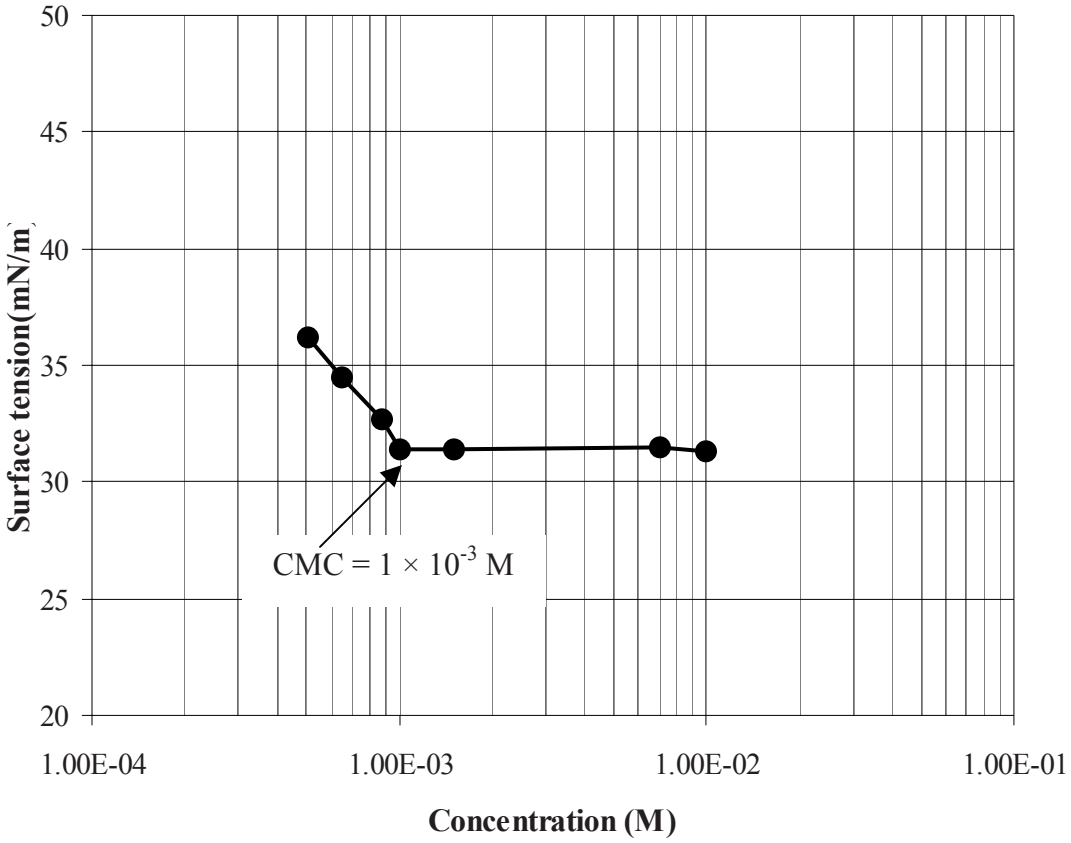


Figure F1. Surface tension versus concentration of SDBS

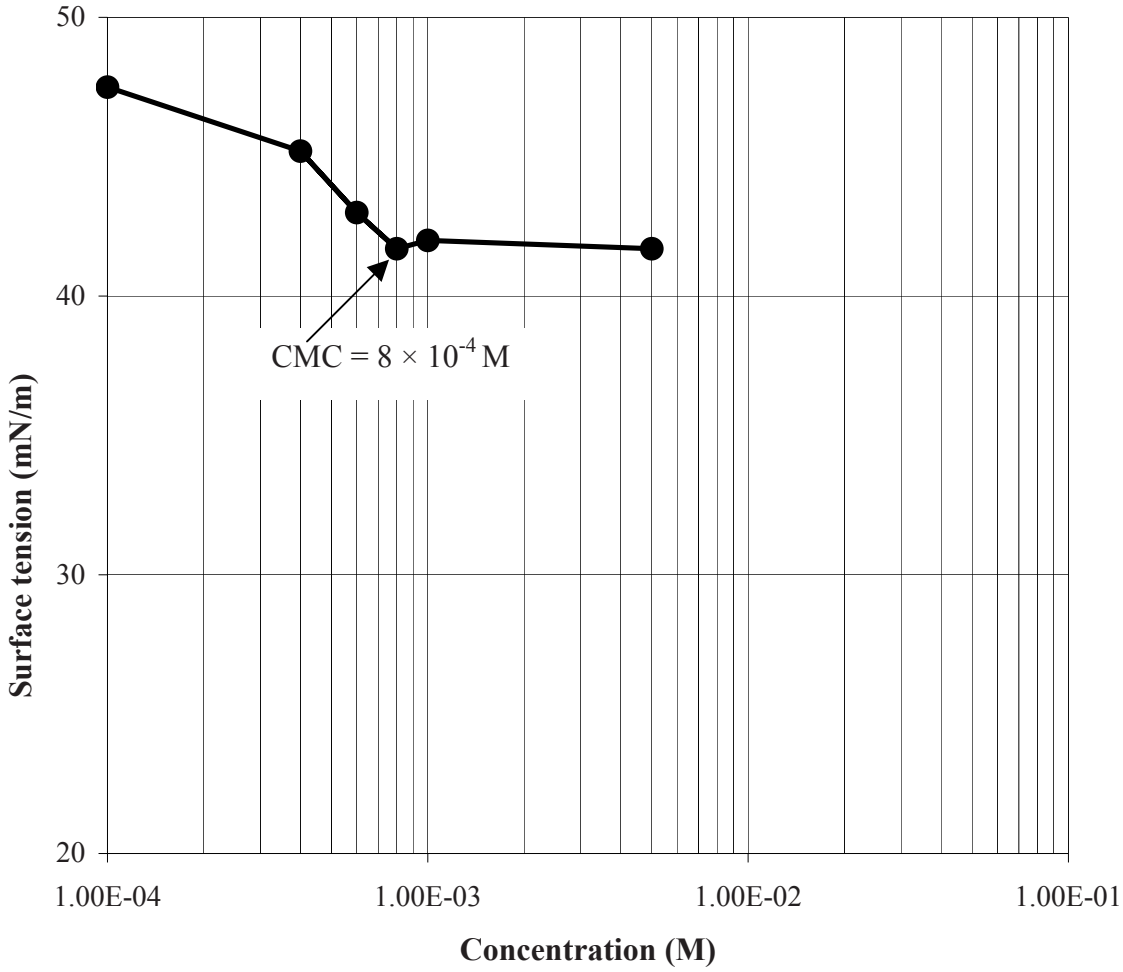


Figure F2. Surface tension versus concentration of CPC

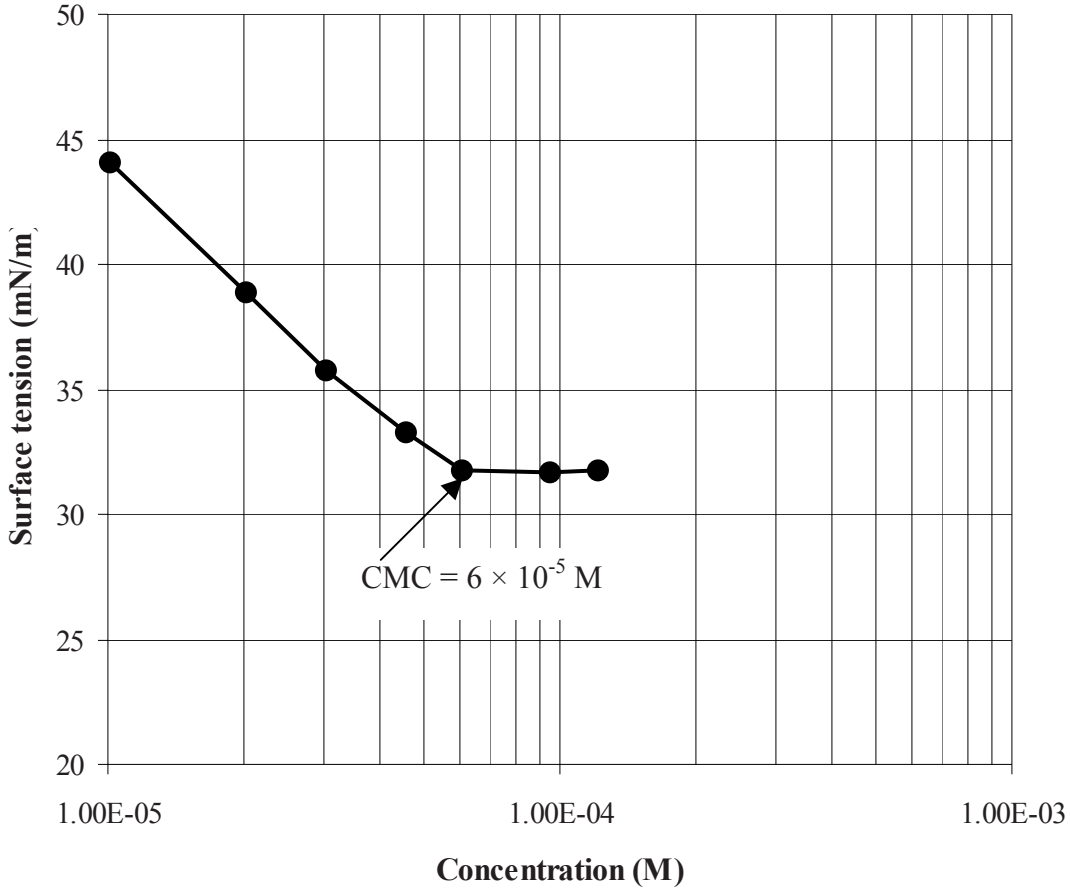


Figure F3. Surface tension versus concentration of NP10

Calculation method for TiO_2 surface coverage by surfactants

Gibbs adsorption equation was used to calculate the surface coverage by a hydrophilic head group of a surfactant (Rosen, 2004, all equations in this appendix are also from this reference). This calculation assumed that the surface was saturated by a surfactant. First a figure of surface tension (γ) as function of natural logarithm of the concentration (C) of surfactant (which is below or equal the CMC) was plotted. The slope of the plot, $\frac{d\gamma}{d\ln C}$, is equal to $-\Gamma_m RT$ ($-2\,\Gamma_m RT$ for an ionic surfactant due to its dissociation), where Γ_m is Gibbs surface excess concentration of a surfactant (mol/m^2) at surface saturation, i.e., the amount of a surfactant per unit m^2 of air-water interface, R is ideal gas constant, and T is absolute temperature (299.15 K in this study). Then Γ_m was obtained from the slope of the plot. The surface area per head group at surface saturation and surface coverage of the surfactant to the TiO_2 surface was then calculated from Γ. An example of surface coverage by NP10 is given below:

The following table lists lnC of NP10 and corresponding surface tension.

Table F1. Concentration of NP10 and surface tension

lnC	Surface tension (N/m)
-11.503	0.0441
-10.810	0.0389
-10.404	0.0358
-9.999	0.0333
-9.711	0.0318

A plot of lnC versus surface tension is presented below (Figure F4) and the slope of the plot is -0.0069 N/m.

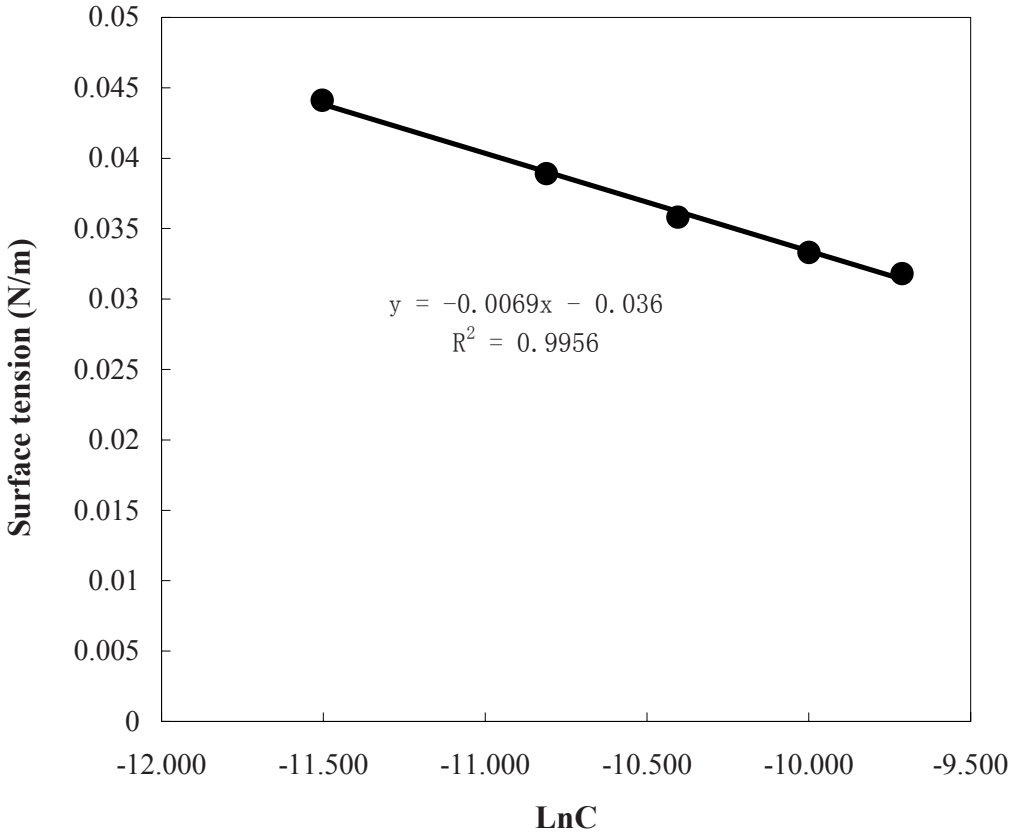


Figure F4. Surface tension as function of natural logarithm of NP10 concentrations

$$\text{So} \quad -\Gamma_m RT = -0.0069 \text{ N/m} \tag{F1}$$

$$\Gamma_m = \frac{0.0069 \text{N/m}}{8.314 \text{J/mol.K} \times (273.15 + 26) \text{K}} = 2.77 \times 10^{-6} \text{ mol/m}^2 \tag{F2}$$

So the surface area per head group at the interface (α_m^s) was calculated:

$$\alpha_m^{\ s} = \frac{1}{2.77 \times 10^{-6} \text{mol/m}^2 \times 6.02 \times 10^{23} \text{molecule/mol}} = 6.00 \times 10^{-19} \text{m}^2/\text{molecule} \tag{F3}$$

So surface coverage was calculated (12% of NP10 is adsorbed to the TiO_2 surface with its initial concentration of 2×10^{-5} M), assuming that the surface area of the TiO_2 is 50 m^2/g (production information from Degussa Corporation):

$$\text{Surface coverage} = \frac{2\times10^{-5}\,\text{mol/L}\times0.12\times6.02\times10^{23}\,\text{molecule/mol}\times5.997\times10^{-19}\,\text{m}^2/\text{molecule}}{3\text{g/L}\times50\text{m}^2/\text{g}}\times100\%$$

$$= 0.6\% \qquad \text{(F4)}$$

This method estimated the minimum surface coverage assuming only the head group of the surfactant was adsorbed to the TiO_2 surface. Table F2 summarizes percentage surfactant adsorbed on the TiO_2 surface, surface area per head group, and the minimum surface coverage by a surfactant, provided a concentration of 2×10^{-5} M surfactants is used.

Table F2. Surface area of head group of surfactants and their surface coverage

Surfactant	Percent adsorbed (%)	Surface area (m^2/molecule)	Surface coverage (%)
NP10	12	6.00×10^{-19}	0.6-4
SDBS	17	3.44×10^{-19}	0.5-5
CPC	77	7.65×10^{-19}	6-27

Next, we estimated the maximum surface coverage assuming the entire surfactant molecule is lying on the TiO_2 surface, which is possible when surfactant concentrations are an order of magnitude below their CMCs. Since the NP10 concentration we used (2

$\times 10^{-5}$ M) was only three times lower than its CMC (6×10^{-5} M, Table S1), the actual surface coverage by NP10 was likely below the maximum value. First, we estimated the surface area of $–CH_2$, $–CH_3$ by dividing the volume by the length of the functional groups (Nagarajan, 1996). Then the total surface area of the surfactant can be calculated by adding the surface area of total $–CH_2$, $-CH_3$, and benzene ring (110A, Senn, 1961) and the head group of the surfactant. The maximum surface coverage can then be calculated from equation F4 using the total surface area of the molecule instead of the surface area of the head group. The values are listed in Table F2.